UNIVERSITAT POLITÈCNICA DE CATALUNYA BARCELONATECH

Multiscale multiphysics simulation in composite materials

Stefano Zaghi

Universitat Politècnica de Catalunya

UPC BarcelonaTech
-
Departament d'Enginyeria Civil i Ambiental - DECA

Multiscale Multiphysics Simulation in Composite Materials

Ph.D. Thesis in Structural Analysis

Thesis submitted as compendium of publications

Author :
Stefano Zaghi

Supervisors :
Prof. Riccardo Rossi
Prof. Xavier Martínez García

Barcelona, September 2018

All things are difficult before they are easy.

Thomas Fuller

Contents

Contents **i**

1 Introduction **1**
1.1 Motivation 1
1.2 Objective 2
1.3 Outline 3

2 State Of The Art **5**
2.1 Introduction 5
2.2 Multiscale Homogenization Methods 8
2.3 First-order Computational Homogenization 9
2.3.1 Macro to micro transition 12
2.3.2 Micro to macro transition 13
2.3.3 Material homogenized properties 13
2.3.4 Representative Volume Element Definition . . . 13
2.4 Thermo dynamic approach of Multiscale Analysis . . . 16
2.4.1 Introduction 16
2.4.2 Multiscale thermo-mechanical formulation . . . 17

3 Multiscale implementation of multiphysical effects in composite materials **21**
3.1 Introduction 21
3.2 Micro-scale continuous and discrete numerical models for nonlinear analysis of masonry shear walls 22
3.3 Multiscale thermo-mechanical analysis of multi-layered coatings in solar thermal applications 23
3.4 Adaptive and Off-Line Techniques for Non-Linear Multiscale Analysis 24

4 Papers **31**

5 Conclusions **103**
5.1 Conclusions 103
5.2 Main Contributions 104
5.3 Future works 105

Appendices **107**

A Interface Element Formulation **109**
A.1 Mixed element u/p formulation for RVE BCs 113

B The GUI (ProblemType) of Kratos **117**
B.1 Overview 117
B.2 Users Interface 118

List of Figures

2.1 Examples of metallic heterogeneous microstructures: (a) SEM image of steel T67CA; the white spots are cementite particles; (b) SEM image of steel T61CA; voids are located around cementite particles; (c) light microscope image of an aluminum polycrystalline microstructure; (d) light microscope image of a shadow mask. [48] . . . 6
2.2 Continuum macrostructure and heterogeneous microstructure associated with the macroscopic point M. [48] . . . 10
2.3 Schematic representation of a macrostructure with (a) a locally and (b) a globally periodic microstructure. [48] 11
2.4 First-order computational homogenization scheme. σ_m is the macroscopic stress tensor and F_m is the macroscopic deformation (gradient) tensor 11
2.5 (a) Several microstructural cells of different sizes. (b) Convergence of the apparent properties [41] to the effective values with increasing microstructural cell size for different types of boundary conditions.[48] 15
2.6 Common boundary conditions for shear of a RVE. (a) Rigid boundary conditions. (b) Periodic boundary conditions. [54] 15

3.1 Masonry micro-structure with nonlinear interface model. [82] 22
3.2 Particle-matrix debonding issues in the nano-absorber: a) matrix damage, b) cohesive damage, c) redistribution of temperature gradient field, and d) change in the heat flux. [63] 24
3.3 Composite Stress Evolution Surfaces. [106] 26

A.1 Initial configuration with zero thickness 109
A.2 Current configuration showing the reference middle surface 109

A.3 Damage Surface for 2D Case 111
A.4 3 Multi Surface theory 112
A.5 Periodic Boundary conditions [38] 114
A.6 Example of Triangular U/P Element 114
A.7 Example of Standard Triangular Element 114
A.8 Displacement distribution on interface element 115

B.1 Masonry micro-structure with nonlinear interface model. 118
B.2 Step 0 of the interface: Application Type. 119
B.3 Step 1 of the interface: Geometry definition. 119
B.4 Step 2 of the interface: Material definition. 120
B.5 Step 2 of the interface: Material definition, import/export. 120
B.6 Step 3 of the interface: Analysis parameter. 121
B.7 Step 4 of the interface: Process information. 121
B.8 Step 5 of the interface: Results. 122

Resumen

En las últimas décadas, el avance en términos de capacidad computacional ofrece la posibilidad de analizar más detalladamente el comportamiento de los materiales. Por un lado, es posible caracterizar y analizar los materiales en una dimensión más pequeña y capturar micro o nanocambios. Por otro lado, la capacidad de memoria computacional permite realizar análisis numéricos, y en particular de elementos finitos, con miles de millones de nodos, lo que permite obtener resultados lo más exacto posible.

En este sentido, el objetivo de este trabajo es la modelización numérica del comportamiento a nivel micro de materiales no homogéneos, con especial atención a los materiales compuestos, en condiciones de carga termo-mecánica. Dado el elevado coste computacional de estos análisis, este trabajo propone la aplicación de herramientas de optimización de las leyes constitutivas a nivel macro y micro estructural.

La tesis se estructura como un compendio de artículos escritos durante los últimos años, todos ellos publicados en revistas internacionales situadas en el primer quartil (Q1).

En la primera publicación, se presenta un micro-modelo capaz de representar el comportamiento mecánico de las estructura de mampostería. El micro-modelo propuesto se basa en un modelo de daño continuo por tensión-compresión. La adopción de criterios de daño apropiados permite controlar la dilatancia del material, aspecto que no suele estar asociado a los modelos de daño contínuo, sino a modelos de plasticidad.

El estudio propone una solución simple a este problema, que consiste en la definición apropiada de las superficies de daño bajo estados de tensión de cortante, junto con la formulación de leyes de evolución apropiadas para las variables de daño. El modelo mantiene el formato simple y eficiente de los modelos de daños clásicos, donde la evaluación explícita de las variables internas evita los procedimientos iterativos anidados, aumentando así el rendimiento computacional. Otro objetivo

de esta investigación es realizar una comparación crítica del micro-modelo continuo propuesto con otras dos estrategias bien conocidas de micro-modelado discreto.

En la siguiente publicación se presenta una metodología termo-mecánica multiescala completa, que cubre las escalas nano, micro y macroscópica. En dicha metodología, derivada directamente del Método Multiescala de Primer Orden. En este trabajo las propiedades fundamentales del material se determinan mediante simulaciones de dinámica a nivel microestructural por medio de análisis de elementos finitos. Finalmente, el problema de macroescala se resuelve considerando el efecto de la microestructura mediante homogeneización termo-mecánica en un elemento de volumen representativo (RVE).

En la publicación que cierra esta tesis se proponen dos procedimientos multiescala computacionalmente eficientes capaces de predecir la respuesta mecánica no lineal de materiales compuestos. Esto se logrará mediante la construcción de una base de datos (DB) calculada a priori. A través de las definiciones de un parámetro de daño equivalente (d_{eq}), función de la tensión global en la microescala. La DB se construye a partir de la realización de una serie de pruebas virtuales en la microscala consistentes en aplicar una deformación y obtener la tensión homogenizada asociada, así como el nivel de daño equivalente d_{eq}. Posteriormente, el comportamiento de la estructura, a nivel macro, se se podrá obtener a partir de los resultados almacenados en la DB, sin ser necesaria la resolución del micro-modelo.

El primer método propuesto, llamado Discrete Multiscale Threshold Surface (DMTS), almacena en la DB únicamente el estado tenso-deformacional que conduce a la rotura del material. Una vez alcado este límite, el método requiere la simulación del RVE para obtener el comportamiento no-lineal. El segundo método, llamado Discrete Multiscale Constitutive Model (DMCM), es completamente independiente del micromodelo ya que en la DB se almacena, tanto el estado tenso-deformacional que conduce a la rotura del material, como la evolución del material a medida que éste daña. En el articulo se ha prestado especial atención a la creación y validación de la base de datos y al estudio de una estructura compuesta completa comparando la mejora, en terminos de coste computacional, obtenida con ambos métodos respecto al metodo multiescala de primer orden.

Abstract

In the last decades, the improvements in terms of computational power provides the capability to analyze with more detail the materials behavior. On one hand, going deeper in the materials to study an increasingly smaller dimension and capture micro- or nano- changes. On the other hand, the increasing computational memory allows to perform finite elements analysis with billions of nodes, that permits to obtain more accurate results.

In this sense, the focus of this work is the numerical modeling of the microscale behavior of inhomogeneous materials, with special attention to composite materials under thermo-mechanical loading conditions. This work also proposes and implements optimization tools, at a constitutive law level, as well as the level of both, macro- and micro-structural algorithms.

The thesis is proposed as compendium of articles written during the last years and all published in Q1 international journals.

In the first publication, a novel damage-mechanics micro-model is presented, able to represent the mechanical behaviors of masonry constituents. The proposed micro-model is based on a tension-compression continuum damage model. The adoption of appropriate failure criteria enables controlling the dilatant behavior of the material, even though this aspect is not generally associated to continuum damage models as it is for plasticity models.

The study proposes a simple solution to this issue, consisting in the appropriate definition of the failure surfaces under shear stress states, together with the formulation of proper evolution laws for damage variables. The model keeps the simple and efficient format of classical damage models, where the explicit evaluation of the internal variables avoids nested iterative procedures, thus increasing computational performance and robustness. Another purpose of this research is to carry out a critical comparison of the proposed continuous micro-model with other two well-known discrete micro-modeling strategies.

The second publication presents a full thermo-mechanical multiscale methodology, covering the nano-, micro-, and macroscopic scales. In such methodology, direcly deriving from the Classical First-Order Multiscale Method, fundamental material properties are determined by means of molecular dynamics simulations. Afterwards, the material properties obtained are used at the microstructural level by means of finite element analyses. Finally, the macroscale problem is solved while considering the effect of the microstructure using a thermo-mechanical homogenization on a representative volume element (RVE).

The publication that close this thesis presents two computationally efficient multiscale procedures able to predict the mechanical non-linear response of composite materials. This is achieved, using an RVE Data Base (DB) calculated a-priori. Through the definitions of an equivalent damage parameter (d_{eq}), function of the global stress at the microscale, a series of strain controlled virtual tests of the RVE are performed storing in the DB the homogenized stress and strain state reached at certain levels of d_{eq}. Afterwards, the solution of the macroscale structure can be solved using the interpolation of the stored data.

The first proposed procedure, named Discrete Multiscale Threshold Surface definition (DMTS), stores in the database the tenso-deformational state in which damage starts. Once reaching this state, a non-linear analysis will require the construction of the RVE to analyze the material damage evolution. On the other hand, the second method proposed, named Discrete Multiscale Constitutive Model (DMCM), is completely based on offline data and uses only the stress information stored in the DB to obtain the failure threshold and the non-linear material performance. In the article, special attention has been paid on the construction and validation of the Data Base, as well as on the study of a complete composite structure comparing the speedup obtained with both methods.

Chapter 1

Introduction

1.1 Motivation

Nowadays, numerous materials used in engineering industrial field, as well as in biological and biomedical area, are characterized by two or more constituents, also called phases.

Carbon fiber composites, polycrystalline structures, concrete, bone or wood are only some examples of components where the constituents could be distinguished at certain length scale. These materials are called inhomogeneous. The length scale as well as the type of constituents are only some example of possible criterion to classify them. Indeed, microstructure take an important rule during the analysis of the material because of the topology and the properties of each phase that determines its behavior.

It is also possible to say that defining a microscale structure means to study the behavior of each phase in order to determine the overall behavior of the global structure in terms of physical properties such as mechanical, thermal, electrical, etc.

Geometry, structure, properties and behavior of the inhomogeneous materials could be separated in two different fields depending on its length scale. On one hand, the microscale (or fine-scale) corresponds to the microstructure where each phase is distinguishable. On the other hand, the macroscale (or coarse-scale) is the largest scale (and length) of the model, in contrast to the microscale that represents the lowest scale.

The most important assumption that has to be made when studying the micromechanical models is the scale separation between micro and macro structures. That assumption allows to separate the contribution of the microscale, defined as fluctuation part, from the macroscale ones,

the constant part.

As it is explained in Bohm [9] these two contributions can be distinguished as fast and slow variables, where the fast variables, microscale fluctuations, can influence the behavior of the macroscale only through their volume average. Instead, the slow variables, the macroscale contribution, are not significant at the microscale level and can be considered as locally constant.

Otero et al. [72] and Petracca et al. [81], also provides an efficient multiscale strategy that, in case of FE2 homogenization, ensures the macro and micro mesh independence taking into account the conservation of the energy dissipation of through the scales.

1.2 Objective

During a finite element analysis, the material response of a structure is taken into account solving almost complex constitutive law for each integration point of the model.

In case of composite material, its constitutive behavior can be compared to the analysis of a complete structure but it is not always possible to use the classical constitutive laws formulations to model it. Therefore, the main objective of this work is the numerical modeling of the behavior of composite materials under mechanical and coupled thermo-mechanical loading conditions.

This objective is achieved by using a multi-scale strategy and implementing optimization tools at the constitutive law level as well as at the macro- and micro-structural scale algorithm. The two and three dimensional mechanical problems are the starting point for the development and implementation of this strategy in the in-house software Kratos-Multiphysics [20, 77].

An important aspect that characterizes the composite materials is the delamination process that can occur under different multiphysical conditions, i.e. severe thermal loading applications. One of the possible numerical implementation able to reproduce this phenomenon is the proposed cohesive interface element: a modified finite element with zero thickness that surrounds the composite constituent. In this work, in addition to the classical one, an extension to the displacement and pressure (U-P) formulation [13, 14, 15, 18] is provided for this element that gives a novel alternative to increase the numerical performance by using iterative solvers A.1.

Frequently, in particular in the engineering industrial field, multi-

scale analyses are not used due to its computational inefficiency. Therefore, with the aim to provide a faster and computationally efficient model, two novel optimization algorithms are developed and implemented. Furthermore, the validation of the optimized methodology is conducted by comparing the results obtained for a benchmark test with the results obtained using a first order multiscale homogenization.

1.3 Outline

The thesis is meant to be a compendium of articles published during last years that show the work conducted to achieve the objectives described in Section 1.2.

In the first part of the thesis the State of the Art is presented providing a background of the subjects studied in this work. Starting from a general overview of the multiscale homogenization methodology, the focus is addressed to the first-order homogenization method, with particular attention to the definition of the representative volume element and the description of a coupled thermo-mechanical multiscale analysis.

The final section of this document draws the conclusions of the work conducted, as well as the original contributions of the research done. It finalizes with a proposal for future works that can give continuity to this one.

Chapter 2

State Of The Art

2.1 Introduction

Physics and mechanics of the microstructure drive various phenomena that occur at the macroscopic level. Size, shape, overall spatial distribution and material properties of the constituents at the microscale level, as well as their respective interfaces, influence the behavior of the heterogeneous material.

Because of the interaction between the different constituent materials, associated to the usually complex composite internal microstructure (see Figure 2.1), the numerical simulation of these non-homogeneous materials has always represented a challenge.

The highest level of accuracy can be provided modelling each single component of the composite, also called Direct Numerical Simulation (DNS), but, at the same time, the simulation of large-scale structures implies a prohibitively expensive computational cost.

One of the simplest methods that aims at increasing the efficiency of these simulations are the phenomenological homogenization methods, where the non-homogeneous composite materials are often treated as homogeneous continua characterized by more complex constitutive models.

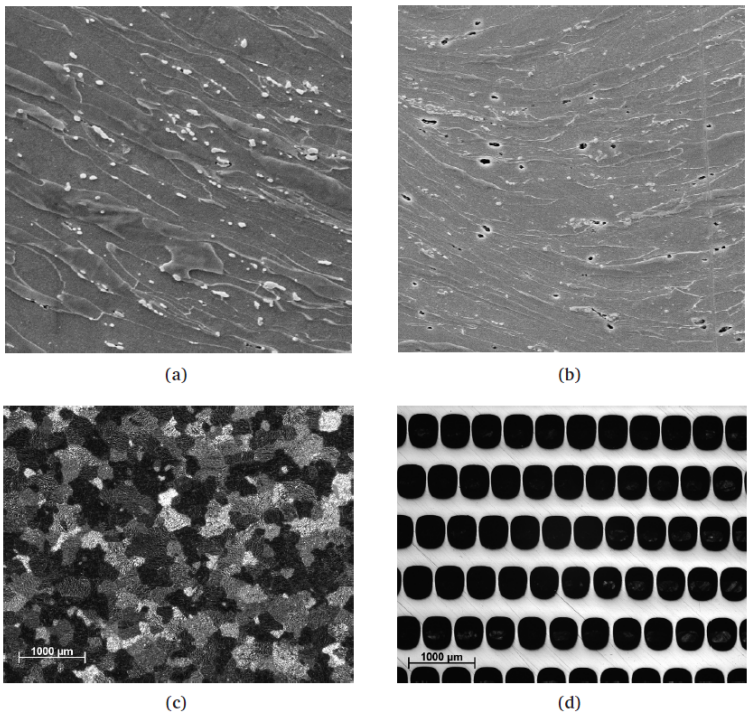

Figure 2.1: Examples of metallic heterogeneous microstructures: (a) SEM image of steel T67CA; the white spots are cementite particles; (b) SEM image of steel T61CA; voids are located around cementite particles; (c) light microscope image of an aluminum polycrystalline microstructure; (d) light microscope image of a shadow mask. [48]

In that field the most used phenomenological homogenization method is the classical rule of mixture [10]. Here, the mechanical behavior of the composite is obtained as the homogenized result of the mechanical properties of the components assuming an iso-strain compatibility equation among them.

As extension of the rule of mixture, Rastellini [85, 55] proposed the Serial/Parallel (SP) mixing theory, which can reproduce a more general topological distribution of the components in the composite. The serial-parallel mixing theory obtains the response of the material assuming iso-stress and iso-strain boundary conditions in the direction in which the fibre is oriented and in the orthogonal directions, respectively. The theory can be also used to characterize laminated composites.

However, phenomenological homogenization describes the behavior of composite materials only at macroscopic level and this method cannot describe accurately some of the complex interactions that can take place among the components specially when dealing with complex

micro-structures (i.e. woven composites).

For this reason, thanks to the increasing computer capabilities, the multiscale homogenization method starts to become a viable alternative. Indeed, this methods compute the stress-strain relationship at every point of interest at the macroscale level solving a Representative Volume Element (RVE) or unit cell, which is modelled as another independent structure. To apply this method, the scale separation from the macro and the microstructure [39] must be preserved.

The Representative Volume Element can be defined as a geometrical representation of the microstructure, subjected to the macroscopic deformation gradient. In this sense, the First-Order Multiscale Method [90, 94], or FE2, represents the classical multiscale homogenization method where the macroscopic behavior depends only on the first gradient of the displacement field.

As studied by [73, 75, 84, 68, 11] and others, complex RVE, with linear and non-linear behaviors, can be modelled with FE2 method but, of course, this methodology has a high computational cost since the microstructure shall be calculated for each integration point of the macroscale.

To address this problem, several model reductions were developed for the optimization of that type of analysis like Response Surface Models (RSM) [105], proper orthogonal decomposition (POD) [39] or others [72, 96].

In case of problems involving localized deformations, we can observe that generally the fracture only involves a very small area of the structure. This means that most of the material is still in the linear-elastic regime and does not require the RVE. In particular, a non-linear activation function was developed by Otero et al. [72] that is defined considering the maximum level of an elastic energy density that can be applied to the RVE before its failure. Despite the high computational gain provided by this procedure, with this method any changes at the macroscale level require the re-computation of the non-linear activation function even when using the same RVE.

Another approach that can be used to optimize the computational cost of multiscale analyses consist on just determining the failure threshold of the structure. In this case the full multiscale analysis is replaced by a linear calculation using the obtained mechanical homogenized properties of the RVE. Then, in a post-process analysis, the most critical RVE are studied, i.e. those with larger elastic stresses, subjecting them to the same loads of the macrostructure. The load step at which the RVE fails defines the maximum load that can be applied to the

macro-structure before material failure.

2.2 Multiscale Homogenization Methods

The fundamental goal of solid mechanics is to determine the best stress and strain relations that replicate the real behavior of the structures. These relations are represented by constitutive laws. Non-linear behavior of the materials needs increasingly complex formulations that frequently a single scale solution is not able to reproduce properly. In these cases, multiscale homogenized methods applied to the solid mechanics aims to study the behavior of the structures substituting the constitutive laws with a second level structure that replicates the micro material properties.

In this thesis a first-order computational homogenization strategy is used, which is essentially based on the derivation of the local macroscopic constitutive response from the lower scale through the correct construction and solution of a microstructural boundary value problem (BVP).

Even though, more complex behaviors were developed to describe the micromechanical models, when significant deformation in the critical regions of the structure are presents. In particular, two methods are worth to be mentioned: the second-order homogenization model [100] and the enhanced first order homogenization procedure [74].

In the second-order homogenization approach the macroscopic deformation and its gradient are imposed on a microstructural representative volume element where every microstructural constituent is modelled as a classical continuum. On the macrolevel, however, a full second gradient equilibrium problem appears. From the solution of the underlying microstructural boundary value problem, the macroscopic stress tensor and the higher-order stress tensor are derived based on an extension of the Hill-Mandel condition [40]. This automatically delivers the microstructurally based constitutive response of the second gradient macrocontinuum.

With the purpose to obtain the best of first-order and second-order methods, the enhanced-first-order computational homogenization preserves a classical BVP at the macro-scale level but taking into account the high-order gradient of the macro-scale in the micro-scale solution.

On one hand, the main advantage of high order homogenization methods is that they can be used in case of local intense deformation so it is preferable during non-linear analysis. On the other hand, the

complex finite element implementation, due to the intricacy mathematical formulation, compared to the first-order homogenization has reduced its dissemination.

2.3 First-order Computational Homogenization

The basic principles of the classical first-order computational homogenization can be explained by the four-step homogenization scheme proposed by Suquet [94]:

1. Definition of a microstructural representative volume element (RVE), of which the constitutive behaviour of individual constituents is assumed to be known.

2. Formulation of the microscopic boundary conditions from the macroscopic input variables and their application on the RVE (macro-to-micro transition).

3. Calculation of the macroscopic output variables from the analysis of the deformed microstructural RVE (micro-to-macro transition).

4. Obtain the (numerical) relation between the macroscopic input and output variables.

At the macrostructural level, the material configuration to be considered is assumed to be enough homogeneous, but microscopically heterogeneous. Indeed, the microscale morphology consists of several components as e.g. inclusions, grains, interfaces, cavities, as illustrated in Figure 2.2, and the phases of the microstructure can also be characterized by different non-linear constitutive models.

It should be emphasised that, in the context of the principle of separation of scales, the microscopic length scale should be much smaller than the characteristic size of the macroscopic structure or the wave length of the macroscopic loading [39]. Moreover, for every constituent, a continuum approach could be justified as solution strategy of the RVE Boundary Value Problem, even if the microscopic length scale is assumed to be much larger than the molecular dimensions.

As well as Suquet, Guedes and Kikuchi [36]; Terada and Kikuchi [99] and Ghosh et al. [31, 32] followed the main ideas of the first-order

computational homogenization divided into four-step scheme. Further developed and improved can be founded in more recent works such as [93, 62, 60, 61, 26, 97, 34, 47].

Among several advantageous characteristics of the computational homogenization technique the following are worth to be mentioned:

1. No explicit assumptions on the format of the macroscopic local constitutive response are compulsory at the macroscale, because the macroscopic constitutive behaviour is the result of the associated microscale BVP solution.

2. The macroscopic constitutive tangent operator comes from the microscopic stiffness matrix through static condensation.

3. Consistency is preserved through this scale transition.

4. The method fit with large strains and large rotations in a trivial way, if the microstructural constituent are properly modelled within a geometrically non-linear framework.

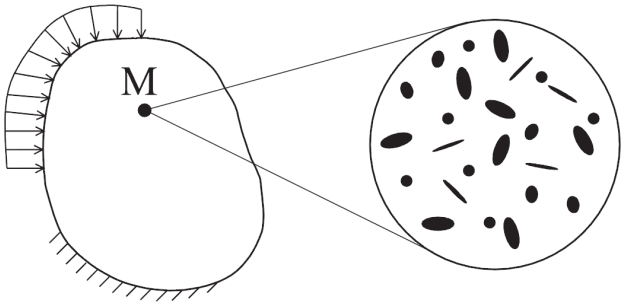

Figure 2.2: Continuum macrostructure and heterogeneous microstructure associated with the macroscopic point M. [48]

Most of the homogenization approaches make an assumption on global periodicity of the microstructure, suggesting that the whole macroscopic continuum consists of spatially repeated unit cells. In the computational homogenization approach a more realistic assumption on local periodicity is suggested. This is the microstructure can have different morphologies corresponding to different macroscopic points, while it repeats itself in a small vicinity of each individual macroscopic point. The concept of local and global periodicity is schematically illustrated in Figure 2.3.

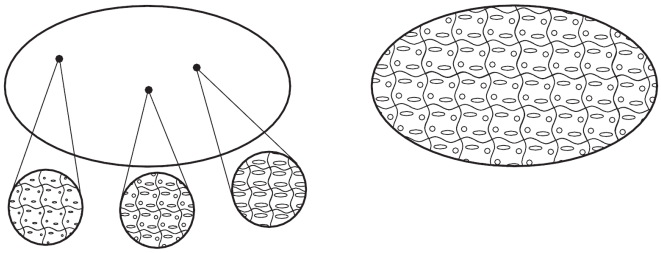

(a) local periodicity **(b)** global periodicity

Figure 2.3: Schematic representation of a macrostructure with (a) a locally and (b) a globally periodic microstructure. [48]

In the first-order computational homogenization procedure, the mechanical properties of the composite are defined by the relationship between the average values of the stresses and strains of the RVE. These average values correspond with the point value of the stress and strain in the macroscale; for this reason are defined as macro-stresses and macro-deformation.

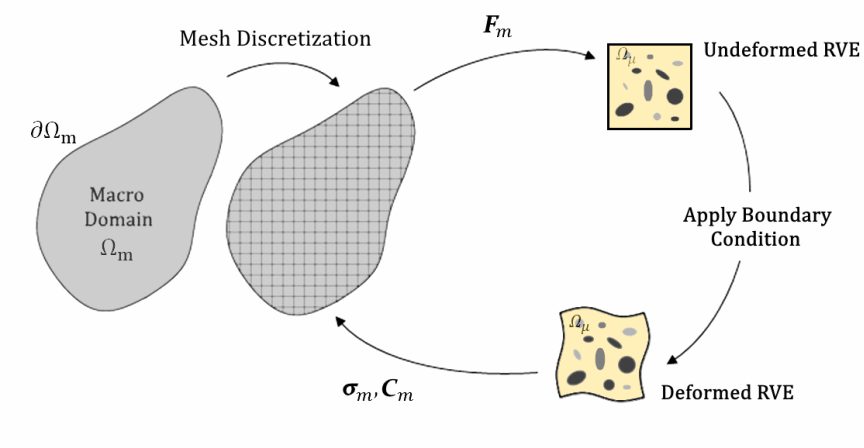

Figure 2.4: First-order computational homogenization scheme. σ_m is the macroscopic stress tensor and F_m is the macroscopic deformation (gradient) tensor

The procedure of homogenization consists of including an average deformation over the RVE with appropriate boundary conditions (BC) and in the calculation of the corresponding average tension.

2.3.1 Macro to micro transition

At the macro level, the starting point for a kinematically based computational homogenization method is the assumption that the mechanical strain tensor, $\boldsymbol{\varepsilon}_m$, at each point of the macroscale domain, Ω_m (where the position is defined through the vector $\boldsymbol{x}_m$), and at a certain instant t, can be obtained as the volume average of the microscopic mechanical strain field, $\boldsymbol{\varepsilon}_\mu$, defined at each point of the microscale domain, Ω_μ (where the position is defined through the vector $\boldsymbol{x}_\mu$), and at the same instant t as:

$$\boldsymbol{\varepsilon}_m(\boldsymbol{x}_m, t) = \frac{1}{V_\mu} \int_{\Omega_\mu} \boldsymbol{\varepsilon}_\mu(\boldsymbol{x}_\mu, t) dV \tag{2.1}$$

From the Eq. [2.1] the microscopic strain field can be expressed as the symmetric gradient of the microscopic displacement field, $\boldsymbol{u}_\mu = (u_\mu^x, u_\mu^y)$:

$$\boldsymbol{\varepsilon}_m(\boldsymbol{x}_m, t) = \frac{1}{V_\mu} \int_{\Omega_\mu} \nabla^s \boldsymbol{u}_\mu dV \tag{2.2}$$

Or using the Gauss theorem:

$$\boldsymbol{\varepsilon}_m(\boldsymbol{x}_m, t) = \frac{1}{V_\mu} \int_{\partial\Omega_\mu} \boldsymbol{u}_\mu \otimes_s \boldsymbol{n} dA \tag{2.3}$$

Where $\boldsymbol{n}$ is the outward unit normal field on the RVE boundary $\delta\Omega_\mu$.

Without loss of generality, we can decompose the microscale displacement as:

$$\boldsymbol{u}_\mu(\boldsymbol{x}_\mu, t) = \boldsymbol{\varepsilon}_m(\boldsymbol{x}_m, t) \cdot (\boldsymbol{x}_\mu - \boldsymbol{x}_g) + \tilde{\boldsymbol{u}}_\mu(\boldsymbol{x}_\mu, t) \tag{2.4}$$

where $\boldsymbol{u}_\mu(\boldsymbol{x}_\mu, t)$ and $\tilde{\boldsymbol{u}}_\mu$ are respectively the constant and fluctuation displacements with respect to the average fields $\boldsymbol{x}_g$ (the centroid of the microscale) at each instant t.

In the same way the microscopic strain can be divided in two parts, a constant one from the macroscopic scale ($\boldsymbol{\varepsilon}_m$) and the contribution of fluctuation ($\tilde{\boldsymbol{\varepsilon}}\mu$).

$$\boldsymbol{\varepsilon}_\mu(\boldsymbol{x}_\mu, t) = \boldsymbol{\varepsilon}_m(\boldsymbol{x}_m, t) + \tilde{\boldsymbol{\varepsilon}}_\mu(\boldsymbol{x}_\mu, t) \tag{2.5}$$

2.3.2 Micro to macro transition

Following the solution of the BVP [40] we get the homogenized macroscopic stress tensor. In addition, we can obtain the homogenized constitutive tensor. The homogenized macroscopic stress tensor can be obtained as the microscopic stress field of the RVE averaged on the volume as [39, 23, 43]

$$\boldsymbol{\sigma}_m = \frac{1}{V_\mu} \int_{\Omega_\mu} \boldsymbol{\sigma}_\mu(\boldsymbol{x}_\mu, t) dV \tag{2.6}$$

2.3.3 Material homogenized properties

The macroscopic constitutive relation defined by the homogenized properties of the RVE can be obtained after the solution of the microscale BVP. Assuming the equilibrium of the microscale expressed as:

$$\int_{\Omega_\mu} \boldsymbol{\sigma}_\mu(\boldsymbol{x}_\mu, t) : \nabla^s \tilde{\boldsymbol{u}}_\mu dV = 0 \tag{2.7}$$

As is described in [33] and [72], the homogenized constitutive tensor $\boldsymbol{C}^H$ can be defined as:

$$\boldsymbol{C}^H = \frac{1}{V_\mu} \int_{\Omega_\mu} \boldsymbol{C}_\mu dV \tag{2.8}$$

where $\boldsymbol{C}_\mu$ is the material constitutive tensor of the RVE.

Among several techniques, one of the most frequently used that provide the linear elastic constitutive law of the composite imply a numerical differentiation. In this work the evaluation of the homogenized constitutive tensor is performed with a perturbation method, also see [75, 72]. For each column j of the constitutive tensor, a small strain perturbation ($\delta\tilde{\varepsilon}_j$) is applied to the RVE in order to obtain, along with Eq. [2.7], a perturbed stress tensor ($\delta\tilde{\sigma}_j$). The j columns of the homogenized constitutive tensor can be obtained as:

$$\boldsymbol{C}^H \equiv \frac{\delta\tilde{\sigma}_j}{\delta\tilde{\varepsilon}_j} \tag{2.9}$$

2.3.4 Representative Volume Element Definition

The computational homogenization approach, as well as most of other homogenization techniques, is based on the concept of a representative

volume element (RVE). An RVE is a model of a material microstructure useful to obtain the response of the corresponding homogenized macroscopic continuum in a macroscopic integration point. Indeed, the accuracy of the model of an heterogeneous material is directly determined by the right choice of the RVE. As explained by Drugan and Willis [24] there are two significantly different ways to define a RVE. The first definition requires an RVE to be a statistically representative sample of the microstructure. Therefore, in the case of a non-regular and non-uniform microstructure, this definition drives to a considerably large RVE.

Another definition characterizes an RVE as the smallest microstructural volume that almost accurately represents the overall macroscopic properties of interest. This usually leads to much smaller RVE sizes than the statistical definition described above. However, in this case the minimum required RVE size also depends on the type of material behaviour, macroscopic loading path and difference of properties between heterogeneities.

This definition of an RVE is closely related to the one established by Hill [40], who described the RVE as a structure satisfying at the same time two conditions:

- The RVE must reflect the material microstructure.
- The responses under uniform different boundary conditions must coincide.

Essentially, if a microstructural cell does not contain sufficient microstructural information, its overall responses depends on the boundary conditions used. This strictly correlation between RVE dimension and BC is crucial when an homogenized multiscale method is used.

Indeed, as illustrated in Figure 2.5, for small size of the RVE, the displacement, periodic and traction boundary condition differs from the effective value of homogenized properties. These properties, also called "apparent" [41], obtained by application of uniform displacement boundary conditions on a microstructural cell, usually overestimate the real effective behavior of the material, while the uniform traction boundary conditions lead to underestimation. On the other hand, a better evaluation can be obtained by increasing the size of the microstructural cell producing a "convergence" of the result, as it is shown by [41, 42, 69, 70, 78, 98].

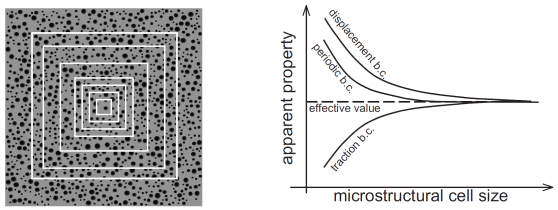

Figure 2.5: (a) Several microstructural cells of different sizes. (b) Convergence of the apparent properties [41] to the effective values with increasing microstructural cell size for different types of boundary conditions.[48]

The most common boundary condition conditions that fulfill the requirements of a first-order multiscale homogenization method can be summarized as follow:

- Taylor model (or zero fluctuations): $\tilde{\boldsymbol{u}}_\mu(\boldsymbol{x}_\mu, t) = 0 \ \forall \ \boldsymbol{x}_\mu \in \Omega_\mu$ This model gives homogeneous deformation in the microstructural scale level.

- Linear boundary displacements (or zero boundary fluctuations): $\tilde{\boldsymbol{u}}_\mu(\boldsymbol{x}_\mu, t) = 0 \ \forall \ \boldsymbol{x}_\mu \in \partial\Omega_\mu$. The deformation of the RVE boundary domain for this class are fully prescribed.

- Periodic boundary fluctuations: $\tilde{\boldsymbol{u}}_\mu(\boldsymbol{x}_\mu^+, t) = \tilde{\boldsymbol{u}}_\mu(\boldsymbol{x}_\mu^-, t) \ \forall \ pair\{\boldsymbol{x}_\mu^+, \boldsymbol{x}_\mu^-\} \in \partial\Omega_\mu$

- Minimal constraint (or uniform boundary traction): In this constraint the nontrivial solution of $\int_{\partial\Omega_\mu} \boldsymbol{u}_\mu \otimes_s \boldsymbol{n} dA$ is obtained.

Figure 2.6 shows two of the most frequently used boundary conditions.

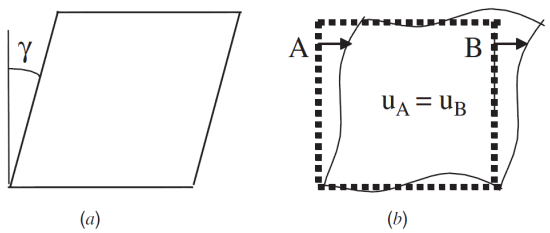

Figure 2.6: Common boundary conditions for shear of a RVE. (a) Rigid boundary conditions. (b) Periodic boundary conditions. [54]

As has been verified by a number of authors [102, 98, 46, 45, 44, 71, 72], for a given microstructural cell size, the periodic boundary conditions provide a better estimation of the overall properties, than the uniform displacement and uniform traction boundary conditions. Moreover, as described by Terada et al. [98] this BC can also be used even if the microstructure does not really has geometrical periodicity.

2.4 Thermo dynamic approach of Multi-scale Analysis

2.4.1 Introduction

An high number of engineering structures can present premature failure of components due to severe thermal loading conditions that can appear as thermal shocks or temperature cycles. This operating temperature variation of a material is frequently accompanied by physical and geometrical changes of the structure. In case of heterogeneous materials, under such thermal loading conditions, the resulting temperature distribution can lead to a complex microscopic mechanical response and a non-uniform degradation of the mechanical and physical properties, generally followed by irreversible geometrical changes at the macroscale level. Furthermore, microstructural changes can produce a critical interaction between the mechanical and thermal fields, i.e. reducing the heat transfer across a damaged interface. Due to the aforementioned problems, the thermo-mechanical analysis of heterogeneous materials represents a challenging task.

Several homogenization techniques have been developed to predict the effective mechanical and thermal properties of materials with complex microstructures. During the '60 and '70, Hashin [37] and [87] starts with the first study of the thermo-mechanical behavior on heterogeneous materials, using simple geometries and a restricted class of constitutive models. More recent homogenization approaches were developed for the determination of the mechanical and thermal constitutive tensors of composites with a periodic microstructure, such as [107].

Starting from the aformentioned methods described in Section 2.3, the use of computational techniques within the homogenization theory has received particular attention including applications to other field problems [103, 19, 35, 30]. Recently the efforts are directed to extend the theory and solution algorithms to the non-linear and inelastic range

[64, 27, 28], and other [108, 7, 51, 109].

As in case of pure mechanical loads, among other, a second-order thermal homogenization method with higher-order fluxes was proposed. Temizer and Wriggers [95] used this approach to capture the size effects when RVE size is not sufficiently small compared to a representative macrostructural length scale.

2.4.2 Multiscale thermo-mechanical formulation

The standard FEM procedure for mechanical problems usually starts with the definition of the strong form of the problem. In classical mechanics, equilibrium, compatibility and constitutive relationships are the three ingredients needed to obtain a solution. We want to consider the mechanical description for the static case in frameworks of linear elasticity and small displacements. The equilibrium of a body $\mathcal{B}$ subjected to body forces f is given by

$$\nabla \cdot \sigma(\varepsilon) + f = 0 \; in \; \Omega \tag{2.10}$$

where σ is the Cauchy's stress. For the kinematic aspect of the problem, small displacements means that the final configuration of the body can be approximated by the initial configuration. Then it is possible to relate displacements and strain in the following way:

$$\varepsilon = \nabla^S \boldsymbol{u} \tag{2.11}$$

ε is the strain tensor whereas $\nabla^S \cdot (\cdot)$ is the symmetric part of the gradient operator

$$\nabla^S(\cdot) = \frac{1}{2}[\nabla(\cdot) + \nabla^T(\cdot)] \tag{2.12}$$

Finally, to close the system of equations one can write the constitutive equation. In a linear elastic problem it will read:

$$\sigma = \mathbb{C} : \varepsilon \tag{2.13}$$

Now consider an isotropic body with temperature-dependent heat transfer. A basic equation of heat transfer has the following form:

$$\nabla \cdot q(T) = \mathcal{Q}_{ext} \tag{2.14}$$

Where,

$$\nabla \cdot q(T) = (\frac{\partial q_x}{\partial x} + \frac{\partial q_y}{\partial y} + \frac{\partial q_z}{\partial z}) \tag{2.15}$$

Here, q_x, q_y and q_z are components of heat flow through the unit area; $\mathcal{Q} = \mathcal{Q}(x, y, z)$ is the inner heat-generation rate per unit volume and T is the temperature. According to Fourier's law the components of heat flow can be expressed as follows:

$$q_x = -\mathbf{k}\frac{\partial T}{\partial x},\ q_y = -\mathbf{k}\frac{\partial T}{\partial y},\ q_z = -\mathbf{k}\frac{\partial T}{\partial z} \tag{2.16}$$

where $\mathbf{k}$ is the conductivity tensor of the media, in general symmetric and positive-definite, in a isotropic medium we can assume $\mathbf{k} = \alpha\mathbb{I}$ where $\mathbb{I}$ is the identity tensor. From 2.16 we obtain

$$q = -\mathbf{k}\nabla T \tag{2.17}$$

Coupling the mechanical and thermal problems for the homogenization multi scale analysis we assume

$$\nabla \cdot \sigma(\varepsilon, T) = f,\ \ \nabla \cdot q(T) = \mathcal{Q}_{ext} \tag{2.18}$$

The object of the proposed method is to calculate, at the micro level, an equivalent stress produced by the heat transfer and add this contribution to the mechanical stress as follow (linear case)

$$\sigma = \mathbb{C} : (\varepsilon_M + \varepsilon_T) = \mathbb{C} : \varepsilon_M + \sigma(\varepsilon_T) \tag{2.19}$$

In the same way of the mechanical homogenization, where we determine $(\sigma, \mathbb{C})$ at the micro level, in the thermo mechanical problem we add two more variables $(q, \mathbf{k})$.

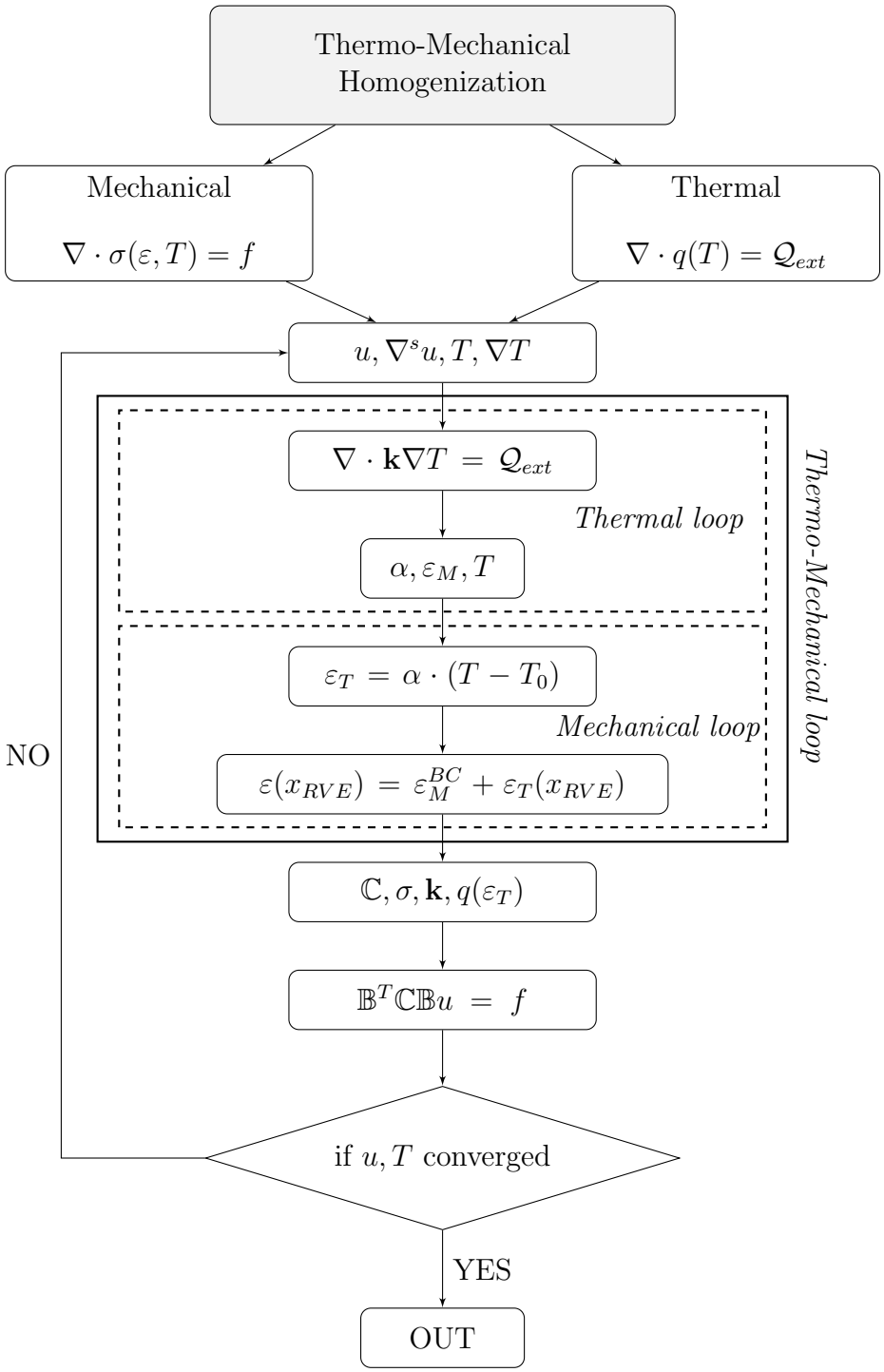
Thermo-Mechanical Homogenization
Mechanical
$\nabla \cdot \sigma(\varepsilon, T) = f$
Thermal
$\nabla \cdot q(T) = \mathcal{Q}_{ext}$
$u, \nabla^s u, T, \nabla T$
$\nabla \cdot \mathbf{k}\nabla T = \mathcal{Q}_{ext}$
Thermal loop
α, ε_M, T
$\varepsilon_T = \alpha \cdot (T - T_0)$
Mechanical loop
$\varepsilon(x_{RVE}) = \varepsilon_M^{BC} + \varepsilon_T(x_{RVE})$
Thermo-Mechanical loop
NO
$\mathbb{C}, \sigma, \mathbf{k}, q(\varepsilon_T)$
$\mathbb{B}^T\mathbb{C}\mathbb{B}u = f$
if u, T converged
YES
OUT

Chapter 3

Multiscale implementation of multiphysical effects in composite materials

3.1 Introduction

The work conducted is reflected in the papers published by the author, and described in this chapter. In fact, the first subject treated during this study is the application of the first-order multiscale method to a real application, as it is the case of masonry structure described in the first paper. This work was followed by the development of multiscale thermo-mechanical framework to improve the capability of the model and to analyze the material behavior of composites such as the multilayered coated receiver tubes illustrated in the paper number two. Finally, it was investigated an optimization algorithm of the first-order multiscale homogenization method in order to improve the performance of the finite element analysis in terms of time and memory consumed. This can be found in the third paper, where the aforementioned developed optimization technique are applied to a reinforced composite structure. In the following are described the most relevant achievements obtained in the aforementioned papers.

3.2 Micro-scale continuous and discrete numerical models for nonlinear analysis of masonry shear walls

In the paper number one it is proposed a novel damage-mechanics based micro-model able to represent the nonlinear response of masonry constituents, especially under shear stress states. The mentioned approach includes a control on the amount of dilatancy of the material, notwithstanding this aspect is not generally taken into account by standard continuum damage models. An existing failure criterion for quasi-brittle materials has been improved under shear conditions, and a novel hardening softening law based on quadratic Bezier curves has been established in order to obtain the control of the dilatant behavior of the material.

The paper presents a comparison of the developed continuous micromodeling technique, with the well-known discrete micro-modeling strategies for the 2D analysis of in-plane loaded masonry structures. The selected modeling strategies to represent the micro-structure of masonry material are reported in Figure 3.1. In the first numerical strategy, both bricks and mortar joints are treated inelastically using the proposed damage model. The other two strategies consist on modeling bricks with continuum elements and mortar joints with interface elements. Bricks are treated either elastically with potential vertical cracks in the middle vertical section, or inelastically.

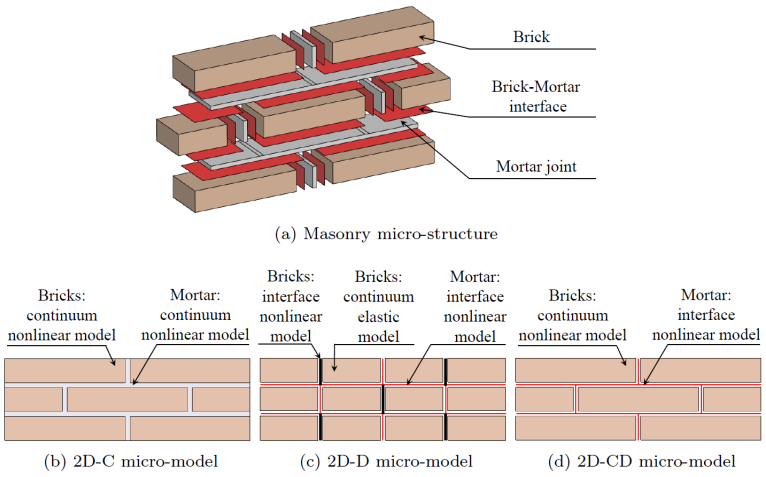

Figure 3.1: Masonry micro-structure with nonlinear interface model. [82]

Even though all the investigated strategies can describe the behavior of shear walls up to their collapse, some differences have been found with higher compressive levels. Indeed, during this loading condition, the 2D-D and 2D-CD micro-models overestimate the maximum shear strength of the wall, whereas the 2D-C micro-model slightly underestimates it in a conservative way.

The main advantages obtained by the proposed continuous micro-model with a continuum description of both bricks and mortar joints are: (i) simple and efficient format inherited from classical damage mechanics models; (ii) increased computational performance and robustness, due to the explicit evaluation of the internal variables that avoids nested iterative procedures; (iii) simple generation of the finite element model during pre-processing; (iv) straightforward interpretation of the results during post-processing.

Moreover, the proposed model can overcome the recurrent disadvantage of standard continuum damage models, for example their poor capability of representing the dilatant behavior of mortar joints under shear stress states.

3.3 Multiscale thermo-mechanical analysis of multi-layered coatings in solar thermal applications

In the second paper a hierarchical multiscale and multiphysical methodology for the analysis of composite materials is presented. This strategy is used to simulate the performance of the receiver tubes with multi-layered coatings that are used in concentrating solar plants.

This methodology provides the possibility to take into account thermo-mechanical simulations that are crucial in this type of plants. Moreover, three different scales are covered via numerical simulations, through an intermediate microscopic analysis of absorber layers, going from the atomistic to the macroscale structural analysis.

Considering the atomistic simulations, an MD methodology has been successfully adopted in order to analyze the material properties of single phases present in nanoabsorbers. In this sense, original results for amorphous carbon have been derived, especially for the elastic constants and the CTE.

At the microscale, an RVE-based thermo-mechanical homogenization scheme has been used. Taking into account both the mechanical and the heat transfer problem, being able to provide homogenized mechanical and thermal properties of the microcomposite. Moreover, it has been validated through experimental results and it has been finally applied to a relevant problem in CSP plants. To conduct this simulation it has been implemented a cohesive zone model to account for the interface between the composite constituents. This model allows accounting for the variation of the thermo-mechanical properties of the composite in case of interface failure.

Finally, a first order multiscale problem (FE2), covering the both micro and macro scales has been conducted, allowing the identification of critical zones in specific layers of solar selective coatings.

In Figure 3.2 it is possible to appreciate the damage distribution along the matrix and internally to the cohesive element; in addition it is also reported the corresponded heat flux and temperature redistribution after the particle-matrix debonding.

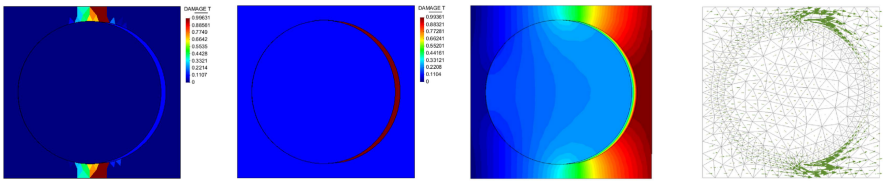

(a) (b) (c) (d)

Figure 3.2: Particle-matrix debonding issues in the nano-absorber: a) matrix damage, b) cohesive damage, c) redistribution of temperature gradient field, and d) change in the heat flux. [63]

This type of homogenization method can entirely explain both linear and non-linear behavior of complex microstructures, and the impact they have on the macroscale response.

3.4 Adaptive and Off-Line Techniques for Non-Linear Multiscale Analysis

The simulations presented in previous research have shown the computational cost required to analyze large structures with multiscale methods. To overcome this problem, in last years many methods have been

proposed aiming to reduce this cost. With this same objective, the last paper presented in this work proposes two techniques that can provide a significant speed-up compared to the classical FE2 without loss of accuracy on the final results.

By conducting a priori finite element analysis of the RVE, the DMTS procedure calculates the linear elastic threshold that leads to composite failure. Once this is achieved, it is necessary to solve the RVE in that given material point to obtain the non-linear material behaviour.

The second method proposed, the Discrete Multiscale Constitutive Model (DMCM) results as a natural extension of the DMTS. With this procedure, during the initial analysis of the RVE, it is computed not only the threshold surface in which the non-linear behavior starts, but also the surfaces associated to different damage values. Aftwerards, the non-linear multiscale anaysis can be realized using only the values stored in the database, without solving the RVE at any time.

The keys of both methods are the precomputed Stress-Strain Data Base and the equivalent damage parameter d_{eq}, essential to reconstruct the correct behavior of the structure. Moreover, the JSON format used to construct the database turns all the data more readable, faster and easier to manage.

A fracture-energy-based regularization procedure is also suggested in order to remove the dependence of the results on macro and micro-scale mesh size. Thanks to the proposed regularization, the Stress-Strain Data Base becomes independent from the macro-scale mesh discretization.

In the paper both DMTS and DMCM methods are validated with a simple benchmark analysis and with a more complex analysis of a reinforced composite beam, showing the capability and robustness of these techniques. The achieved speed-up of more than 600 times respect to FE2 and the accuracy of the results, justifies the time spent to obtain the Stress-Strain Data Base.

In Figure 3.3 it is shown an example of the obtained threshold surface evolution for a carbon-epoxy composite microstructure.

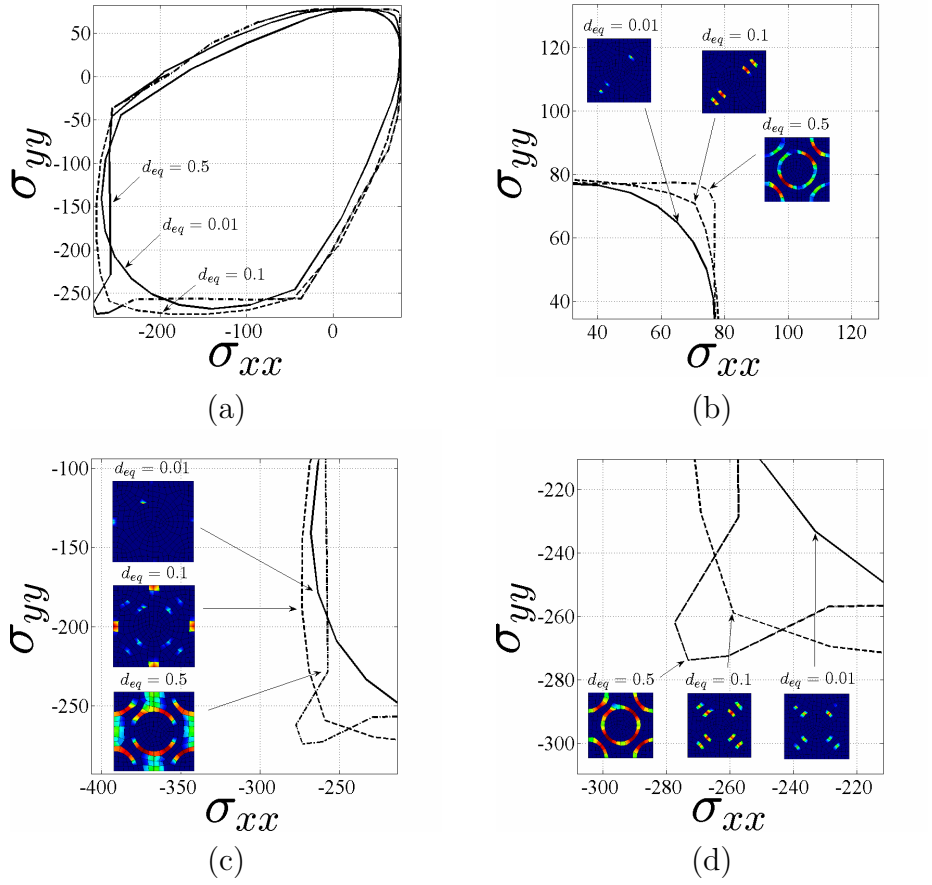

Figure 3.3: Composite Stress Evolution Surfaces. [106]

Contributed Pubblications

	Name	Journal	Quartil Index in JCR	Impact Factor
Paper 1	Micro-scale continuous and discrete numerical models for nonlinear analysis of masonry shear walls	Construction and Building Materials	Q1	3.485
Paper 2	Multiscale thermo-mechanical analysis of multi-layered coatings in solar thermal applications	Finite Elements in Analysis and Design	Q1	2.253
Paper 3	Adaptive and Off-Line Techniques for Non-Linear Multiscale Analysis	Composite Structures	Q1	4.101

Paper 1

Massimo Petracca, Luca Pelà, Riccardo Rossi, Stefano Zaghi, Guido Camata, Enrico Spacone. Micro-scale continuous and discrete numerical models for nonlinear analysis of masonry shear walls, Construction and Building Materials - 2017, Volume 149, Pages 296-314

Abstract A novel damage mechanics-based continuous micro-model for the analysis of masonry-walls is presented and compared with other two well-known discrete micro-models. The discrete micro-models discretize masonry micro-structure with nonlinear interfaces for mortar-joints, and continuum elements for units. The proposed continuous micro-model discretizes both units and mortar-joints with continuum elements, making use of a tension/compression damage model, here refined to properly reproduce the nonlinear response under shear and to control the dilatancy. The three investigated models are validated

against experimental results. They all prove to be similarly effective, with the proposed model being less time-consuming, due to the efficient format of the damage model. Critical issues for these types of micro-models are analysed carefully, such as the accuracy in predicting the failure load and collapse mechanism, the computational efficiency and the level of approximation given by a 2D plane-stress assumption.

Paper 2

F. Montero-Chacón, S. Zaghi, R. Rossi, E. García-Pérez, I. Heras-Pérez, X. Martínez, S. Oller, M. Doblaré. Multiscale thermo-mechanical analysis of multi-layered coatings in solar thermal applications, Finite Elements in Analysis and Design - 2017, Volume 127, Pages 31-43

Abstract Solar selective coatings can be multi-layered materials that optimize the solar absorption while reducing thermal radiation losses, granting the material long-term stability. These layers are deposited on structural materials (e.g., stainless steel, Inconel) in order to enhance the optical and thermal properties of the heat transfer system. However, interesting questions regarding their mechanical stability arise when operating at high temperatures. In this work, a full thermo-mechanical multiscale methodology is presented, covering the nano-, micro-, and macroscopic scales. In such methodology, fundamental material properties are determined by means of molecular dynamics simulations that are consequently implemented at the microstructural level by means of finite element analyses. On the other hand, the macroscale problem is solved while taking into account the effect of the microstructure via thermo-mechanical homogenization on a representative volume element (RVE). The methodology presented herein has been successfully implemented in a reference problem in concentrating solar power plants, namely the characterization of a carbon-based nanocomposite and the obtained results are in agreement with the expected theoretical values, demonstrating that it is now possible to apply successfully the concepts behind Integrated Computational Materials Engineering to design new coatings for complex realistic thermo-mechanical applications.

Paper 3

Stefano Zaghi, Xavier Martinez, Riccardo Rossi, Massimo Petracca. Adaptive and Off-Line Techniques for Non-Linear Multiscale Analysis,

Composite Structures - 2018, Volume 206, Pages 215-233

Abstract This paper presents two procedures, based on the numerical multiscale theory, developed to predict the mechanical non-linear response of composite materials under monotonically increasing loads. Such procedures are designed with the objective of reducing the computational cost required in these types of analysis. Starting from virtual tests of the microscale, the solution of the macroscale structure via Classical First-Order Multiscale Method will be replaced by an interpolation of a discrete number of homogenized surfaces previously calculated. These surfaces describe the stress evolution of the microscale at fixed levels of an equivalent damage parameter (d_{eq}). The information required for these surfaces to conduct the analysis is stored in a Data Base using a json format. Of the two methods developed, the first one uses the pre-computed homogenized surface just to obtain the material non-linear threshold, and generates a Representative Volume Element (RVE) once the material point goes into the nonlinear range; the second method is completely off-line and is capable of describing the material linear and non-linear behavior just by using the discrete homogenized surfaces stored in the Data Base. After describing the two procedures developed, this manuscript provides two examples to validate the capabilities of the proposed methods.

Chapter 4

Papers

Micro-scale continuous and discrete numerical models for nonlinear analysis of masonry shear walls

Massimo Petracca[a,b,c,*], Luca Pelà[a,b], Riccardo Rossi[a,b], Stefano Zaghi[a,b], Guido Camata[c], Enrico Spacone[c]

[a] *Department of Civil and Environmental Engineering, Universitat Politècnica de Catalunya (UPC-BarcelonaTech), Barcelona 08034, Spain*
[b] *CIMNE - Centre Internacional de Metodes Numerics en Enginyeria, Universitat Politècnica de Catalunya (UPC-BarcelonaTech), Barcelona 08034, Spain*
[c] *Department of Engineering, University "G.d'Annunzio" of Chieti and Pescara, Pescara 65127, Italy*

Abstract

A novel damage mechanics-based continuous micro-model for the analysis of masonry-walls is presented and compared with other two well-known discrete micro-models. The discrete micro-models discretize masonry micro-structure with nonlinear interfaces for mortar-joints, and continuum elements for units. The proposed continuous micro-model discretizes both units and mortar-joints with continuum elements, making use of a tension/compression damage model, here refined to properly reproduce the nonlinear response under shear and to control the dilatancy. The three investigated models are validated against experimental results. They all prove to be similarly effective, with the proposed model being less time-consuming, due to the efficient format of the damage model. Critical issues for these types of micro-models are analysed carefully, such as the accuracy in predicting the failure load and collapse mechanism, the computational efficiency and the level of approximation given by a 2D plane-stress assumption.

Keywords: Masonry, Continuous micro-modeling, Discrete micro-modeling, Continuum damage model, Interface model, Dilatancy

1. Introduction

Masonry is a composite material, with a micro-structure consisting of bricks and joints, with or without mortar. These micro-structural constituents, their very different elastic and inelastic properties, and their arrangement lead to very complex behaviors and different failure mechanisms. Several computational strategies were proposed to deal with the numerical analysis of such a complex material [1]. Several macro-models, also known as continuum finite element models, are available in the existing literature to study

*corresponding author
Email addresses: mpetracca@cimne.upc.edu (Massimo Petracca), luca.pela@upc.edu (Luca Pelà), rrossi@cimne.upc.edu (Riccardo Rossi), zstefano@cimne.upc.edu (Stefano Zaghi), g.camata@unich.it (Guido Camata), espacone@unich.it (Enrico Spacone)

masonry structures. The most recent macro-models regard the material as a fictitious homogeneous orthotropic continuum, without making any explicit distinction between units and joints in the discrete model [2, 3, 4]. This approach presents some intrinsic difficulties mainly related to the identification of the mechanical parameters of the continuum and the definition of realistic phenomenological failure criteria. However, macro-models are still a suitable option for the numerical analysis of large and complex structures due to their limited computational cost. More sophisticated numerical strategies were proposed by several authors for detailed analysis of single structural members, where a full description of the interaction between units and mortar is necessary (Figure 1a). Very popular approaches used nowadays to study masonry, including its heterogeneous micro-structure in the discretization, are based on micro-modeling [5, 6, 7, 8]. Midway between macro- and micro-modeling there are the homogenization methods [9, 10, 11, 12, 13, 14, 15, 16, 17, 18, 19].

A complete and detailed description of masonry micro-structure would require the full three-dimensional discretization of bricks, mortar joints, and the interface between them. In this way all masonry constituents and their complex interaction would be explicitly accounted for. However, three-dimensional modeling requires a complex model generation and high computational costs. For the case of a wall made of one layer of bricks with a regular pattern, the 2D plane stress assumption can be made to simplify the problem. This however can lead to imprecise results when the wall is subjected to high levels of compressions, since the state of triaxial compression in the mortar joints cannot be represented with the plane-stress assumption. A more accurate solution can be the adoption of generalized plane state [20, 21].

The objective of this paper is to propose a novel damage-mechanics based continuous micro-model able to represent the mechanical behaviors of masonry constituents. The proposed micro-model is based on a tension-compression continuum damage model [22, 23, 24], here refined in order to accurately reproduce the nonlinear response of masonry constituents, especially in shear. The adoption of appropriate failure criteria enables the analyst to control the dilatant behavior of the material, even though this aspect is not generally associated to continuum damage models as it is for plasticity models. The study proposes a simple solution to this issue, consisting in the appropriate definition of the failure surfaces under shear stress states together with the formulation of proper evolution laws for damage variables. For this aim, a failure criterion for quasi-brittle materials [25] is suitably enhanced under shear conditions and a novel hardening-softening law based on quadratic Bézier curves is established. The model keeps the simple and efficient format of classical damage models, where the explicit evaluation of the internal variables avoids nested iterative procedures, thus increasing computational performance and robustness.

Another purpose of this research is to carry out a critical comparison of the proposed continuous micro-model with other two well-known discrete micro-modeling strategies for the numerical simulation of shear walls made of periodic masonry. The three micro-models explicitly take into account the interaction between units and mortar joints by including their separate discretizations. The main distinction made here between continuous and discrete micro-models is referred to the different type of elements and constitutive models used for the discretization of masonry micro-structure. Discrete micro-modeling has been widely adopted by several authors in literature [5, 7, 26, 27, 28, 29, 30] using a discrete description of masonry micro-structure, mixing continuum and interface elements for bricks and mortar joints, respectively. On the contrary, the proposed contin-

uous micro-modeling uses a continuum discretization of all components of the masonry micro-structure, without resorting to interface elements.
The investigated approaches are validated against experimental tests of masonry shear walls under different level of vertical compression [31], proving to be similarly effective and accurate in predicting the global strength of shear walls up to their collapse. All three micro-modeling techniques are able to properly reproduce the main failure mechanisms of the material, such as tensile cracking, sliding, shear and crushing. However, each one of the selected models introduces different approximations that lead to slight differences in accuracy, robustness and computational cost. The validation of the novel continuous micro-model, together with the critical review of available discrete micro-models, leads to a fruitful discussion on advanced computational strategies for the analysis of masonry structures at the level of material constituents.

2. Adopted modeling strategies

The three selected modeling strategies to represent the micro-structure of masonry material (see Figure 1a) are:

1. **2D Continuous micro-model (2D-C)**: Both units and mortar joints are modeled using 2D plane-stress continuum elements with nonlinear behavior (see Figure 1b). This paper presents a novel formulation for this approach at the level of the constitutive law.
2. **2D Discrete micro-model (2D-D)**: All non-linearity is lumped into interface elements. Both horizontal and vertical mortar joints are discretized by this type of elements. Units are composed of 2D continuum elastic elements and vertical interfaces at their mid-length for potential splitting cracks (see Figure 1c).
3. **2D Mixed Continuous/Discrete micro-model (2D-CD):** The mortar joints (vertical and horizontal) are represented by nonlinear interface elements, whereas the units are modeled with 2D plane-stress continuum elements with nonlinear behavior, to avoid forcing the crack pattern inside the units, differently from 2D-D approach (see Figure 1d).

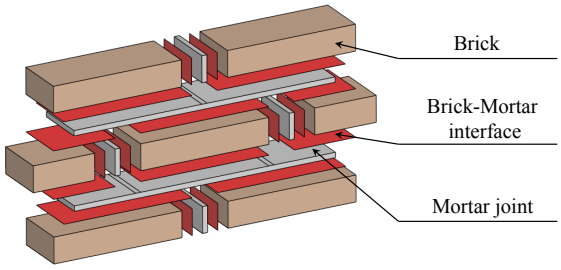

(a) Masonry micro-structure

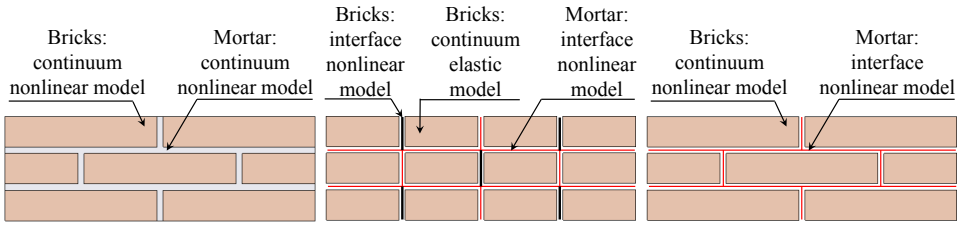

(b) 2D-C micro-model (c) 2D-D micro-model (d) 2D-CD micro-model

Figure 1: Masonry modeling strategies

The aforementioned 2D-D and 2D-CD micro-modeling strategies for masonry structures are very well-known and they have been used by several authors in the available literature [5, 7, 26, 27, 28, 29, 30]. In the present comparative study, the adopted constitutive model for the interfaces is the one presented in [5]. The 2D-D and 2D-CD strategies are also known as "simplified micro-models", while "detailed micro-models" would consider a distinct discretization for units and mortar (by means of continuum finite elements) and unit-mortar interface (by means of interface elements).

On the other hand, the proposed 2D-C micro-modeling strategy considers a more classical approach, discretizing both bricks and mortar joints with continuum elements. In this context, and to propose an efficient and robust numerical method, a constitutive law based on continuum damage mechanics is adopted, taking advantage of its explicit evaluation, thus avoiding local iterative procedures typically necessary to integrate plasticity-based models. In particular, the d^+/d^- tension-compression damage framework [22, 23, 24] has been used. This model introduces two failure criteria for tensile and compressive stress states, as well as two scalar damage indexes, allowing the description of different behaviors under tension and compression. A novel failure criterion for compression is presented in Section 3.2 to be combined with a novel hardening-softening law based on quadratic Bézier curves (Section 3.3). Section 4 describes how this criterion can be used to control the dilatant behavior of the damage model.

In the following, Section 3 describes the continuum damage model here proposed, and used for both bricks and mortar joints in the modeling strategy 2D-C, and for bricks in the modeling strategy 2D-CD, while Section 5 describes the constitutive model used for mortar interfaces in the modeling strategies 2D-D and 2D-CD.

Note that the modeling strategy 2D-CD features both a plasticity-based model (in mortar joints), and a damage-based one (in bricks). The choice of a damage model for bricks stems from the brittle nature of bricks failure mechanism. In fact, in in-plane loaded shear walls, the main failure mechanism that can be expected at the brick level is a brittle tensile split, which can be accurately represented by a damage model.

3. Proposed Tension/Compression Continuum Damage Model

3.1. Constitutive Model

The 2-parameter d^+/d^- damage model, based on the works in [22, 23, 24], defines the stress tensor as

$$\boldsymbol{\sigma} = \left(1 - d^+\right) \bar{\boldsymbol{\sigma}}^+ + \left(1 - d^-\right) \bar{\boldsymbol{\sigma}}^- \tag{1}$$

where $\bar{\boldsymbol{\sigma}}$ is the effective (elastic) stress tensor

$$\bar{\boldsymbol{\sigma}} = \boldsymbol{C} : \boldsymbol{\varepsilon} \tag{2}$$

while $\bar{\boldsymbol{\sigma}}^+$and $\bar{\boldsymbol{\sigma}}^-$are, respectively, its positive and negative components, computed as:

$$\bar{\boldsymbol{\sigma}}^+ = \sum_{i=1}^{3} \langle \bar{\sigma}_i \rangle \, \boldsymbol{p}_i \otimes \boldsymbol{p}_i \tag{3}$$

$$\bar{\boldsymbol{\sigma}}^- = \bar{\boldsymbol{\sigma}} - \bar{\boldsymbol{\sigma}}^+ \tag{4}$$

d^+ and d^- are tensile and compressive damage indexes, affecting, respectively, the positive $\bar{\boldsymbol{\sigma}}^+$ and negative $\bar{\boldsymbol{\sigma}}^-$ components of the effective stress $\bar{\boldsymbol{\sigma}}$. These damage indexes are scalar variables ranging from 0 (intact material) to 1 (completely damaged material).

3.2. Failure Criteria

Two scalar measures, referred to as equivalent stresses τ^+ and τ^-, are introduced to properly identify "loading", "unloading" or "reloading" conditions.

The compressive surface employed in this research represents an improvement of the one described in [25]. The equivalent stress τ^- is computed as

$$\tau^- = \frac{1}{1-\alpha} \left(\alpha \bar{I}_1 + \sqrt{3\bar{J}_2} + k_1 \beta \left\langle \bar{\sigma}_{max} \right\rangle \right) \tag{5}$$

$$\alpha = \frac{k_b - 1}{2k_b - 1} \tag{6}$$

$$\beta = \frac{f_{cp}}{f_t} (1 - \alpha) - (1 + \alpha) \tag{7}$$

where $\bar{I}_1$ is the first invariant of the effective stress tensor, $\bar{J}_2$ is the second invariant of the effective deviatoric stress tensor, $\bar{\sigma}_{max}$ is the maximum effective principal stress, f_{cp} is the compressive peak stress and k_b is the ratio of the bi-axial strength to the uniaxial strength in compression. The constant k_1 in Eq. (5) is proposed in this research to control the influence that the compressive criterion has on the dilatant behavior of the model, as described in Section 4. k_1 ranges from 0 to 1. A value of 0 leads to the Drucker-Prager criterion, while a value of 1 leads to the criterion presented in [25]), as shown in Figure 2.

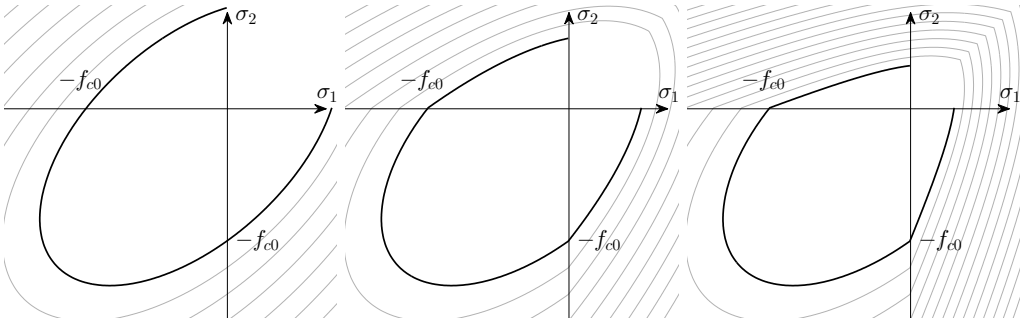

(a) $k_1 = 0$ (b) $k_1 = 0.16$ (c) $k_1 = 0.5$

Figure 2: Proposed compressive failure surface for the continuum model. Influence of the parameter k_1

The tensile surface is similar to the compressive one

$$\tau^+ = \frac{1}{1-\alpha}\left(\alpha\bar{I}_1 + \sqrt{3\bar{J}_2} + \beta\left\langle\bar{\sigma}_{max}\right\rangle\right)\frac{f_t}{f_{cp}} \tag{8}$$

but without the k_1 parameter. Here the term $\frac{f_t}{f_{cp}}$ is introduced to compare τ^+ with the uniaxial tensile strength f_t. Figure 3 shows the two initial damage surfaces, for the plane-stress case, superimposed in the principal stress space. The negative surface τ^- is represented for various values of the constant k_1. Being the two surfaces defined for any state of stress, it may happen that negative damage evolves under uniaxial or biaxial tension and vice-versa for the tensile damage. This can be avoided inactivating the tensile and compressive criteria under conditions, so that (i) the compressive surface can evolve if and only if at least one of the principal stresses is negative, and (ii) the tensile surface can evolve if and only if at least one the principal stresses is positive.
These conditions can be taken into account by rewriting the damage surfaces as:

$$\tau^- = H\left(-\bar{\sigma}_{min}\right)\left[\frac{1}{1-\alpha}\left(\alpha\bar{I}_1 + \sqrt{3\bar{J}_2} + k_1\beta\left\langle\bar{\sigma}_{max}\right\rangle\right)\right] \tag{9}$$

$$\tau^+ = H\left(\bar{\sigma}_{max}\right)\left[\frac{1}{1-\alpha}\left(\alpha\bar{I}_1 + \sqrt{3\bar{J}_2} + \beta\left\langle\bar{\sigma}_{max}\right\rangle\right)\frac{f_t}{f_{cp}}\right] \tag{10}$$

where $H\left(x\right)$ is the Heaviside function, defined as

$$H\left(x\right) = \begin{cases} 0 & x < 0 \\ 1 & x > 0 \end{cases} \tag{11}$$

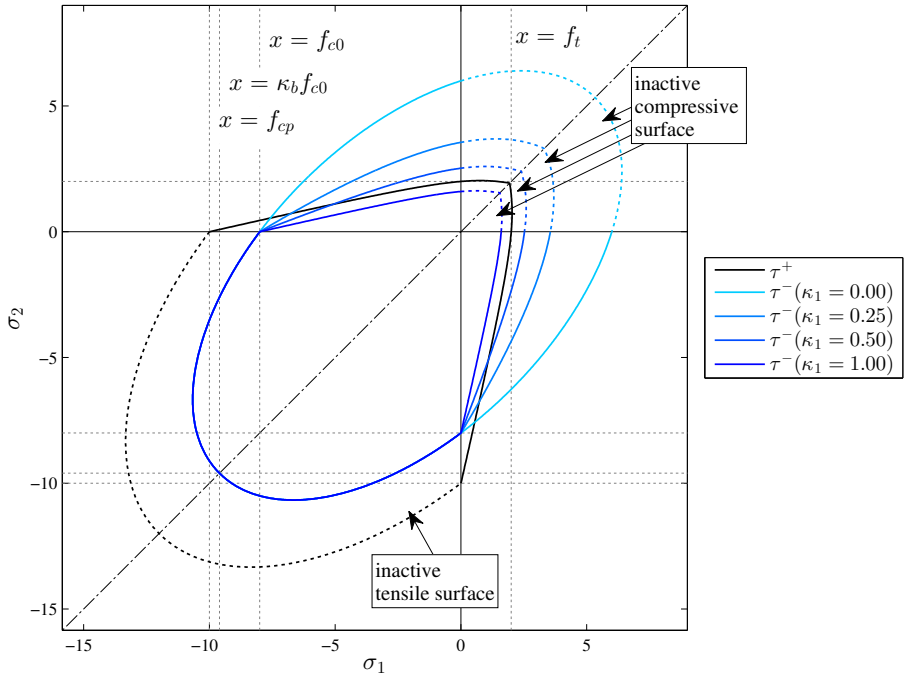

Figure 3: Initial damage surfaces for the plane-stress case.

To account for the irreversible nature of damage, two scalar quantities are used, referred to as damage thresholds $r^{\pm}$. The thresholds $r^{\pm}$ denote the largest values attained by the equivalent stresses $\tau^{\pm}$ throughout the whole loading history up to the current time instant. $r^{\pm}$ at time $t + \Delta t$ are explicitly evaluated as

$$r^{\pm} = max\left(r_0^{\pm}, \max_{0 \le n \le t} \tau_n^{\pm}\right)$$

$$r_0^{+} = f_t \tag{12}$$

$$r_0^{-} = f_{c0} \tag{13}$$

with r_0^{+} and r_0^{-} being the initial damage thresholds, i.e. the elastic limits in uniaxial tension f_t and uniaxial compression f_{c0}. n denotes the time instant. With $\tau^{\pm}$ and $r^{\pm}$ at hand, the damage criteria can be defined as:

$$\Phi\left(\tau^{\pm}, r^{\pm}\right) = \tau^{\pm} - r^{\pm} \le 0 \tag{14}$$

3.3. Evolution laws for damage variables

The tensile (positive) damage d^+ is obtained from the following exponential softening law (see Figure 4):

$$d^+\left(r^+\right) = 1 - \frac{r_0^+}{r^+} exp\left\{2H_{dis}\left(\frac{r_0^+ - r^+}{r_0^+}\right)\right\} \tag{15}$$

where H_{dis} is the discrete softening parameter. In the discrete problem, in order to achieve invariance of the response with respect to the discretization size, the softening law must be modified according to the size of the damaging zone (l_{dis}) [32, 33, 34], so that the following equation holds:

$$g_f\, l_{dis} = G_f \tag{16}$$

where G_f is the fracture energy per unit area in tension. The specific fracture energy g_f per unit volume, for the exponential softening law, is obtained as:

$$g_f = \left(1 + \frac{1}{H_{dis}}\right)\frac{f_t^2}{2E} \tag{17}$$

The discrete softening parameter H_{dis} is given by

$$H_{dis} = \frac{l_{dis}}{l_{mat} - l_{dis}} \tag{18}$$

where $l_{mat} = 2EG_f/f_t^2$. l_{dis} is taken equal to the characteristic size of the finite element ($l_{dis} = l_{ch}$).

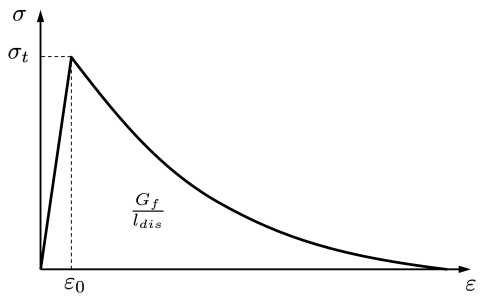

Figure 4: Tensile uniaxial law

The evolution of the compressive damage index d^-, instead, is governed by an ad hoc uniaxial law proposed in this paper, as shown in Figure 5.

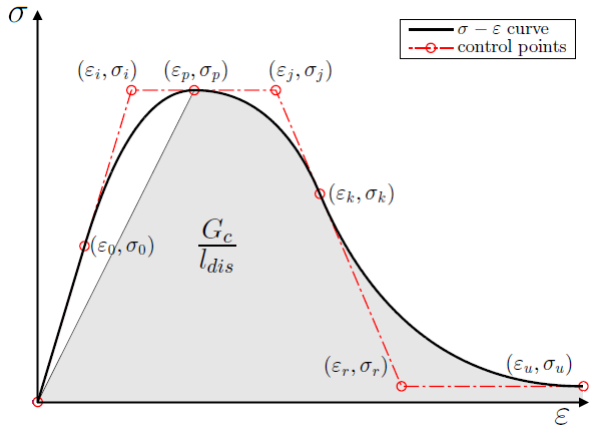

Figure 5: Compressive uniaxial law

This curve is made of a linear part $[(0,0)-(\varepsilon_0,\sigma_0)]$, a hardening part $[(\varepsilon_0,\sigma_0)-(\varepsilon_p,\sigma_p)]$ and two softening parts $[(\varepsilon_p,\sigma_p)-(\varepsilon_k,\sigma_k)]\,[(\varepsilon_k,\sigma_k)-(\varepsilon_u,\sigma_u)]$, followed by a final residual plateau $[(\varepsilon_u,\sigma_u)-(+\infty,\sigma_u)]$.
The hardening and softening portions are three quadratic Bézier curves. Each one of them has three control points that define their shape, the end-positions, and the tangents to the curve at the end-positions.
We can define a function $\mathscr{B}$ that evaluates the Y-coordinate of a Bézier curve at a given X-abscissa, given the three control points, as follows:

$$\mathscr{B}\left(X,\ x_1,x_2,x_3,\ y_1,y_2,y_3\right) = \left(y_1-2y_2+y_3\right)t^2 + 2\left(y_2-y_1\right)t + y_1 \tag{19}$$

where

$$\begin{aligned} A &= x_1 - 2x_2 + x_3 \\ B &= 2\left(x_2 - x_1\right) \\ C &= x_1 - X \\ D &= B^2 - 4AC \\ t &= \frac{-B+\sqrt{D}}{2A} \end{aligned}$$

Given the current compressive damage threshold r^-, its strain-like counterpart ξ can be obtained

$$\xi = \frac{r^-}{E} \tag{20}$$

and then it is used to calculate the corresponding hardening variable $\Sigma\left(\xi\right)$:

$$\Sigma\left(\xi\right)=\begin{cases}\mathscr{B}\left(\xi,\ \varepsilon_0,\varepsilon_i,\varepsilon_p,\ \sigma_0,\sigma_i,\sigma_p\right) & \varepsilon_0<\xi\leq\varepsilon_p\\ \mathscr{B}\left(\xi,\ \varepsilon_p,\varepsilon_j,\varepsilon_k,\ \sigma_p,\sigma_j,\sigma_k\right) & \varepsilon_p<\xi\leq\varepsilon_k\\ \mathscr{B}\left(\xi,\ \varepsilon_k,\varepsilon_r,\varepsilon_u,\ \sigma_k,\sigma_r,\sigma_u\right) & \varepsilon_k<\xi\leq\varepsilon_u\\ \sigma_u & \xi>\varepsilon_u\end{cases}\tag{21}$$

Finally the damage index d^- can be calculated as follows:

$$d^-\left(r^-\right)=1-\frac{\Sigma\left(\xi\right)}{r^-}\tag{22}$$

This novel formulation for the evolution law of the compressive damage parameter d^- is more flexible than conventional ones. In fact, the control points of the Bézier curves may be set so that the curve can match the experimental response obtained from an uniaxial compressive test. Then the compressive fracture energy G_c (shaded area in Figure 5) is evaluated with the following relations:

$$G_{c,1}=\frac{\sigma_p\varepsilon_p}{2}\tag{23}$$

$$G_{c,2}=\mathscr{G}\left(\varepsilon_p,\varepsilon_j,\varepsilon_k,\ \sigma_p,\sigma_j,\sigma_k\right)\tag{24}$$

$$G_{c,3}=\mathscr{G}\left(\varepsilon_k,\varepsilon_r,\varepsilon_u,\ \sigma_k,\sigma_r,\sigma_u\right)\tag{25}$$

$$G_c=G_{c,1}+G_{c,2}+G_{c,3}\tag{26}$$

where the area $\mathscr{G}$ under each Bézier curve reads:

$$\mathscr{G}\left(x_1,x_2,x_3,\ y_1,y_2,y_3\right)=\frac{x_2y_1}{3}+\frac{x_3y_1}{6}-\frac{x_2y_3}{3}+\frac{x_3y_2}{3}+\frac{x_3y_3}{2}-x_1\left(\frac{y_1}{2}+\frac{y_2}{3}+\frac{y_3}{6}\right)\tag{27}$$

It should be noted that here G_c is not the total area under the uniaxial curve, but only the portion that needs to be regularized (post-peak regime).
In the discrete problem the compressive curve shown in Figure 5 needs to be regularized so that the shaded area underneath be G_c/l_{dis}. This can be achieved by *"stretching"* the strain abscissas ε_j, ε_k, ε_r and ε_u (before using them in Eq. (21)):

$$\tilde{\varepsilon}_\alpha=\varepsilon_\alpha+\mathcal{S}\left(\varepsilon_\alpha-\varepsilon_p\right),\qquad\alpha=j,k,r,u\tag{28}$$

where $\mathcal{S}$ is a stretching factor calculated as

$$\mathcal{S}=\frac{\dfrac{G_c}{l_{dis}}-G_{c,1}}{G_c-G_{c,1}}-1\tag{29}$$

This factor should be greater than -1.0 to avoid a constitutive snap-back. In fact for a stretch factor $\mathcal{S}=-1.0$ every post-peak strain-abscissa would collapse to the peak strain ε_p, leading to a sudden fall of the uniaxial curve. To avoid this, the characteristic length l_{dis} should satisfy the following restriction:

$$l_{dis} < \frac{2G_c}{\sigma_p \varepsilon_p} \tag{30}$$

The effect of this regularization on the uniaxial law can be seen in Figure 6.

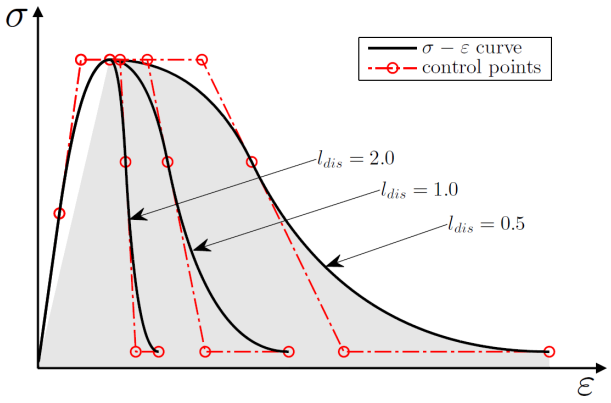

Figure 6: Regularization of compressive uniaxial law

4. Shear behavior and dilatancy of the Tension/Compression Continuum Damage Model

This section describes the shear behavior of the proposed d^+/d^- damage model. The present formulation includes the possibility to calibrate the dilatant behavior of the material under shear stresses. This crucial aspect has been usually disregarded by available models based on classical damage mechanics theory. Such disadvantage has often favored the use of plasticity models since they can control explicitly the dilatancy through the definition of a proper plastic potential. This work proposes an improvement of the well-known d^+/d^- damage model [22, 23, 24] to control the dilatant behavior of the material. The material dilatancy is described without resorting to the formulation of a plastic potential, i.e. differently from well-established plasticity models (e.g. Eq. (36)). The objective of the proposed approach is to describe phenomenologically the dilatant behavior without spoiling the simple and efficient format of the classical damage mechanics models.

4.1. Shear response of the Tension/Compression Damage Model

The models adopted in this paper are based on the 2D plane stress hypothesis. In this specific case, and in the framework of the d^+/d^- damage model, when the two principal stresses have different sign, both tensile and compressive surfaces might be active. In this case the positive principal stress is affected by the tensile damage while the minimum principal stress is affected by the compressive damage. If the damage was isotropic, i.e. the tension and compression damage variables are equal, the damaged stress tensor would

be an isotropic scaling of the effective (elastic) stress tensor. On the other hand, in the d^+/d^- damage model the damaged stress tensor is actually obtained by an anisotropic scaling of the effective (elastic) stress tensor, as it was already demonstrated in [2].
Figure 7 graphically shows this behavior for the simple case of a pure shear distortion, in an isotropic damage model (Figure 7a) and d^+/d^- damage model (Figure 7b). Let us suppose that the material point is subject to a given strain state whose components are ($\varepsilon_{xx} = 0$, $\varepsilon_{yy} = 0$, $\gamma_{xy} \neq 0$). Point A represents the effective stress state $\bar{\boldsymbol{\sigma}} = \boldsymbol{C} : \boldsymbol{\varepsilon}$ due to pure shear, with coordinates $(\bar{\sigma}_1, \bar{\sigma}_2 = -\bar{\sigma}_1)$ in the principal stresses reference system. Point B represents the damaged stress state $\boldsymbol{\sigma}$ denoted by coordinates $(\sigma_1, \sigma_2 = -\sigma_1)$ obtained in the case of an isotropic damage model, i.e. if $d^+ = d^-$. In this case the damaged stress tensor is an isotropic scaling of the effective stress tensor, since the isotropic scalar damage index scales the whole effective stress tensor $\bar{\boldsymbol{\sigma}}$. Consequently the damaged stress would stay in a pure shear state as the effective stress (Figure 7a). Point C, instead, corresponds to the damaged stress $\boldsymbol{\sigma}$ obtained by the d^+/d^-damage model. In this case, due to the existence of two different failure surfaces, the tensile and compressive damage indexes do not have in general the same value, being their evolution laws different. Consequently the damaged stress is not an isotropic scaling of the effective stress. In the specific example depicted in Figure 7b, the compressive damage increment is smaller then the tensile one. Thus, due to the preassigned null values for ε_{xx} and ε_{yy}, the damaged stress $\boldsymbol{\sigma}$ must denote a shear-compression state.
In the compressive damage surface in Eq. (5), the parameter k_1 is introduced to control the "weight" of the compressive surface on the constitutive shear response in the nonlinear range. As shown in Figure 2, the parameter k_1 controls the size of the compressive surface in tension/compression quadrants. As a consequence, this parameter controls implicitly also the dilatancy of the model, taking into account that the larger the compressive surface (with respect to the tensile surface), the higher the dilatancy. This effect is shown in Figure 8 for decreasing values of k_1, moving from Figure 8a to Figure 8c. It can be seen how decreasing k_1 from 1 to 0, the size of the compressive surface in the tension/compression quadrants increases. As a consequence, the increment of the compressive damage index d^- diminishes, thus predicting increasing compressive stresses.

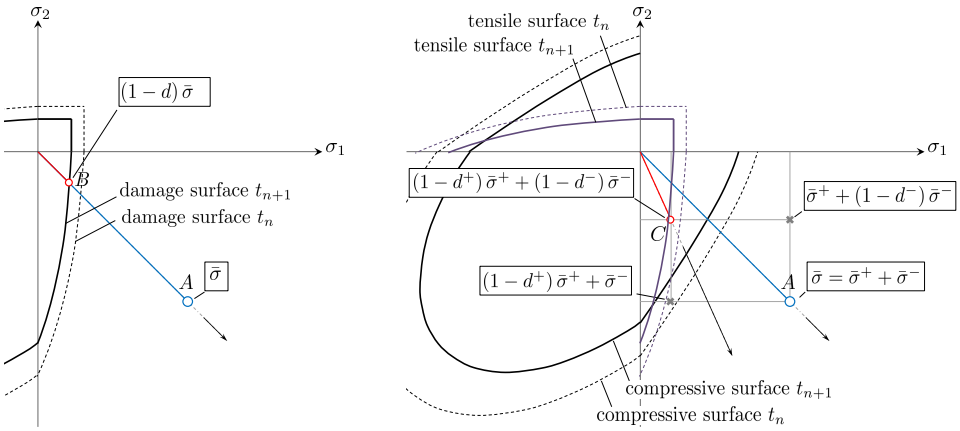

(a) Isotropic damage (b) d^+/d^- damage

Figure 7: Behavior of isotropic and d^+/d^- damage models in tension/compression quadrants

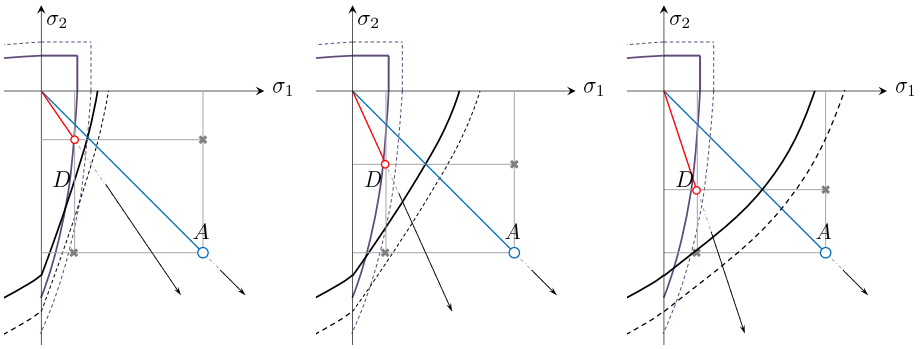

(a) (b) (c)

Figure 8: Behavior of d^+/d^- damage model in tension/compression quadrants for values of k_1 decreasing from (a) to (c)

4.2. Numerical modeling of shear behavior of mortar joints

To assess the performance of the proposed constitutive model in shear, the experimental shear tests conducted in [35] are numerically reproduced here. Figure 9a shows the test set-up. These tests aim at producing a constant stress state in the mortar joint. Mortar joints are subjected to shear under a constant confining stress.

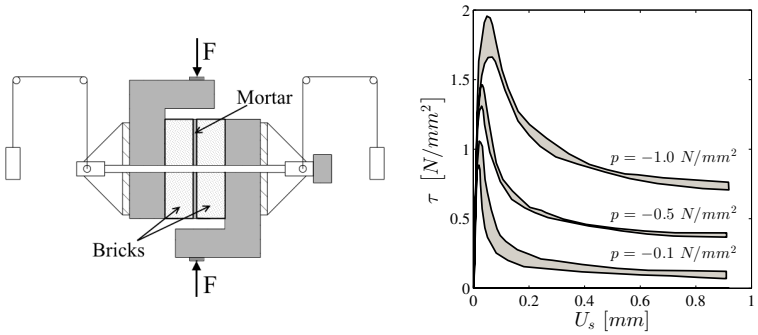

(a) (b)

Figure 9: Van Der Pluijm (1993). (a) test set-up; (b) test results for different values of confinement

The experimental tests were conducted with three different confining stress levels of -0.1, -0.5 and $-1.0\,N/mm^2$. Experimental results are given in Figure 9b in terms of envelope curves of shear stress τ vs. shear displacement U_s along the mortar joint. It can be seen how the maximum shear stress increases with increasing confining stress. After reaching a peak value, the shear stress decreases with increasing shear displacement, reaching a residual value due to dry friction. Another important aspect of this kind of experiment is the dilatancy of the mortar joint (Figure 10a), which describes the appearance (in the nonlinear range) of normal displacement perpendicular to the shear displacement. The ratio between the normal and shear displacements is denoted as the tangent to the dilatancy angle ψ. This behavior is related to the roughness of the crack surface. Experimental results show how dilatancy decreases with increasing normal stresses, as shown in Figure 10b. In the same way, for a constant normal stress, the dilatancy decreases to zero upon increasing shear displacement, as shown in Figure 10c.

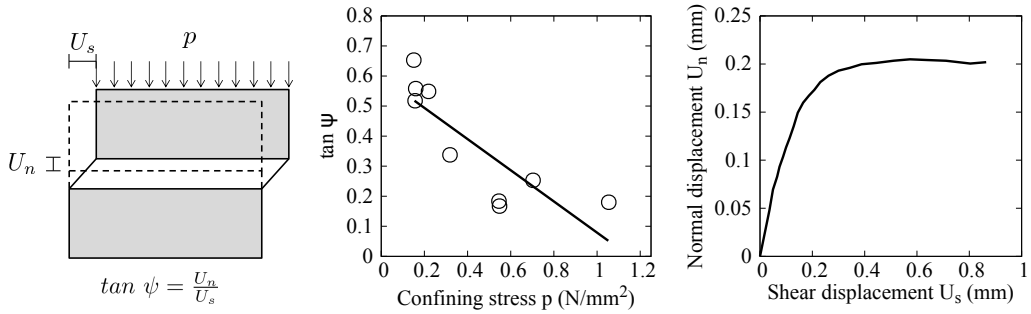

(a) (b) (c)

Figure 10: Van Der Pluijm (1993). (a) dilatancy of mortar joints; (b) dilatancy $tan\,\psi$ as a function of confining stress; (c) typical evolution of normal displacement for increasing values of shear displacement. Adapted from [6].

To study the control of the dilatancy in the proposed model, an elemental test has been performed. The geometry and boundary conditions are shown in Figure 11. Material parameters, obtained from [35], are given in Table 1. For each level of confining stress ($p = -0.1$, $p = -0.5$, and $p = -1.0\, N/mm^2$) two analyses have been conducted, using $k_1 = 0$, and $k_1 = 0.16$. The value $k_1 = 0.16$ has been found as optimal for these tests as well as for the shear walls analyzed in Section 6.

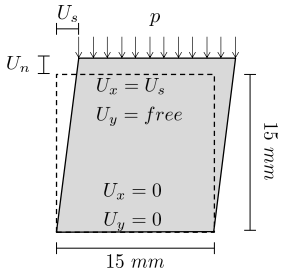

Figure 11: Elemental shear test. Geometry and boundary conditions

E	ν	σ_t	G_t	σ_0	σ_p	σ_r	G_c	ε_p	k_b
2970.0	0.15	0.62	0.02	8.0	11.0	1.0	20.0	0.005	1.16
$\frac{N}{mm^2}$	-	$\frac{N}{mm^2}$	$\frac{N}{mm}$	$\frac{N}{mm^2}$	$\frac{N}{mm^2}$	$\frac{N}{mm^2}$	$\frac{N}{mm}$	-	-

Table 1: Mortar material properties for the shear tests

Results of the analyses are given in Table 2 in terms of shear strength and dilatancy, for each level of pre-compression. The first column show the shear stress - shear displacement curves, with the shear strength increasing for higher values of pre-compression. The second column show the uplift (positive vertical displacement) generated upon shear displacement. Finally the third column shows the dilatancy coefficient (which is the tangent to the curves reported in the second column). It can be clearly seen that if the standard Drucker-Prager failure surface ($k_1 = 0$) is chosen for compression, an overestimation of the dilatant behavior (with respect to the values shown in Figure 10b and Figure 10c) is obtained.
Overall, these analyses show how the size of the compressive surface in the tension/compression quadrants has a major impact on the dilatancy of the model. As explained in the introduction of this section, the d^+/d^- damage model as proposed in [22, 23, 24] does not explicitly impose the direction of the inelastic strain, as opposed to plastic models. This elemental test has shown how a careful definition of the compressive damage surface, and

especially of its shape in the II and IV quadrants of the principal (plane)stress space, can help in controlling the dilatant behavior in the proposed continuum damage model. It can be noticed, however, that for higher levels of vertical compression, the maximum shear strength is slightly underestimated (see Table 2, case p=-1 N/mm2). The same effect will be found in the results of the analysis of the shear walls given in Section 6.2. This slight underestimation may be due to the limitations given by plane-stress assumption. In fact, for high levels of compression, the plane-stress hypothesis is not able to represents the triaxial compression state in the mortar bed joint given by its interaction with the surrounding units.

$\tau - U_s$	$U_n - U_s$	$tan\,\psi - U_s$
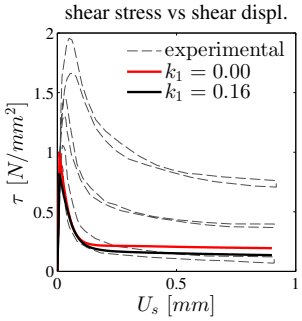	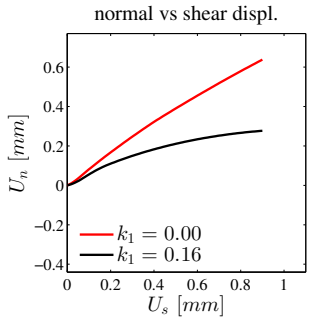	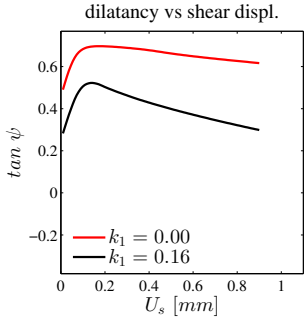
$p = -0.1\,N/mm^2$		
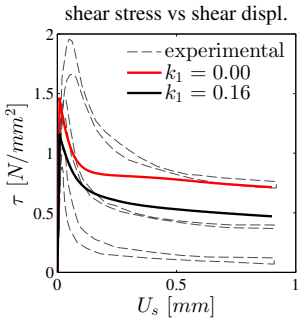	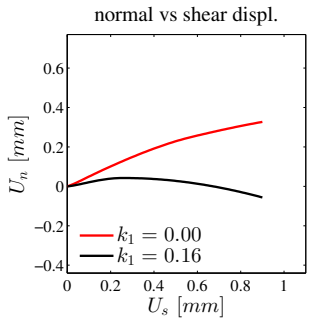	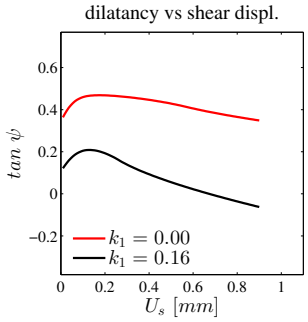
$p = -0.5\,N/mm^2$		
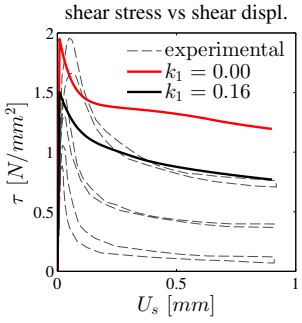	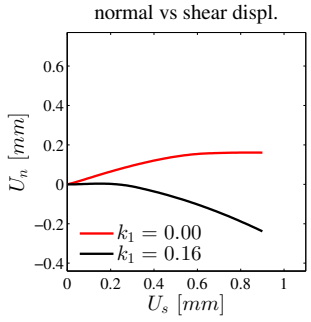	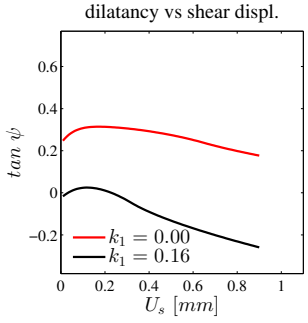
$p = -1.0\,N/mm^2$		

Table 2: Numerical results of the elemental shear test

5. Multisurface Plasticity Interface Model

Mortar joints are modeled using interface elements, allowing to incorporate discontinuities in the displacement field. Thus a constitutive law in terms of relative displacement and traction vector is required. The constitutive model adopted in this work is the one formulated in [5]. For the sake of completeness, only a brief description of the model is given here, and for further details the reader should refer to [5]. This model is based on the concept of multisurface plasticity to better describe all failure mechanisms of masonry, through the definition of three surfaces for tension, shear and compressive failures, as shown in Figure 12.

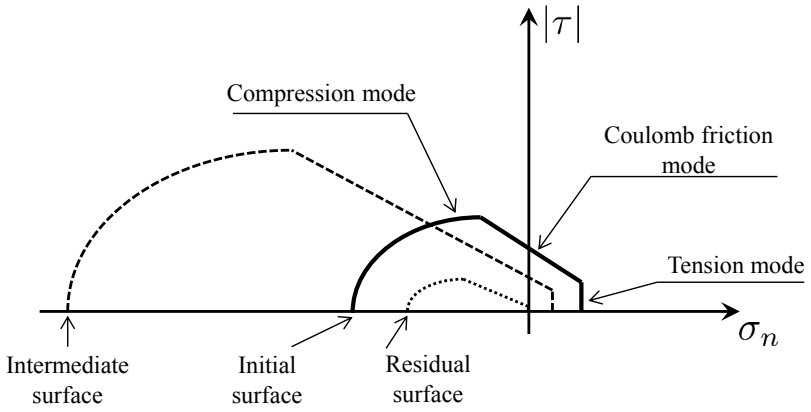

Figure 12: Composite yield surface for mortar joints, from [5].

For an interface element, the elastic response relating the generalized stresses $\boldsymbol{\sigma} = \{\sigma_n, \tau\}^T$ and the generalized strains $\boldsymbol{\varepsilon} = \{u_n, u_s\}^T$ is given by

$$\boldsymbol{\sigma} = \boldsymbol{D}\boldsymbol{\varepsilon} = diag\{k_n, k_s\}\boldsymbol{\varepsilon} \tag{31}$$

where k_n and k_s are the stiffness parameters (not meant as dummy stiffnesses to simulate contact) in the normal and tangential directions, and can be obtained by the elastic properties of brick and mortar as follows:

$$k_n = \frac{E_b E_m}{t_m (E_b - E_m)};\ k_s = \frac{G_b G_m}{t_m (G_b - G_m)} \tag{32}$$

where E_b, E_m, t_m, G_b, G_m are respectively the brick Young's modulus, the mortar Young's modulus, the mortar thickness, the brick Shear modulus and the mortar Shear modulus. To describe the nonlinear regime, three yield functions are employed in the framework of multisurface plasticity:

$$f_1(\boldsymbol{\sigma}, \kappa_1) = \sigma_n - f_t(\kappa_1) \tag{33}$$

$$f_2(\boldsymbol{\sigma}, \kappa_2) = |\tau| + \sigma_n tan\phi(\kappa_2) - c(\kappa_2) \tag{34}$$

$$f_3(\boldsymbol{\sigma}, \kappa_3) = C_{nn}\sigma_n^2 + C_{ss}\tau^2 + C_n\sigma_n - fc(\kappa_3)^2 \tag{35}$$

f_1 is the tension cut-off criterion, where $f_t(\kappa_1)$ is the yield value and k_1 is the hardening-softening parameter. Associated flow rule is considered.
f_2 is the Coulomb friction criterion, where $c(\kappa_2)$ is the cohesion, $\phi(\kappa_2)$ is the friction angle, and k_2 is the hardening-softening parameter. To properly describe dilatancy in mortar joints, a non-associated flow rule is considered, replacing the friction angle with the dilatancy angle ψ:

$$g_2(\boldsymbol{\sigma}, \kappa_2) = |\tau| + \sigma_n tan\psi(\kappa_2) - c(\kappa_2) \tag{36}$$

f_3 is the elliptical cap criterion, where $f_c(\kappa_3)$ is the yield value and k_3 is the hardening/softening parameter. C_{nn}, C_{ss} and C_n are parameters describing the shape of the elliptical cap. An associated flow rule is assumed.
The evolution of the yield value f_t is described by an exponential softening:

$$f_t(\kappa_1) = f_{t0} exp\left(-\frac{f_{t0}}{G_f^I}\kappa_1\right) \tag{37}$$

where f_{t0} is the initial tensile strength and G_f^I is the tensile fracture energy. Similarly, the evolution of the cohesion is given by same exponential softening:

$$c(\kappa_2) = c_0 exp\left(-\frac{c_0}{G_f^{II}}\kappa_2\right) \tag{38}$$

where c_0 is the initial cohesion and G_f^{II} is the shear fracture energy. The evolution of friction and dilatancy angles is linked to the evolution of the cohesion:

$$tan\phi(\kappa_2) = tan\phi_0 + (tan\phi_r - tan\phi_0)\left(\frac{c_0 - c}{c_0}\right) \tag{39}$$

$$tan\psi(\kappa_2) = tan\psi_0 + (tan\psi_r - tan\psi_0)\left(\frac{c_0 - c}{c_0}\right) \tag{40}$$

where ϕ_0 and ψ_0 are the initial friction and dilatancy angles, while ϕ_r and ψ_r are the residual friction and dilatancy angles.
The evolution of $f_c(\kappa_3)$ is described by a hardening-softening law in terms of plastic displacements, explained in Section 3.2.

6. Numerical modeling of shear walls

The adopted modeling strategies are used to model the experimental response of masonry shear walls [31]. Section 6.1 describes the experimental tests, then the results of each modeling strategy is described in detail. Finally, Section 6.5 compares the adopted modeling strategies, highlighting similarities/differences and advantages/disadvantages.
The analyses were performed using an enhanced version of the software Kratos Multiphysics [36, 37], while pre- and post-processing were done with GiD [38].

6.1. Numerical simulation of experimental test: TU Eindhoven shear wall

The geometry and boundary conditions of the wall are given in Figure 13. The wall consists of single layer of solid bricks ($210\,mm \times 52\,mm \times 100\,mm$), and $10\,mm$ of mortar [31]. Loading conditions are applied in two stages. In the first stage, the top of the wall is subjected to a uniform vertical compression. In the second stage, a horizontal force is applied via displacement control, while keeping the top of the wall horizontal. The test is performed for three increasing values of vertical compression (0.30, 1.21 and $2.12\,N/mm^2$). The experimentally obtained crack patterns are shown in Figure 14. Two tests were carried out only for a pre-compression level of $0.3\,N/mm^2$, and the envelope of their load-displacement curves is represented as a shaded area in Figure 15, Figure 17 and Figure 18.

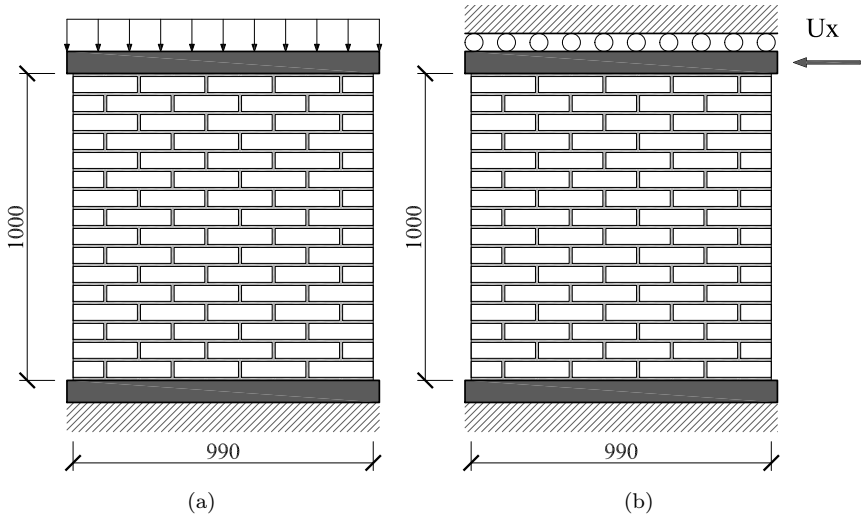

Figure 13: TU Eindhoven shear wall [31]. Geometry and loading conditions: (a) first stage: uniform vertical compression $p = 0.3,\ 1.21,\ 2.12\,N/mm^2$; (b) second stage: horizontal displacement.

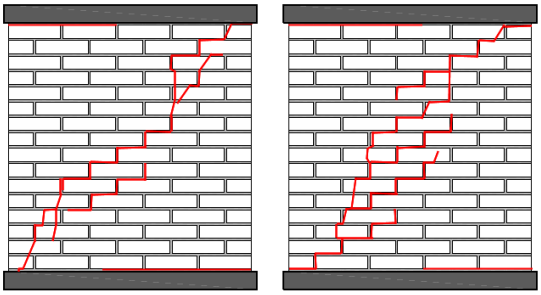

(a) $p = 0.3\,N/mm^2$ (b) $p = 0.3\,N/mm^2$

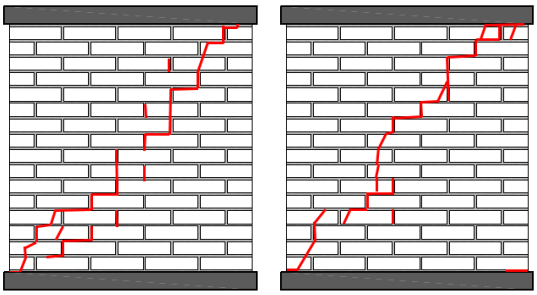

(c) $p = 1.21\,N/mm^2$ (d) $p = 2.12\,N/mm^2$

Figure 14: Experimental failure patterns, adapted from [6].

For each one of the three modeling strategies, three analyses have been carried out, one for each level of vertical compression, for a total of nine analyses.
Each nonlinear static analysis is carried out in two stages. During the 1^{st} stage, the top of the wall is subjected to a uniform vertical compression of respectively $0.3\,N/mm^2$, $1.21\,N/mm^2$ and $2.12\,N/mm^2$, under load control. During the 2^{nd} stage, a horizontal concentrated force is applied on the top-right corner, via displacement control. The vertical displacement on top of the wall is fixed at the value achieved at the previous time-step.
The pseudo-time is adaptively incremented from $t = 0\,s$ to $t = 1\,s$, with an initial time step of $1.0 \times 10^{-2}\,s$, and a minimum time step of $1.0 \times 10^{-9}\,s$. The duration of the two stages are respectively $0.02\,s$ and $0.98\,s$. In each time step the equilibrium is achieved with a full Newton-Raphson iteration process. Convergence is accepted with a relative tolerance of the residual norm of 1.0×10^{-5}. For all three models, the adopted FEM discretization size is $h = 10.0\,mm$ (i.e. the thickness of the mortar layer). 4-node displacement-based quadrilateral elements with full 2x2 gauss integration are used for bricks. For the 2D-C and 2D-CD micro-models, the characteristic length used to regularize the softening behavior of the damage model, is equal to the discretization size ($l_{ch} = h = 10.0\,mm$). In all three models, both the bottom and the top steel beams were modeled, with their corresponding loads and boundary conditions.

6.2. 2D Continuous micro-model (2D-C)

This section reports the results obtained using the 2D-C model. Table 3 shows the material parameters for the damage constitutive model used for both bricks and mortar joints, adapted from the values reported in [6]. Figure 15 shows the obtained force-displacement curves for the three levels of vertical pre-compression. A good agreement with experimental results are obtained, with a slight underestimation of the wall capacity for the highest level of pre-compression. This is probably due to the plane-stress assumption made for both bricks and mortar joints, that becomes hardly applicable to describe the complex interaction between bricks and mortar joints under high levels of compression. A detailed comparison with a full 3D model will be given in Section 6.7. Table 4 shows the obtained results in terms of maximum principal strain, minimum principal stress, tensile and compressive damage.

E	ν	σ_t	G_t	σ_0	σ_p	σ_r	G_c	ε_p	k_b	k_1
850.0	0.15	0.2	0.016	3.0	10.0	2.0	80.0	0.04	1.2	0.16
$\frac{N}{mm^2}$	-	$\frac{N}{mm^2}$	$\frac{N}{mm}$	$\frac{N}{mm^2}$	$\frac{N}{mm^2}$	$\frac{N}{mm^2}$	$\frac{N}{mm}$	-	-	-

(a)

E	ν	σ_t	G_t	σ_0	σ_p	σ_r	G_c	ε_p	k_b	k_1
16700.0	0.15	2.0	0.08	8.0	12.0	1.0	6.0	0.004	1.2	0.0
$\frac{N}{mm^2}$	-	$\frac{N}{mm^2}$	$\frac{N}{mm}$	$\frac{N}{mm^2}$	$\frac{N}{mm^2}$	$\frac{N}{mm^2}$	$\frac{N}{mm}$	-	-	-

(b)

Table 3: Model 2D-C. (a) Material properties for mortar joints (damage model); (b) Material properties for bricks (damage model)

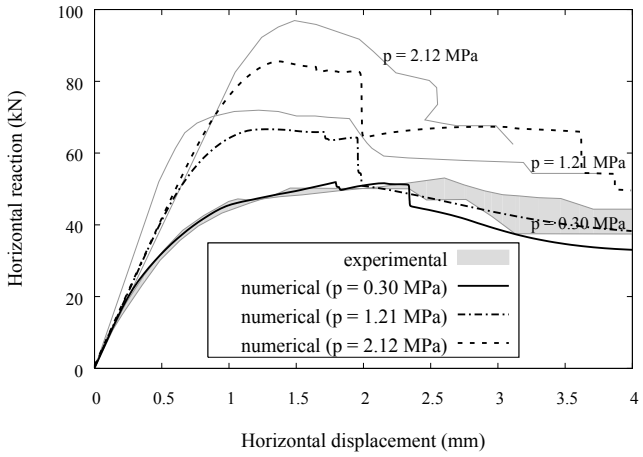

Figure 15: Model 2D-C. load-displacement curves for different values of pre-compression

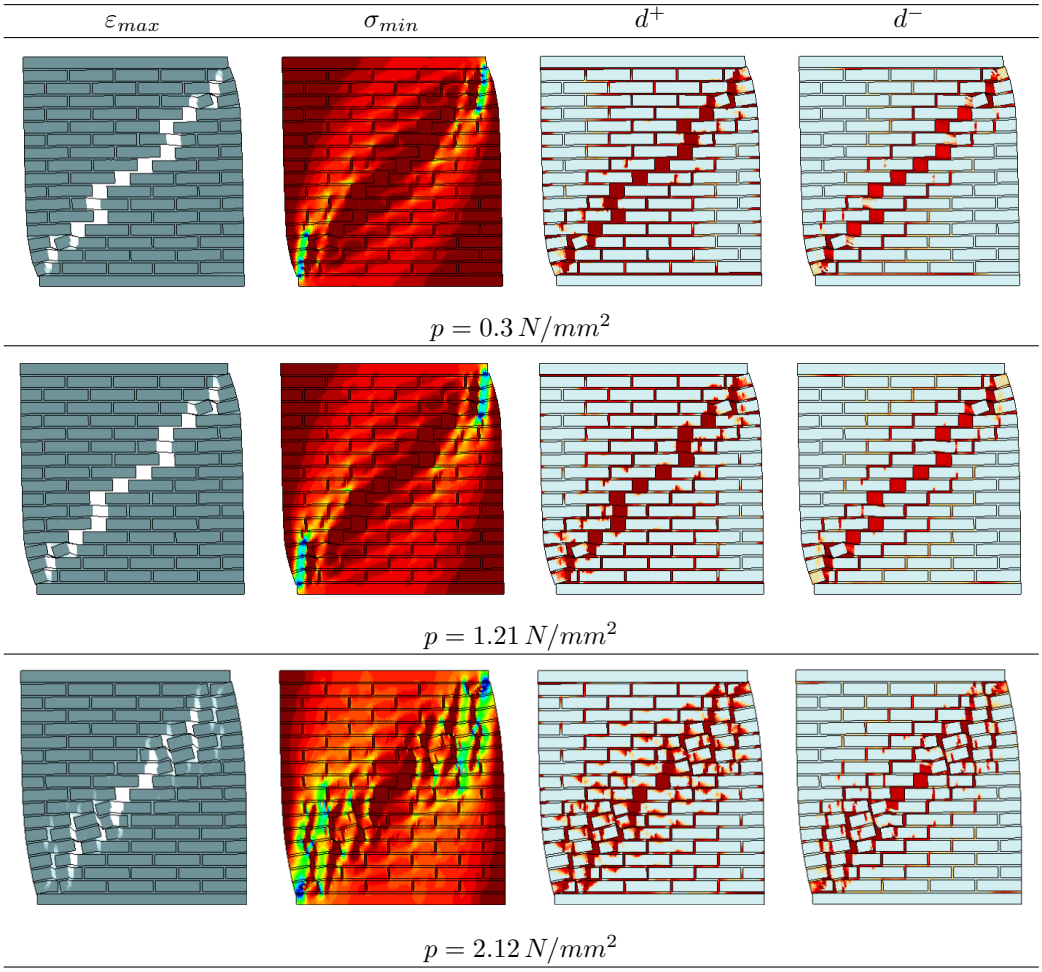

Table 4: Model 2D-C. Results in terms of maximum principal strains, minimum principal stresses, tensile damage and compressive damage, at the ultimate displacement $U_x = 4.0\,mm$

The results of the model 2D-C for a vertical compression of $0.3\,N/mm^2$ are carefully commented to explain the behavior of the shear walls and to better understand the evolution of the micro-structure up to the complete failure of the wall. For this reason, five meaningful points of the analysis are considered, identified by instants $t = [0.14, 0.30, 0.47, 0.64, 1.0]\,s$, and by horizontal top-displacements $U_x = [0.5, 1.1, 1.8, 2.5, 4.0]\,mm$. The obtained results are shown in Figure 16, in terms of maximum principal strains.
The very first non-linear behavior takes place at a horizontal top-displacement $U_x = 0.5\,mm$, when horizontal cracks appears at the bottom-right and top-left corners of the wall. At a horizontal top-displacement $U_x = 1.1\,mm$, staircase cracks emerge from the central part, advancing towards the corners and passing through mortar joints. At this stage, several cracks are visible, but not yet a completely open unique crack. This is

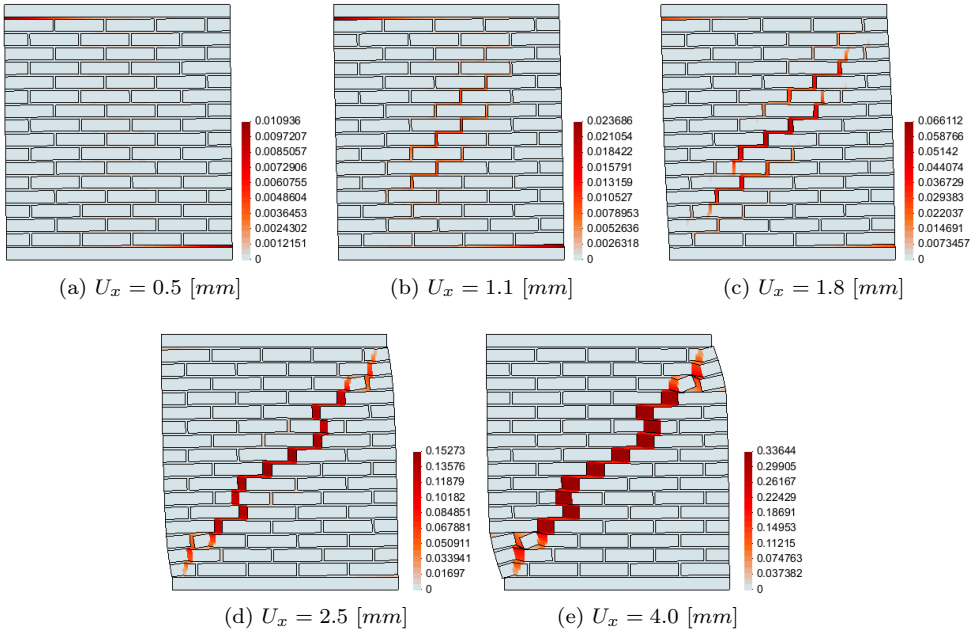

(a) $U_x = 0.5\ [mm]$ (b) $U_x = 1.1\ [mm]$ (c) $U_x = 1.8\ [mm]$

(d) $U_x = 2.5\ [mm]$ (e) $U_x = 4.0\ [mm]$

Figure 16: Model 2D-C, $P = 0.3\,N/mm^2$. Incremental contour plots of maximum principal strain ε_{max}

mainly related to the presence of bricks, whose stress state is still far from their tensile strength. The appearance of these diagonal cracks produces the first significant change in the slope of the global load-displacement curve. At a later stage of the analysis, approximately between top-displacements $U_x = 1.8\,mm$ and $U_x = 2.5\,mm$, the tensile strength in some bricks is exceeded, leading to their splitting. As a consequence, the previously mentioned staircase cracks coalesce into a single well defined diagonal cracks. The further opening of this diagonal crack finally leads to the complete development of the shear/crushing mechanism determining the collapse of the wall.

6.3. 2D Discrete micro-model (2D-D)

This section reports the results obtained using the 2D-D model. Table 5 shows the material parameters for the interface constitutive model used for mortar joints, and the elastic properties for the bricks. The potential crack in the bricks have been simulated using a simple damage interface model with a tensile strength $\sigma_t = 2.0\,N/mm^2$. Figure 17 shows the obtained force-displacement curves for the three levels of vertical pre-compression. Also in this case, a good agreement with experimental results have been reached. As opposed to the 2D-C model, the 2D-D model shows an overestimation of the wall capacity for higher level of pre-compression. This is probably due to assuming only a vertical potential crack in the bricks. This assumption is more appropriate for low values of vertical pre-compression. For higher values of pre-compression, diagonal cracks in the bricks cannot appear, and the main diagonal "crack" has to find its path through the pre-defined

interfaces. Table 6 shows the obtained results in terms of deformed shape, minimum principal stress, tensile/shear and compressive equivalent plastic displacements.

E	ν
16700.0	0.15
$\frac{N}{mm^2}$	-

(a)

k_n	k_s	ν
82.0	36.0	0.15
$\frac{N}{mm^3}$	$\frac{N}{mm^3}$	-

(b)

f_t	G_I	c	G_{II}	$tan\phi$	$tan\psi$	σ_0	σ_p	σ_r	G_{III}	C_{ss}
0.2	0.016	0.35	0.125	0.75	0	6.0	11.0	2.0	6.0	9.0
$\frac{N}{mm^2}$	$\frac{N}{mm}$	$\frac{N}{mm^2}$	$\frac{N}{mm}$	-	-	$\frac{N}{mm^2}$	$\frac{N}{mm^2}$	$\frac{N}{mm^2}$	$\frac{N}{mm}$	-

(c)

Table 5: Model 2D-D. (a) Material properties for elastic bricks; (b)(c) Material properties for mortar joints (interface model)

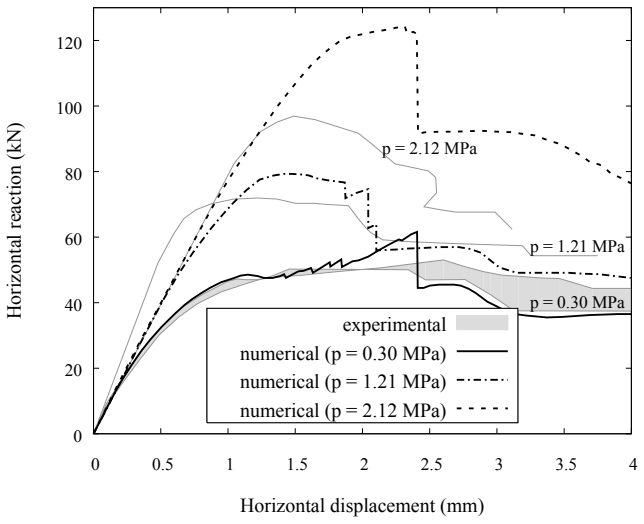

Figure 17: Model 2D-D. load-displacement curves for different values of pre-compression

deformed shape	σ_{min}	tensile/shear $u_{p,eq}$	compressive $u_{p,eq}$
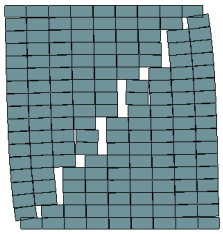	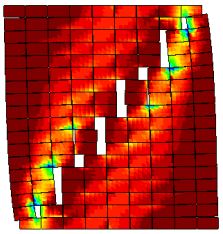	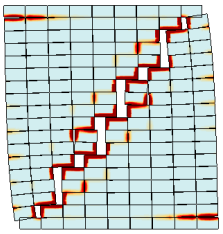	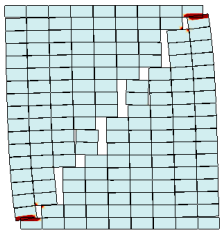
$p = 0.3\,N/mm^2$			
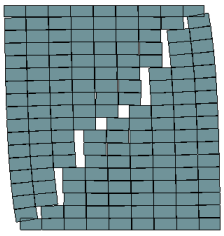	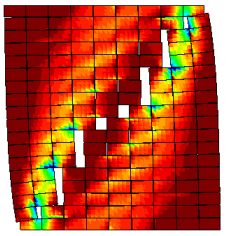	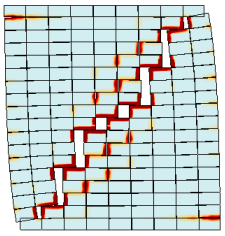	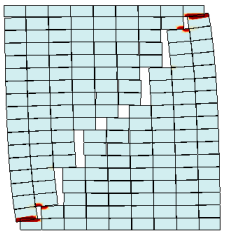
$p = 1.21\,N/mm^2$			
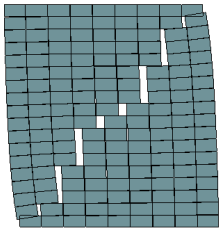	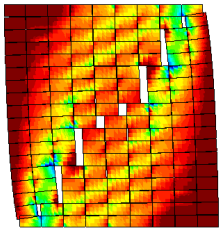	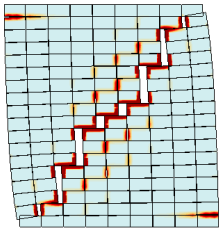	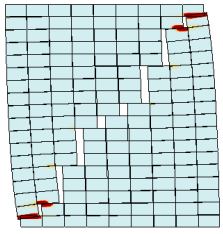
$p = 2.12\,N/mm^2$			

Table 6: Model 2D-D. Results in terms of deformed shape, minimum principal stresses, tensile/shear and compressive equivalent plastic displacement, at the ultimate displacement $U_x = 4.0\,mm$

6.4. 2D Mixed Continuous/Discrete micro-model (2D-CD)

This section reports the results obtained using the 2D-CD model. Table 7 shows the material parameters for the interface constitutive model used for mortar joints, and for the damage model used for the bricks. Figure 18 shows the obtained force-displacement curves for the three levels of vertical pre-compression. A good agreement with experimental results have been obtained also in this case. As expected, this model shows a response which is in-between the 2D-C and the 2D-D models. The overestimation for higher levels of vertical pre-compression is reduced compared to the 2D-D model, by allowing any possible damage pattern in the bricks.Table 8 shows the obtained results

in terms of deformed shape, minimum principal stress, tensile/shear and compressive equivalent plastic displacements.

k_n	k_s	ν
82.0	36.0	0.15
$\frac{N}{mm^3}$	$\frac{N}{mm^3}$	-

f_t	G_I	c	G_{II}	$tan\phi$	$tan\psi$	σ_0	σ_p	σ_r	G_{III}	C_{ss}
0.2	0.016	0.35	0.125	0.75	0	6.0	11.0	2.0	6.0	9.0
$\frac{N}{mm^2}$	$\frac{N}{mm}$	$\frac{N}{mm^2}$	$\frac{N}{mm}$	-	-	$\frac{N}{mm^2}$	$\frac{N}{mm^2}$	$\frac{N}{mm^2}$	$\frac{N}{mm}$	-

(a)

E	ν	σ_t	G_t	σ_0	σ_p	σ_r	G_c	ε_p	k_b	k_1
16700.0	0.15	2.0	0.08	8.0	12.0	1.0	6.0	0.004	1.2	0.0
$\frac{N}{mm^2}$	-	$\frac{N}{mm^2}$	$\frac{N}{mm}$	$\frac{N}{mm^2}$	$\frac{N}{mm^2}$	$\frac{N}{mm^2}$	$\frac{N}{mm}$	-	-	-

(b)

Table 7: Model 2D-CD. (a) Material properties for mortar joints (interface model); (b) Material properties for bricks (damage model)

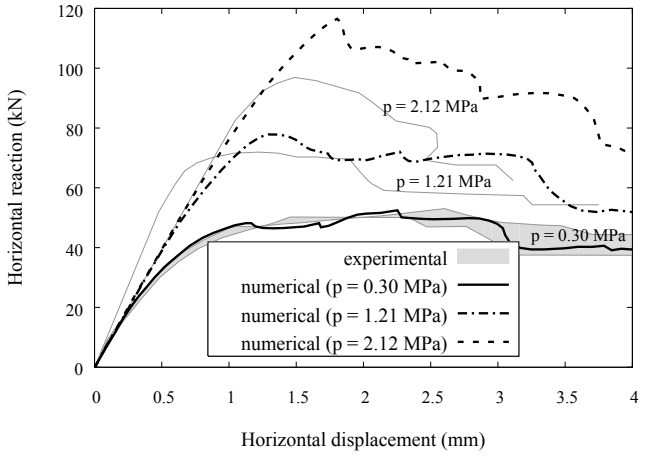

Figure 18: Model 2D-CD. load-displacement curves for different values of pre-compression

deformed shape	σ_{min}	tensile/shear $u_{p,eq}$	compressive $u_{p,eq}$
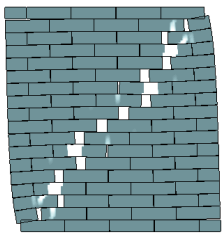	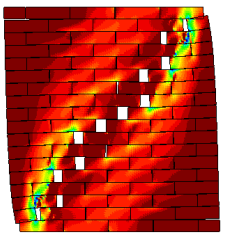	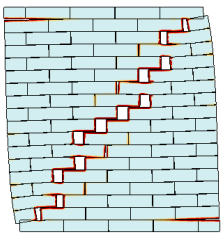	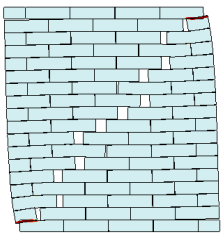
$p = 0.3\,N/mm^2$			
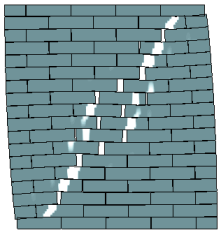	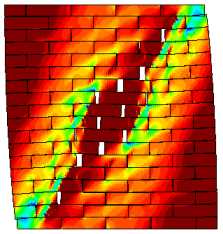	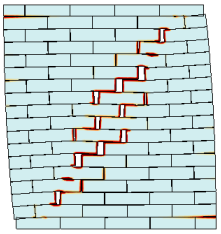	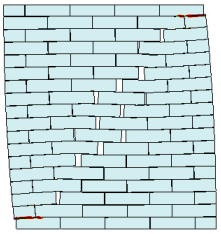
$p = 1.21\,N/mm^2$			
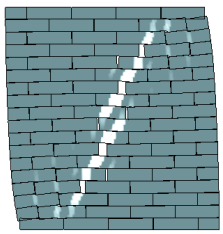	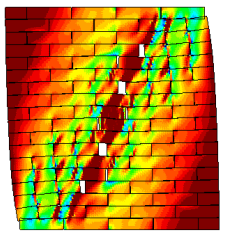	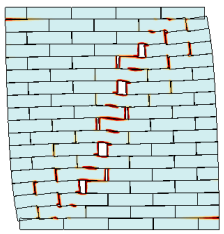	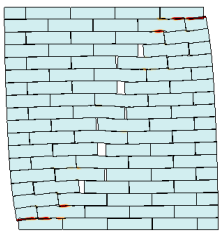
$p = 2.12\,N/mm^2$			

Table 8: Model 2D-CD. Results in terms of deformed shape, minimum principal stresses, tensile/shear and compressive equivalent plastic displacement, at the ultimate displacement $U_x = 4.0\,mm$

6.5. Comparison and discussion of numerical results

The presented results demonstrate that all the three selected models perform relatively well and give similar results, all in good agreement with the experimental tests. Each modeling strategy introduces simplifications with respect to a more general 3D detailed micro-modeling, thus giving slightly different results.

The model 2D-C uses a tension/compression continuum damage model for both bricks and mortar joints. This leads to a very efficient and robust analysis due to the explicit evaluation of the internal variables. The concept of dilatancy (which is of paramount importance for the simulation of shear walls) cannot be easily defined in the context of

damage models, differently from the case of plasticity. Nevertheless, both failure surfaces are active in a tension/compression damage model when the two principal stresses have different sign. In this case, the Cauchy stress is not an isotropic scaling of the effective (elastic) stress. Taking advantage of this feature, a novel compressive model has been formulated to provide a satisfactory shear behavior, in terms of dilatancy and shear strength, as described in Section 4. The proposed model requires a careful definition of the parameter k_1 that sets the shape of the compressive failure surface in the tension/compression quadrants of the principal stresses plane. A value of 0.16 has shown to be be adequate for the investigated case studies, see Section 6.6. Also the novel evolution law for the compressive damage variable, based on quadratic Bézier curves, has shown to be adequate for the description of the shear-compression nonlinear response of masonry. The proposed model is remarkably efficient from the point of view of the computation of the constitutive response.

The model 2D-D lumps all the main non-linearity in mortar joints, modeled as interface elements with a composite yield criterion based on the concept of multisurface plasticity. The dilatancy of mortar joints are easily defined due to the non-associativity of the shear mode. Another advantage is that this model separately defines the shear and compressive failure mechanisms. In this way the compressive cap criterion can be used to properly model the compressive behavior of the wall without affecting the shear behavior of the mortar joints. The choice of allowing only the tensile failure of the brick, through a vertical potential crack in the mid-section, limits the number of DOFs of the model, but at the same time it does not allow a natural failure of the bricks when a diagonal crack is likely to appear, as in cases of shear at high compression. It should be mentioned that this model takes into account the reduction in shear strength for high level of compression through the elliptical cap mode. However, this happens at the interface constitutive level but at the structural level the "crack" is forced to find its path through the predefined interfaces. This is probably the cause of overestimation of the strength of the wall for higher vertical compression levels and sudden drops as the vertical cracks in the bricks open, as can be seen in Figure 17.

Finally the model 2D-CD seems to join the features of both the previous models, at the price of a higher computational cost. In this model the accurate description of the mortar joint behavior is achieved with the composite interface model, while the non-linearity in the bricks is described through the continuum damage model, thus without making any assumption on the direction of the cracks in the bricks. Compared to the 2D-D model, the overestimation of the shear strength of the wall under high vertical compression is alleviated, as can be seen in Figure 18.

Slight differences in the crack patterns can be seen by comparing the obtained results for each model and for each level of vertical compression, as shown in Table 9. Model 2D-CD shows a progressively changing direction in the main diagonal crack, becoming more vertical as the vertical compression increases, due to the propagation of diagonal cracks in the bricks, while the model 2D-D shows almost the same failure pattern for all vertical compression levels. Model 2D-C instead shows an overall diagonal crack running from corner to corner, similar to model 2D-D, but with a more diffuse damage pattern in bricks as the vertical compression increases.

$P = 0.30\,N/mm^2$	$P = 1.21\,N/mm^2$	$P = 2.12\,N/mm^2$
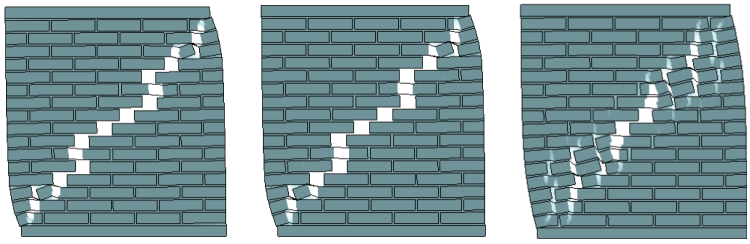		
2D Continuous micro-model (2D-C)		
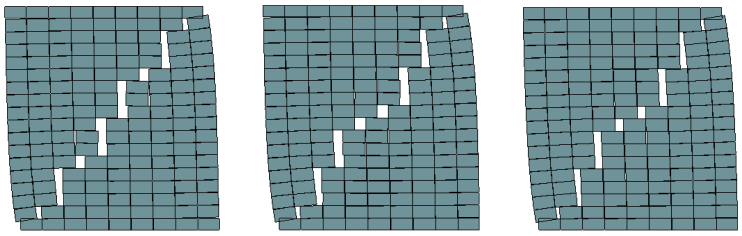		
2D Discrete micro-model (2D-D)		
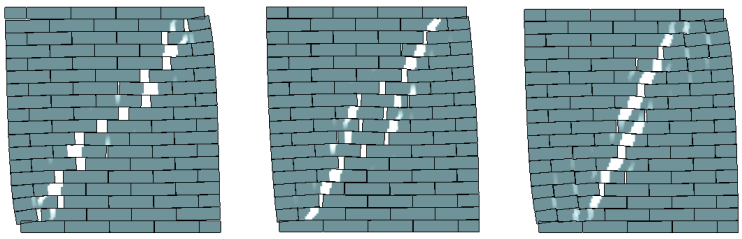		
2D Mixed Continuous/Discrete micro-model (2D-CD)		

Table 9: Comparison of failure patterns

Table 10 shows the total simulation time for each one of the analyses with micro-models, carried out with a single standard PC equipped with an Intel Core i7-2670QM CPU and 8 GB RAM. Model 2D-C and model 2D-D are the most efficient ones in terms of computational costs, with model 2D-C giving a slightly better performance. In relative terms, the models 2D-D and 2D-CD provide an increment of the computation time of +23% and + 91% compared with the 2D-C model. The main reason is the efficient formulation typical of damage-models, where the evolution of the internal variables is performed explicitly. On the contrary, the interface model used in model 2D-D is based on multi-surface plasticity (see [6, 5] for further details), where an iterative procedure at the constitutive law level is also necessary in order to integrate the constitutive relation. However, in model 2D-D, this higher cost for the interface constitutive model is amortized by the assumption of an elastic-behavior for bricks. Obviously, model 2D-CD shows the highest computational cost, due to the use of both the interface model for mortar joints,

and the damage model for bricks.

Total simulation time (hh:mm:ss)		
Model 2D-C	Model 2D-D	Model 2D-CD
00 : 09 : 16	00 : 11 : 23 +23%	00 : 17 : 41 +91%

Table 10: Total simulation time for each one of the three micro-models

6.6. Dilatant behavior in the continuous micro-model 2D-C

This section presents a further assessment of the tension/compression damage model proposed for the 2D-C model. A parametric study is carried out to evaluate the model's capability of handling the dilatant behavior of mortar joints. The effect of the compressive surface on the global response of the wall is evaluated.

For the 2D-C modeling strategy, with the lowest of the three vertical compression levels, $0.3\,N/mm^2$, three analyses have been carried out, varying the k_1 parameter in Eq. (5). Three values have been selected: 0.0, 0.16, and 1.0. Recalling that this parameter affects the shape of the compressive surface in tension/compression quadrants, the value of 0.0 leads to a Drucker-Prager criterion, while the value of 1.0 leads to the Lubliner criterion [25]. The intermediate value of 0.16 has been found as optimal for the required dilatancy. The results of the three analyses are shown in Figure 19 in terms of global force-displacement response, and in Figure 20 in terms of maximum principal strains. As expected the Drucker-Prager criterion ($k_1 = 0$) overestimates the dilatancy of the model, and since no vertical displacement is allowed on top of the wall while loaded in shear, this induces an excessive state of compression to the material with a consequent overestimation of the global strength, as well as a more brittle behavior. Furthermore the crack pattern clearly shows how the slip of mortar joints is inhibited, while a unique diagonal crack opens through the bricks. On the contrary, a k_1 value of 1.0 makes the compressive surface very close to the tensile one in the tension/compression quadrants. In this case the dilatancy of mortar joints is not captured at all, and consequently the global shear strength of the model is largely underestimated. The failure in this case is almost only due to slip of mortar joints in the middle of the wall, and only when the crack reaches the boundaries of the wall, it finally propagates vertically through the bricks. On the other hand, the case with $k_1 = 0.16$ provides a more realistic result, by giving a better estimate of the dilatancy of mortar joints.

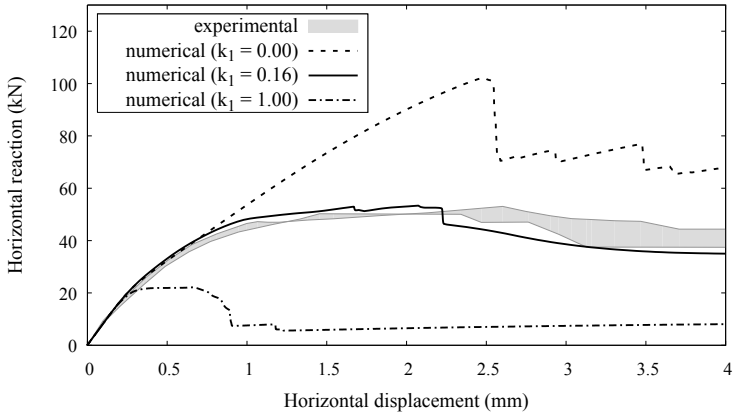

Figure 19: Model 2D-C, $p = 0.3\,N/mm^2$. Force-displacement curves for three different values of k_1

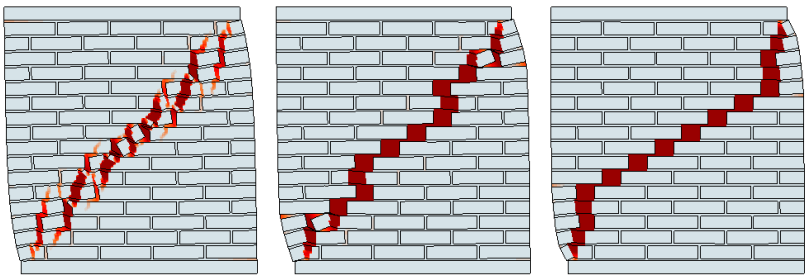

(a) $k_1 = 0.0$ (b) $k_1 = 0.16$ (c) $k_1 = 1.0$

Figure 20: Model 2D-C, $p = 0.3\,N/mm^2$. Failure patterns for three different values of k_1

6.7. Comparison of 2D-plane stress and full 3D modeling

The adoption of the plane stress hypothesis is widely diffused in the FE analyses of in-plane loaded shear walls [39]. However, as shown in the results presented in Section 6.2, the plane-stress assumption in the model 2D-C, while reducing the computational cost of the simulation, leads to a slight underestimation of the shear strength of walls as the vertical compression level increases. With stiff bricks and soft mortar, high levels of vertical compression induce a state of triaxial compression in mortar joints, thus increasing their strength. This effect is neglected with the plane-stress hypothesis, since the out-of-plane stress is assumed to be zero. This section shows how a full 3D continuous model (3D-C) can provide more accurate results, but at the price of higher computational costs. Another alternative solution that retains the efficiency of 2D modeling is the so called generalized plane state [20, 21].

To account for the increase strength under stress states of triaxial compression, Eq. (9) given for the 2D-plane stress model, should be rewritten for a generic 3D stress state as follows:

$$\tau^{-} = H\left(-\bar{\sigma}_{min}\right)\left[\frac{1}{1-\alpha}\left(\alpha\bar{I}_1 + \sqrt{3\bar{J}_2} + k_1\beta\left\langle\bar{\sigma}_{max}\right\rangle + \gamma\left\langle-\bar{\sigma}_{max}\right\rangle\right)\right] \tag{41}$$

$\gamma \geq 0$ is a material parameter that increases the strength in states of triaxial compression, effectively "enlarging" the damage surface around the hydrostatic axis when all three principal stresses are negative: $\bar{\sigma}_3 \leq \bar{\sigma}_2 \leq \bar{\sigma}_1 = \bar{\sigma}_{max} \leq 0$. In the following simulations this parameter is set equal to 3 (see [25]).
Figure 21 shows, for the case of highest vertical compression level ($p = 2.12\,N/mm^2$), the load-displacement response of the model 2D-C compared to the respective 3D-C model, while Figure 22 shows the failure pattern obtained from the 3D-C micro-model. As expected, the 3D model shows an improved global response in terms of maximum strength of the wall, while the failure pattern is similar to that obtained from the 2D model.

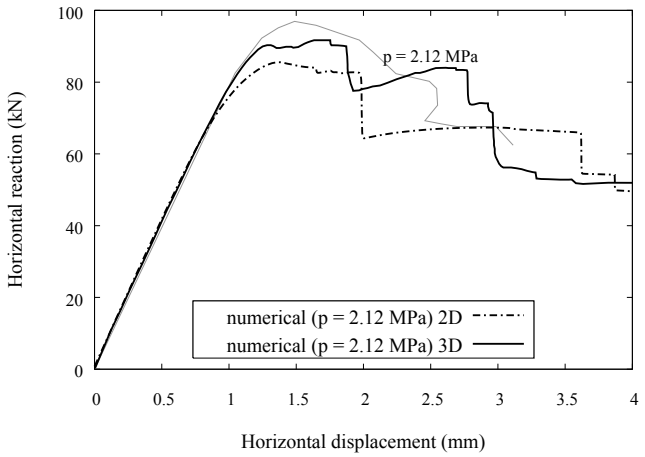

Figure 21: Load-displacement curve of the model 2D-C compared to a full-3D simulation

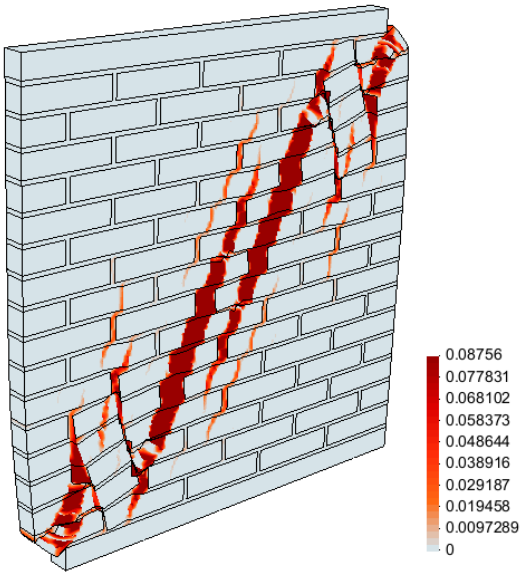

Figure 22: Continuous 3D micro-model (3D-C), maximum principal strain

7. Conclusions

This work has proposed a novel damage-mechanics based micro-model able to represent the nonlinear response of masonry constituents, especially under shear stress states. The presented approach includes the control of the dilatant behavior of the material, even though this aspect is not generally handled by standard continuum damage models. In order to obtain a control on the amount of dilatancy, an existing failure criterion for quasi-brittle materials has been improved under shear conditions and a novel hardening-softening law based on quadratic Bézier curves has been established.

The paper has presented also the critical comparison of the novel continuous micro-modeling technique with well-known discrete micro-modeling strategies for the 2D analysis of in-plane loaded masonry structures. The first numerical strategy, here named 2D Continuous micro-model (2D-C), is based on a classical continuum description of both bricks and mortar joints, both of them treated inelastically using the proposed damage model. The other two strategies, named 2D Discrete micro-model (2D-D) and 2D Mixed Continuous/Discrete micro-model (2D-CD) are already well-known in the literature, and they are based on a discrete description of the micro-structure, modeling bricks with continuum elements and mortar joints with interface elements. Bricks are treated either elastically with potential vertical cracks in the middle vertical section, or inelastically.

The critical analysis of the results has shown how all the investigated strategies are equivalently capable of describing the behavior of shear walls up to their collapse. The main differences have been found with higher compressive levels, where the 2D-D and 2D-CD micro-models overestimate the maximum shear strength of the wall, whereas the 2D-C micro-model slightly underestimates it in a conservative way.

The advantage of the proposed micro-model mainly resides in its simple and efficient format that it inherits from classical damage mechanics models, where the explicit evaluation of the internal variables avoids nested iterative procedures, thus increasing computational performance and robustness. The recurrent disadvantage of standard continuum damage models, i.e. their poor capability of representing the dilatant behavior of mortar joints under shear stress states, has been overcome by the proposed model. Other remarkable advantages offered by the proposed continuous micro-model with a continuum description of both bricks and mortar joints are the simple generation of the finite element model during pre-processing, as well as the straightforward interpretation of the results during post-processing. As regarding the response of the proposed damage model with respect to the dilatant behavior of mortar joints, through the use of the k_1 parameter, future research will be devoted to further assess the reliability of the model on different types of masonry walls.

Acknowledgments

This research has received the financial support from the Graduate School of the University "G. d'Annunzio" of Chieti-Pescara, from the MINECO (Ministerio de Economia y Competitividad of the Spanish Government) through the MULTIMAS project (Multiscale techniques for the experimental and numerical analysis of the reliability of masonry structures, ref. num. BIA2015-63882-P) and the EACY project (Enhanced accuracy computational and experimental framework for strain localization and failure mechanisms, ref. MAT2013-48624-C2-1-P). Partial financial support by the ReLUIS (Network of Earthquake Engineering Experimental Laboratories, funded by the Prime Minister Office - Civil Protection Department) project is acknowledged and greatly appreciated. This publication, however, might not necessarily reflect the viewpoint of the Civil Protection Department.

References

[1] P. Roca, M. Cervera, G. Gariup, L. Pelà, Structural Analysis of Masonry Historical Constructions. Classical and Advanced Approaches, Archives of Computational Methods in Engineering 17 (3) (2010) 299–325, ISSN 1134-3060.

[2] L. Pelà, M. Cervera, P. Roca, Continuum damage model for orthotropic materials: Application to masonry, Computer Methods in Applied Mechanics and Engineering 200 (9-12) (2011) 917–930, ISSN 0045-7825, URL http://www.sciencedirect.com/science/article/pii/S0045782510003257.

[3] L. Pelà, M. Cervera, P. Roca, An orthotropic damage model for the analysis of masonry structures, Construction and Building Materials 41 (2013) 957–967, ISSN 0950-0618, URL http://www.sciencedirect.com/science/article/pii/S0950061812004837.

[4] L. Pelà, M. Cervera, S. Oller, M. Chiumenti, A localized mapped damage model for orthotropic materials, Engineering Fracture Mechanics 124-125 (2014) 196–216, ISSN 0013-7944, URL http://www.sciencedirect.com/science/article/pii/S0013794414001386.

[5] P. B. Lourenço, J. G. Rots, Multisurface interface model for analysis of masonry structures, Journal of engineering mechanics 123 (7) (1997) 660–668.

[6] P. B. Lourenco, Computational strategies for masonry structures, Ph.D. thesis, TU Delft, Delft University of Technology, 1996.

[7] D. V. Oliveira, P. B. Lourenço, Implementation and validation of a constitutive model for the cyclic behaviour of interface elements, Computers & structures 82 (17) (2004) 1451–1461.

[8] A. Drougkas, L. Pelà, P. Roca, Numerical modelling of masonry shear walls failure mechanisms, in: Proceedings of 9th International Masonry Conference, Guimarães, Portugal, 2014.

[9] M. Petracca, L. Pelà, R. Rossi, S. Oller, G. Camata, E. Spacone, Regularization of first order computational homogenization for multiscale analysis of masonry structures, Computational Mechanics 57 (2) (2016) 257–276, ISSN 1432-0924, URL http://dx.doi.org/10.1007/s00466-015-1230-6.

[10] M. Petracca, L. Pelà, R. Rossi, S. Oller, G. Camata, E. Spacone, Multiscale computational first order homogenization of thick shells for the analysis of out-of-plane loaded masonry walls, Computer Methods in Applied Mechanics and Engineering 315 (2017) 273–301.

[11] R. D. Quinteros, S. Oller, L. G. Nallim, Nonlinear homogenization techniques to solve masonry structures problems, Composite Structures 94 (2) (2012) 724–730.

[12] A. Zucchini, P. Lourenço, A micro-mechanical model for the homogenisation of masonry, International Journal of Solids and Structures 39 (12) (2002) 3233–3255.

[13] A. Zucchini, P. B. Lourenço, A micro-mechanical homogenisation model for masonry: Application to shear walls, International Journal of Solids and Structures 46 (3) (2009) 871–886.

[14] M. L. De Bellis, A Cosserat based multi-scale technique for masonry structures, in: PHD Thesis, 2009.

[15] M. L. De Bellis, D. Addessi, A Cosserat based multi-scale model for masonry structures, International Journal for Multiscale Computational Engineering 9 (5).

[16] T. J. Massart, Multi-scale modeling of damage in masonry structures, Ph.D. thesis, 2003.

[17] T. Massart, R. Peerlings, M. Geers, An enhanced multi-scale approach for masonry wall computations with localization of damage, International Journal for Numerical Methods in Engineering 69 (5) (2007) 1022–1059.

[18] B. Mercatoris, P. Bouillard, T. Massart, Multi-scale detection of failure in planar masonry thin shells using computational homogenisation, Engineering fracture mechanics 76 (4) (2009) 479–499.

[19] B. Mercatoris, T. Massart, A coupled two-scale computational scheme for the failure of periodic quasi-brittle thin planar shells and its application to masonry, International journal for numerical methods in engineering 85 (9) (2011) 1177–1206.

[20] D. Addessi, E. Sacco, Nonlinear analysis of masonry panels using a kinematic enriched plane state formulation, International Journal of Solids and Structures 90 (2016) 194–214.

[21] A. Anthoine, Homogenization of periodic masonry: plane stress, generalized plane strain or 3D modelling?, International Journal for Numerical Methods in Biomedical Engineering 13 (5) (1997) 319–326.

[22] M. Cervera, J. Oliver, R. Faria, Seismic evaluation of concrete dams via continuum damage models, Earthquake engineering & structural dynamics 24 (9) (1995) 1225–1245.

[23] R. Faria, J. Oliver, M. Cervera, A strain-based plastic viscous-damage model for massive concrete structures, International Journal of Solids and Structures 35 (14) (1998) 1533–1558.

[24] J. Y. Wu, J. Li, R. Faria, An energy release rate-based plastic-damage model for concrete, International Journal of Solids and Structures 43 (3) (2006) 583–612.

[25] J. Lubliner, J. Oliver, S. Oller, E. Oñate, A plastic-damage model for concrete, International Journal of solids and structures 25 (3) (1989) 299–326.
[26] M. L. Raffa, F. Lebon, E. Sacco, H. Welemane, A multi-level interface model for damaged masonry, in: E. B.H.V. Topping, P. Iv/'anyi (Ed.), "Proceedings of the Fourteenth International Conference on Civil, Structural and Environmental Engineering Computing", Civil-Comp Press, Stirlingshire, UK, 2013.
[27] E. Sacco, J. Toti, Interface Elements for the Analysis of Masonry Structures, International Journal for Computational Methods in Engineering Science and Mechanics 11 (6) (2010) 354–373, URL http://www.tandfonline.com/doi/abs/10.1080/15502287.2010.516793.
[28] C. Citto, Two-dimensional interface model applied to masonry structures, ProQuest, 2008.
[29] L. Gambarotta, S. Lagomarsino, Damage models for the seismic response of brick masonry shear walls. Part I: The mortar joint model and its applications, Earthquake Engineering & Structural Dynamics 26 (4) (1997) 423–439, ISSN 1096-9845.
[30] H. R. Lotfi, P. B. Shing, Interface model applied to fracture of masonry structures, Journal of structural engineering 120 (1) (1994) 63–80.
[31] T. Raijmakers, A. Vermeltfoort, Deformation controlled tests in masonry shear walls: report B-92-1156, URL http://books.google.it/books?id=HUmTPgAACAAJ, 1992.
[32] Z. Bažant, B. Oh, Crack Band Theory for Fracture of Concrete, Bordas-Dunod, URL http://books.google.it/books?id=x9citwAACAAJ, 1983.
[33] J. Oliver, A consistent characteristic length for smeared cracking models, International Journal for Numerical Methods in Engineering 28 (2) (1989) 461–474.
[34] S. Oller, Fractura Mecánica: Un Enfoque Global, Ediciones CIMNE y UPC, 2001.
[35] R. V. D. Pluijm, Shear behavior of bed joints, Proc. 6 th North American Masonry Conf. (1993) 125–136.
[36] P. Dadvand, R. Rossi, E. Oñate, An object-oriented environment for developing finite element codes for multi-disciplinary applications, Archives of computational methods in engineering 17 (3) (2010) 253–297.
[37] P. Dadvand, R. Rossi, M. Gil, X. Martorell, J. Cotela, E. Juanpere, S. R. Idelsohn, E. Oñate, Migration of a generic multi-physics framework to HPC environments, Computers & Fluids 80 (2013) 301–309.
[38] GiD: The personal pre and post preprocessor, 2002.
[39] S. Saloustros, L. Pelà, M. Cervera, P. Roca, Finite element modelling of internal and multiple localized cracks, Computational Mechanics (2016) 1–18.

Finite Elements in Analysis and Design 127 (2017) 31–43

Contents lists available at ScienceDirect

Finite Elements in Analysis and Design

journal homepage: www.elsevier.com/locate/finel

Multiscale thermo-mechanical analysis of multi-layered coatings in solar thermal applications

F. Montero-Chacón[a,*], S. Zaghi[b], R. Rossi[b], E. García-Pérez[c], I. Heras-Pérez[c], X. Martínez[b], S. Oller[b], M. Doblaré[d]

[a] Universidad Loyola Andalucía, Dpto. Ingeniería, Calle Energía Solar, 1, 41014 Seville, Spain
[b] Centre Internacional de Mètodes Numèrics a l'Enginyeria, C/ Gran Capità, s/n, 08034 Barcelona, Spain
[c] Abengoa Research, Calle Energía Solar, 1, 41014 Seville, Spain
[d] Group of Structural Mechanics and Materials Modelling (GEMM), Aragon Institute of Engineering Research (I3A), University of Zaragoza, Spain

ARTICLE INFO

Keywords:
Multiscale analysis
Thermo-mechanical homogenization
Finite element method
Representative Volume Element (RVE)
Molecular dynamics
Solar selective coatings

ABSTRACT

Solar selective coatings can be multi-layered materials that optimize the solar absorption while reducing thermal radiation losses, granting the material long-term stability. These layers are deposited on structural materials (e.g., stainless steel, Inconel) in order to enhance the optical and thermal properties of the heat transfer system. However, interesting questions regarding their mechanical stability arise when operating at high temperatures. In this work, a full thermo-mechanical multiscale methodology is presented, covering the nano-, micro-, and macroscopic scales. In such methodology, fundamental material properties are determined by means of molecular dynamics simulations that are consequently implemented at the microstructural level by means of finite element analyses. On the other hand, the macroscale problem is solved while taking into account the effect of the microstructure via thermo-mechanical homogenization on a representative volume element (RVE). The methodology presented herein has been successfully implemented in a reference problem in concentrating solar power plants, namely the characterization of a carbon-based nanocomposite and the obtained results are in agreement with the expected theoretical values, demonstrating that it is now possible to apply successfully the concepts behind Integrated Computational Materials Engineering to design new coatings for complex realistic thermo-mechanical applications.

* Corresponding author.
E-mail address: fpmontero@uloyola.es (F. Montero-Chacón).

http://dx.doi.org/10.1016/j.finel.2016.12.006
Received 26 October 2016; Received in revised form 29 December 2016; Accepted 30 December 2016
Available online 26 January 2017
0168-874X/

Composite Structures 206 (2018) 215–233

Contents lists available at ScienceDirect

Composite Structures

journal homepage: www.elsevier.com/locate/compstruct

Adaptive and off-line techniques for non-linear multiscale analysis

Stefano Zaghi[a], Xavier Martinez[a,c,*], Riccardo Rossi[a,b], Massimo Petracca[d]

[a] CIMNE – Centre Internacional de Metodes Numerics en Enginyeria, Universitat Politécnica de Catalunya (UPC-BarcelonaTech), Barcelona 08034, Spain
[b] Department of Civil and Environmental Engineering, Universitat Politécnica de Catalunya (UPC-BarcelonaTech), Barcelona 08034, Spain
[c] Department of Nautical Science and Engineering, Universitat Politécnica de Catalunya (UPC-BarcelonaTech), Barcelona 08003, Spain
[d] Department of Engineering, University "G.d'Annunzio" of Chieti and Pescara, Pescara 65127, Italy

ARTICLE INFO

Keywords:
Multiscale
Multiphysics
Optimization

ABSTRACT

This paper presents two procedures, based on the numerical multiscale theory, developed to predict the mechanical non-linear response of composite materials under monotonically increasing loads. Such procedures are designed with the objective of reducing the computational cost required in these types of analysis. Starting from virtual tests of the microscale, the solution of the macroscale structure via Classical First-Order Multiscale Method will be replaced by an interpolation of a discrete number of homogenized surfaces previously calculated. These surfaces describe the stress evolution of the microscale at fixed levels of an equivalent damage parameter (d_{eq}). The information required for these surfaces to conduct the analysis is stored in a Data Base using a json format. Of the two methods developed, the first one uses the pre-computed homogenized surface just to obtain the material non-linear threshold, and generates a Representative Volume Element (RVE) once the material point goes into the nonlinear range; the second method is completely off-line and is capable of describing the material linear and non-linear behavior just by using the discrete homogenized surfaces stored in the Data Base. After describing the two procedures developed, this manuscript provides two examples to validate the capabilities of the proposed methods.

* Corresponding author at: CIMNE – Centre Internacional de Metodes Numerics en Enginyeria, Universitat Politécnica de Catalunya (UPC-BarcelonaTech), Barcelona 08034, Spain.
E-mail addresses: zstefano@cimne.upc.edu (S. Zaghi), xmartinez@cimne.upc.edu (X. Martinez), rrossi@cimne.upc.edu (R. Rossi), mpetracca@cimne.upc.edu (M. Petracca).

https://doi.org/10.1016/j.compstruct.2018.08.022

Available online 20 August 2018

Chapter 5

Conclusions

5.1 Conclusions

In this thesis it has been presented an application of the first-order multiscale method to real composite structures used in various engineering fields involving different physical phenomena.

Following the initial outlined objective, a thermo dynamic multiscale algorithm has been implemented providing a software able to reproduce the composite behavior at the microscale level under coupled thermo-mechanical loading condition. Furthermore, the delamination process that frequently occurs in the composite materials has been addressed implementing an interface cohesive element with midsurface plasticity based model for 2D and 3D analysis. This element has been also extended to the displacement and pressure (U-P) formulation providing significant advantages, in particular:

- it can increase the numerical performance allowing the use of iterative solvers;
- it represents a better alternative to the standard one in case of high compression loading because the compenetration is automatically avoided through the formulation without any additional parameters, such as lagrangian multipliers or penalty methods.

The multiscale thermo-mechanical analysis and the cohesive interface element formulation have been validated in the case studied of solar plant, where a multilayered tube has been simulated in order to obtain the structural response under severe working conditions. In addition, inside of a collaboration with ABENGOA Research, a GUI B.2 has been developed and implemented in the GiD pre-post process software

giving a powerful and user friendly industrial tool for multiscale evaluation of homogenized composite material properties for 2D analysis as well as 3D cases.

One of the most critical problems for both academic and industrial field is the computational cost of multiscale procedures. Therefore, two novel optimization methods have been developed and implemented. These methods, the DMTS and DMCM procedures, take in to account the linear and non linear behavior of the microscale structure, respectively, by decoupling the first order multiscale analysis from the macroscale problem. In the first method (DMTS), the elastic limit boundary of the material is stored and only if the amount of stress exceeds this limit the microscale structure is solved. The second method (DMCM), provides multiple threshold surfaces in order to describe the material behavior up to the complete failure without any additional multiscale analysis.

To achieve this goal, a key parameter named "equivalent damage" d_{eq} and a novel database structure has been implemented. The d_{eq} identifies the amount of non-linearity inside of the microstructure, while the database allows to store the information of the linear and non linear behavior in terms of stress and strain.

These methods have been also tested and validated by classical benchmarks as well as more complex cases, i.e. reinforced composite structure where, with the DMCM method, a speed up greater than 600 times has been obtained.

In conclusion, this work provides a thermo-mechanical approach to the classical first-order multiscale analysis, able to capture linear and non-linear phenomena that occur in composite materials at the constitutive law level and at the structural one, as i.e. the delamination process. The mechanical and thermal homogenized properties of the microstructure can be also directly evaluated through the implemented GUI. Moreover, a significant speed-up is obtained with the optimized algorithms, in order to extend the multiscale approach to wide and complex range of structures.

5.2 Main Contributions

The main features provided by this work are reported below:

- Extension, from two-dimensions to three-dimensions, of the first order homogenization model implemented in the in-house soft-

ware Kratos-Multiphysics [20, 77]. Followed by validation tests to ensure the correct implementation.

- Implementation of a cohesive interface element based on the concept of midsurface plasticity [76], see Annex A.1.
- Extension of the cohesive interface element to the U-P formulation in order to increase the numerical performance using iterative solvers, see Annex A.1.
- Development of thermo dynamic approach applied to a first order multiscale homogenization model.
- Extension of the thermo dynamic formulation to the cohesive interface elements in order to simulate the heat transfer problem.
- Application of the thermo-mechanical model to a receiver tube with multilayered coatings used in solar plant application.
- Development of Graphic User Interface in GiD Pre-Post Processor [2] coupled to Kratos Multiphysics software able to perform Thermo-Mechanical analysis and to obtain the corresponding homogenized properties, see Annex B.2.
- Development and implementation of two novel optimization algorithms, DMTS and DMCM, to provide a faster and computationally efficient model derived from the first order homogenization method. These methods are based on the definitions of an RVE Data Base (DB) implementated in JSON [1] format.

5.3 Future works

This thesis showed the importance of including multiphysical effects in multiscale simulations of composite materials with special attention to the thermo-mechanical behavior. Following this research line, some future developments can be proposed as follow:

- Implementation of thermo-mechanical behavior to the zero-thickness U-P cohesive element described in the Annex A.1. This modified element could be useful to describe the behavior of the fiber and matrix interface as well as the mortar joints interaction under higher compression loading that can produce numerical instabilities with classical penalty method or lagrangian formulation.

- The natural extension of the linear thermo-mechanical fully coupled technique is the non-linear thermo dynamic behavior applied to the first-order homogenization method.

- Design and development of a complete and user-friendly tool able to perform a complete thermo-mechanical full-multiscale analysis as extension of the GUI already implemented in GiD pre-postprocessor.

- Extension of the proposed DMTS and DMCM optimized multiscale formulations to 3D simulations.

- An optimization of the DMTS and DMCM database construction. These procedures requires a first analysis to determine the threshold elastic surface, under the different loads applied to them. The computational cost of this operation could be reduced thanks to the implementation of the Smart First Step (SFS) algorithm developed by Otero et al. [72].

- Development and implementation of thermo dynamic behavior in DMTS and DMCM technique. The thermal part of the multiscale homogenized model implies, considering only the linear regime, to add an additional dimension to the problem.

- Extension of the DMTS and DMCM technique to dynamic loading in order to extend the range of application of these methodology.

Appendices

Annex A

Interface Element Formulation

The element formulation implemented was made for 2D and 3D; we report only the 3D case with prismatic interface and tetrahedral boundary element [91]. The prismatic element is composed by two triangular surfaces. This surface lie together in the initial configuration (zero thickness) and separate as the adjacent solid elements Figure A.2. The relative displacement of the element faces generate normal and shear stresses depending on the constitutive equation of the cohesive crack, which is independent of the element formulation. The interface element has 18 degrees of freedom. The nodal displacements in the global coordinate system are given by the 18×1 column vector $\mathbf{d}_N$ defined

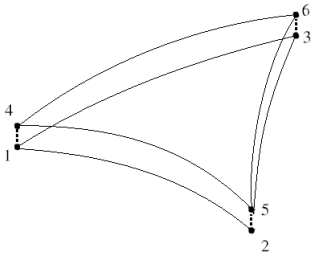

Figure A.1: Initial configuration with zero thickness

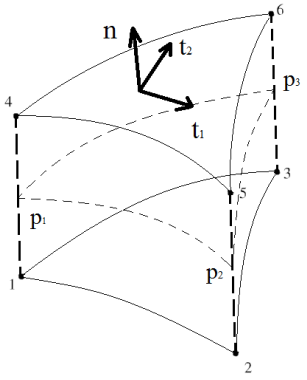

Figure A.2: Current configuration showing the reference middle surface

as:

$$\mathbf{d}_N = \left(d_x^1, d_y^1, d_z^1, \quad d_x^2, d_y^2, d_z^2, \quad \dots \quad d_x^6, d_y^6, d_z^6\right)^T \tag{A.1}$$

and the relative displacement between paired nodes in the element surfaces is given in global coordinates by the 9×1 column vector Δu_N

$$\mathbf{\Delta u}_N = \mathbf{N}^* \mathbf{d}_N = \left(\mathbf{I}_{9\times 9} \quad | \quad -\mathbf{I}_{9\times 9}\right)\mathbf{d}_N \tag{A.2}$$

where $\mathbf{I}_{n\times n}$ is the identity matrix. Let $N_i(\xi, \eta)$ be the shape function for the node pair $i(i = 1, 3)$, where ξ and η stand for the natural element coordinates $0 \leq \xi \leq 1, 0 \leq \eta \leq 1$. The relative displacement between the element faces at the point (ξ, η) can be interpolated as a function of relative displacement between paired nodes as

$$\mathbf{\Delta u}(\xi, \eta) = \begin{pmatrix} \Delta u_x(\xi, \eta) \\ \Delta u_y(\xi, \eta) \\ \Delta u_z(\xi, \eta) \end{pmatrix} = \mathbf{\Phi}^{**}(\xi, \eta)\mathbf{\Delta u}_N \tag{A.3}$$

where $\mathbf{N}^{**}$ is a 3×9 matrix given by

$$\mathbf{N}^{**}(\xi, \eta) = (N_1\mathbf{I}_{3\times 3} \quad | \quad N_2\mathbf{I}_{3\times 3} \quad | \quad N_3\mathbf{I}_{3\times 3}) \tag{A.4}$$

Finally we can obtain:

$$\mathbf{\Delta u}(\xi, \eta) = \mathbf{N}^{**}\mathbf{N}^* = \mathbf{N}\mathbf{d}_N \tag{A.5}$$

where $\mathbf{N}$ is the 3×18 matrix which computes the relative crack opening at any point of the interface element from the nodal displacements. For this geometry the *Jacobian* is a 3×2 matrix. If we define the middle surface points like:

$$\begin{cases} \bar{x}_1 = 0.5(\mathbb{X}_1 + \mathbb{X}_4) \\ \bar{x}_2 = 0.5(\mathbb{X}_2 + \mathbb{X}_5) \\ \bar{x}_3 = 0.5(\mathbb{X}_3 + \mathbb{X}_6) \end{cases} \tag{A.6}$$

where $\mathbb{X}_i$ are the coordinates at the $i - th$ node, we obtain J as:

$$J = \begin{bmatrix} -(\bar{x}_1^x + \bar{x}_2^x), & (\bar{x}_1^x + \bar{x}_3^x) \\ -(\bar{x}_1^y + \bar{x}_2^y), & (\bar{x}_1^y + \bar{x}_3^y) \\ -(\bar{x}_1^z + \bar{x}_2^z), & (\bar{x}_1^z + \bar{x}_3^z) \end{bmatrix} \tag{A.7}$$

The 18×18 tangent stiffness matrix for the element, K_{el}, can be defined as:

$$\mathbf{K}_{el} = \mathbf{N}^T\mathbf{D}\mathbf{N} \tag{A.8}$$

where the Elastic Constitutive matrix $\mathbf{D}$ is a 3×3 matrix:

$$\mathbf{D} = \begin{bmatrix} k_n & 0 & 0 \\ 0 & k_{t1} & 0 \\ 0 & 0 & k_{t2} \end{bmatrix} \tag{A.9}$$

and k_n, k_{t1}, k_{t2} are respectively the normal and tangential stiffness modules. *Remark* : In order to use the interface element with Hexaedral Elements in the boundary, and in 2D condition, other 2 new type of geometry has been implemented, in addition to the Prismatic ones, that accomplished the condition of zero thickness:

- Quadrilateral 2D - 4 Nodes
- Hexahedral 3D - 8 Nodes

Constitutive Law Formulation The Constitutive law formulation used to simulate the cohesive crack model is a variation of the Multi-surface model developed by Lourenço [76]. This theory is similar to the Coulomb friction cone with a $cut-off$ for the traction mode. The Fig-

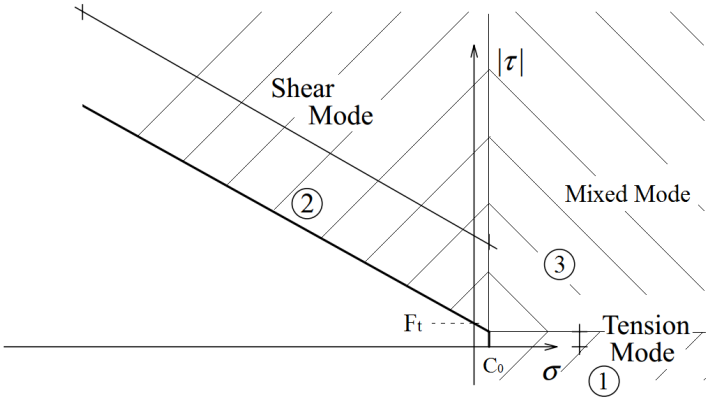

Figure A.3: Damage Surface for 2D Case

ure A.3 represent the Flux Surface of this Constitutive Law, where F_t (Yield Stress) and C_0 (Initial Cohesion) are material parameters passed as input at the code. In this specific case, when the separation create a vacuum space, the initial cohesion value (C_0) represent the adhesion force between the aluminum and the sphere. The no-compenetration condition in addition to the friction, if the sliding is present, is accomplished imposing a Compression Stiffness. The two flux surface can't move independently because they must to be continue. To join the two

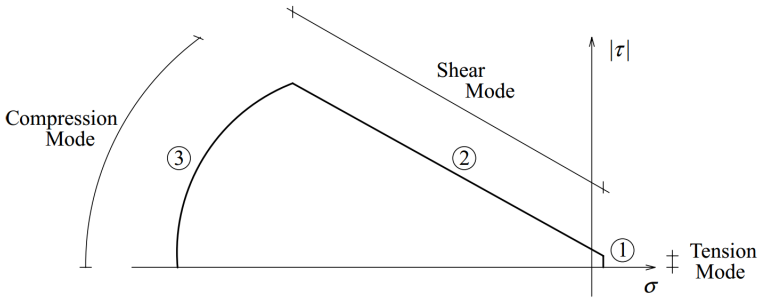

Figure A.4: 3 Multi Surface theory

mode we have define a coefficient (M_{ratio}) function of F_t, C_0 and the $FractureEnergy$ for both mode I and II:

$$M_{ratio} = \frac{F_t}{C_0}\frac{G_I}{G_{II}} \tag{A.10}$$

In case of (F_t and/or C_0) ≤ 0 the M_{ratio} is imposed equal to 1 and F_t and C_0 equal to 0.

Damage Calculation It is possible to assume this theory like a scalar damage law where are introduced more parameters. *Remark* : Lourenço use a Plasticity theory assumption and 3 flux surface like in the Figure A.4: This parameters are a *damage multipliers* and are defined as:

$$\begin{cases} \lambda_1 = \sigma_n - F_t \\ \lambda_2 = \sigma_n + |\tau| - C_0 \end{cases} \tag{A.11}$$

where σ_n and $|\tau|$ are:

$$\sigma_n = \sigma_{11}\,, \qquad |\tau| = \sqrt{\sigma_{22}^2 + \sigma_{33}^2} \tag{A.12}$$

In this way the multisurface yield function are define as:

$$f_i(\sigma, \kappa_i) \tag{A.13}$$

where the scalar κ_i is introduced as a measure for the amount of damage. we have assumed for each zone a different value of κ_i:

$$Zone\ 1 \begin{cases} \kappa_1 = \lambda_1 \\ \kappa_2 = \lambda_1 M_{ratio} \end{cases} \tag{A.14}$$

$$Zone\ 2 \begin{cases} \kappa_1 = \lambda_2 M_{ratio} \\ \kappa_2 = \lambda_2 \end{cases} \tag{A.15}$$

$$Zone\ 3 \begin{cases} \kappa_1 = \sqrt{\lambda_1^2 + (\frac{\lambda_2}{M_{ratio}})^2} \\ \kappa_2 = \sqrt{\lambda_2^2 + (\frac{\lambda_1}{M_{ratio}})^2} \end{cases} \tag{A.16}$$

Finally it's possible to calculate the actual value of damage as:

$$Tension\ Mode\,(in\ n\ direction) \qquad \mathbf{D}_1 = 1.0 - \left(\frac{F_t}{\kappa_1 + F_t}\right)^{-\frac{F_t}{G_I k_n}\kappa_1} \tag{A.17}$$

$$Compression\ Mode\,(in\ n\ direction) \qquad \mathbf{D}_1 = 1.0 - \left(\frac{F_t}{\kappa_1 + F_t}\right)^{-\frac{F_t}{G_I k_n^*}\kappa_1} \tag{A.18}$$

$$Shear\ Mode\,(in\ t_1\ direction) \qquad \mathbf{D}_2 = 1.0 - \left(\frac{C_0}{\kappa_2 + C_0}\right)^{-\frac{C_0}{G_{II} k_{t1}}\kappa_2} \tag{A.19}$$

$$Shear\ Mode\,(in\ t_2\ direction) \qquad \mathbf{D}_3 = 1.0 - \left(\frac{C_0}{\kappa_2 + C_0}\right)^{-\frac{C_0}{G_{II} k_{t2}}\kappa_2} \tag{A.20}$$

where $k_n^* = CompressionStiffness$.

Update Stress After the calculation of the damage it's possible update the stress as:

$$\begin{cases} \sigma_{11} = \sigma_n = \sigma_{11}(1.0 - D_1) \\ \sigma_{22} = \sigma_{22}(1.0 - D_2) \\ \sigma_{33} = \sigma_{33}(1.0 - D_3) \end{cases} \tag{A.21}$$

A.1 Mixed element u/p formulation for RVE BCs

To compute the micro structure in the MultiScale analysis one of the geometrical assumption is the periodicity of the relative displacement (Δu) of the opposite surface of the RVE.

In Kratos, now, this problem was resolved by lagrangian multiplier. This approach add an additional term at the global matrix in order to achieve the periodic conditions of the displacement's field.

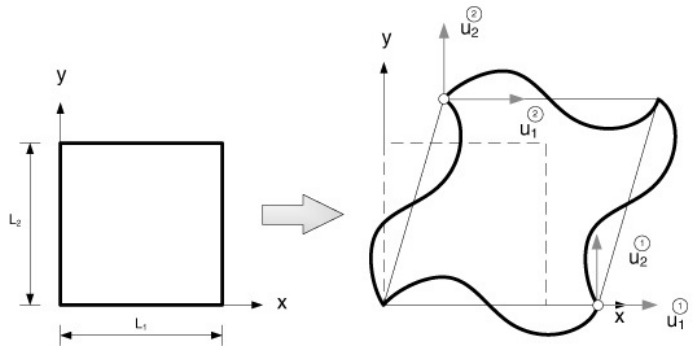

Figure A.5: Periodic Boundary conditions [38]

In term of computational costs the MultiScale analysis required a lot of memory to solve the micro scale. For this reasons it is better to use an Iterative Solver in order to use a Direct Solver, because it stores less memory and it's possible to calculate more complex micro structure. Using the lagrangian multiplier is pratically not possible to use an Iterative solver because the global dof are different form the nodal dof. To solve this problem the PLCd program uses the reduced method, F.Otero et al. [75], but in this case the idea is to implement an equivalent u/p (displacement/pressure) element to represent the boundary condition of the RVE. In this case the dof are the same for each node:

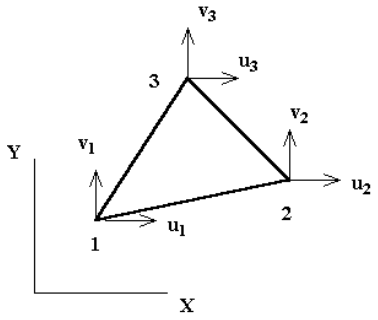

Figure A.6: Example of Triangular U/P Element

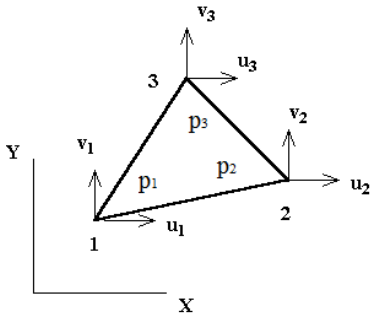

Figure A.7: Example of Standard Triangular Element

Before that implementation, to prove the capability of the formulation, a u/p element will be implemented to simulate an interface material. For this analysis, to ensure the non compenetration from the boundary elements, the "periodic" condition is that the gap should not drop below to zero:

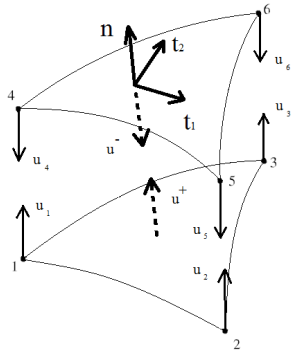

Figure A.8: Displacement distribution on interface element

$$\Delta u = n(u^+ - u^-) = 0 \tag{A.22}$$

The benefit to use the u/p formulation instead of the classical penalty method is that there is no need extra parameters, the $\Delta u = 0$ condition is automatically satisfied.

Annex B

The GUI (ProblemType) of Kratos

In order to provide a Graphical User Interface (GUI) able to solve a multiscale analysis a ProblemType of Kratos Multiphysics has been implemented in GiD pre-post process software.

Kratos FEM Program Kratos is a framework for building multi-disciplinary finite element programs. It provides several tools for easy implementation of finite element applications and a common platform providing effortless interaction between them. Kratos has an innovative variable base interface designed to be used at different levels of abstraction and implemented to be very clear and extendible. It also provides an efficient yet flexible data structure which can be used to store any type of data in a type-safe manner. The Python scripting language is used to define the main procedure of Kratos which significantly improves the flexibility of the framework in time of use [20, 21].

B.1 Overview

This ProblemType, that represents the user interface from GiD (Pre-Post Process Program) and Kratos (see Figure B.1), it's a complex and quite encapsulated code written using TCL (Tool Command Language). This code is often, like in this case, used to develop graphical interface.

Figure B.1: Masonry micro-structure with nonlinear interface model.

B.2 Users Interface

Implementing these applications offers the possibility to resolve the multiscale problem directly from the user interface. Below are reported the main steps of the GUI to perform the multiscale analysis and to obtain the homogenized properties of the composite material:

1. When the Kratos ProblemType is loaded the user can select the Application Type to start the Analysis. The Structural analysis button starts the classical macroscale analysis, while the Rve wizard button starts the multiscale one.

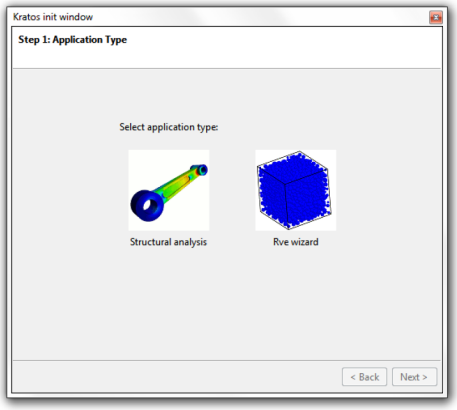

Figure B.2: Step 0 of the interface: Application Type.

2. The first step of the Rve wizard is the selection of the geometry, where the user is allowed to to import an existing geometry or to use a new one. The Rve, in this first release of the GUI must be respectively a square or a cube for the 2D and 3D analyses.

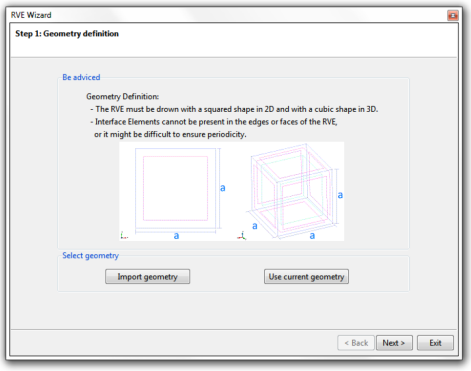

Figure B.3: Step 1 of the interface: Geometry definition.

3. The second step regards the material definition. The GUI, depending on the geometry of the microstructure, can recognize the total number of materials, the number of inclusions and, if presents, the additional cohesive interface elements. In presence of interface, additional constitutive laws appears to the corresponding window.

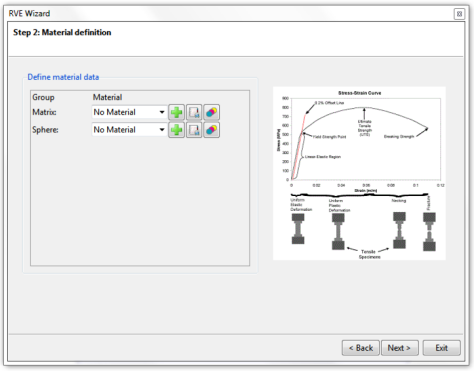

Figure B.4: Step 2 of the interface: Material definition.

4. In the Material Definition step it is also possible ti import or export material. The standard extension of the materials file is .kmdb. This feature is convenient for the users that does not want to hand-write the material properties for each analysis.

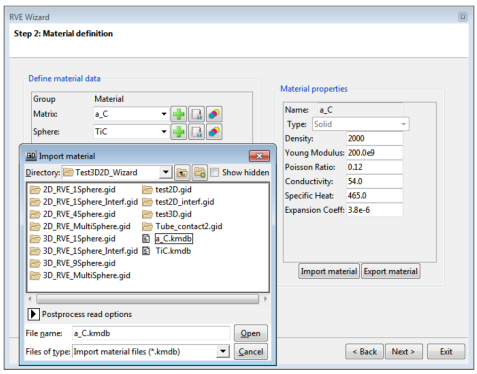

Figure B.5: Step 2 of the interface: Material definition, import/export.

5. In the third step, the GUI provides a window with the Analysis parameter setup. In this step the user can select the type of analysis, i.e. mechanical or thermal, as well as the amount of strain or temperature to be applied on the RVE.

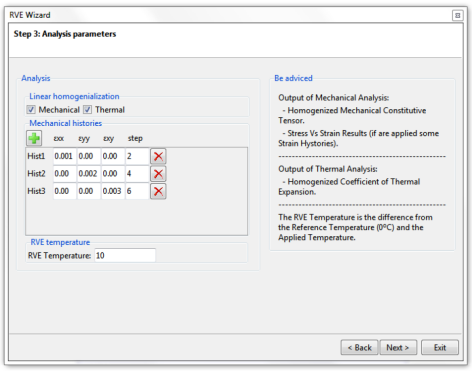

Figure B.6: Step 3 of the interface: Analysis parameter.

6. The step number four, the mesh must be checked by the user before to run the simulation with the corresponding button. The process information can be also seeing in an external window in order to check the analysis status or errors.

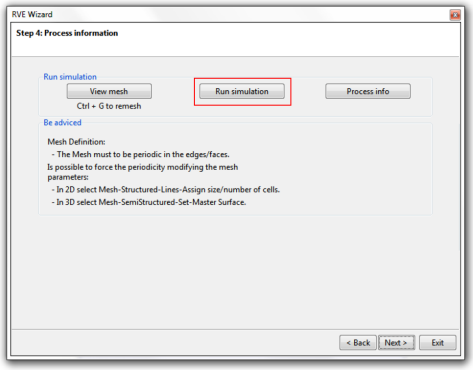

Figure B.7: Step 4 of the interface: Process information.

7. At the end of the analysis the last window provide the homogenized properties of the composite: the constitutive tensor, the coefficient of thermal expansion as well as the homogenized stress state for each prescribed analysis.

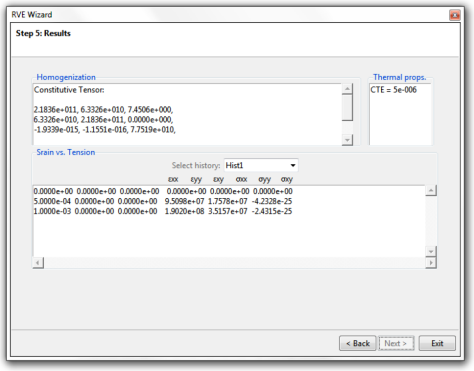

Figure B.8: Step 5 of the interface: Results.

These results could be used to define correctly the Orthotropic or Anisotropic equivalent Material for a Linear Elastic Analysis instead of using the complete MultiScale procedure. In case of applied loading, the deformed microstructure and the additional contour plot are stored in the main folder and can be opened with the post-process interface.

Bibliography

[1] Json (javascript object notation), 1999.

[2] *GiD: The personal pre and post preprocessor*. 2002.

[3] P. B. Lourenço A. Zucchini. A micro-mechanical model for the homogenisation of masonry. *International Journal of Solids and Structures*, 39(12):3233 – 3255, 2002.

[4] Daniela Addessi and Elio Sacco. Nonlinear analysis of masonry panels using a kinematic enriched plane state formulation. *International Journal of Solids and Structures*, 90:194 – 214, 2016.

[5] Daniela Addessi and Elio Sacco. Nonlinear analysis of masonry panels using a kinematic enriched plane state formulation. *International Journal of Solids and Structures*, 90:194–214, 2016.

[6] Armelle Anthoine. Homogenization of periodic masonry: plane stress, generalized plane strain or 3d modelling? *International Journal for Numerical Methods in Biomedical Engineering*, 13(5):319–326, 1997.

[7] Yusuke Asakuma, Shinsuke Miyauchi, Tsuyoshi Yamamoto, Hideyuki Aoki, and Takatoshi Miura. Homogenization method for effective thermal conductivity of metal hydride bed. *International Journal of Hydrogen Energy*, 29(2):209 – 216, 2004.

[8] Z.P. Bažant and B.H. Oh. *Crack Band Theory for Fracture of Concrete*. Bordas-Dunod, 1983.

[9] Helmut J. Böhm. *A Short Introduction to Continuum Micromechanics*, pages 1–40. Springer Vienna, Vienna, 2004.

[10] E. Car, S. Oller, and E. Oñate. An anisotropic elastoplastic constitutive model for large strain analysis of fiber reinforced com-

posite materials. *Computer Methods in Applied Mechanics and Engineering*, 185(2):245 – 277, 2000.

[11] E Car, Fernando Zalamea, Sergio Oller, J Miquel, and Eugenio Oñate. Numerical simulation of fiber reinforced composite materials - two procedures. *International journal of solids and structures*, 39:1967–1986, 04 2002.

[12] M Cervera and M Chiumenti. Mesh objective tensile cracking via a local continuum damage model and a crack tracking technique. *Computer Methods in Applied Mechanics and Engineering*, 196(1):304–320, 2006.

[13] M. Cervera, M. Chiumenti, and C. Agelet de Saracibar. Shear band localization via local j2 continuum damage mechanics. *Computer Methods in Applied Mechanics and Engineering*, 193(9):849 – 880, 2004.

[14] M. Cervera, M. Chiumenti, Q. Valverde, and C. Agelet de Saracibar. Mixed linear/linear simplicial elements for incompressible elasticity and plasticity. *Computer Methods in Applied Mechanics and Engineering*, 192(49):5249 – 5263, 2003.

[15] Miguel Cervera, Michele Chiumenti, and Carlos Agelet de Saracibar. Softening, localization and stabilization: Capture of discontinuous solutions in j2 plasticity. 28:373 – 393, 04 2004.

[16] Miguel Cervera, Javier Oliver, and Rui Faria. Seismic evaluation of concrete dams via continuum damage models. *Earthquake engineering & structural dynamics*, 24(9):1225–1245, 1995.

[17] Miguel Cervera, Luca Pelà, Roberto Clemente, and Pere Roca. A crack-tracking technique for localized damage in quasi-brittle materials. *Engineering Fracture Mechanics*, 77(13):2431–2450, 2010.

[18] Michele Chiumenti, Quino Valverde, Carlos Agelet de Saracibar, and Miguel Cervera. A stabilized formulation for incompressible plasticity using linear triangles and tetrahedra. 20:1487–1504, 08 2004.

[19] Peter W. Chung and Kumar K. Tamma. Woven fabric composites—developments in engineering bounds, homogenization and applications. *International Journal for Numerical Methods in Engineering*, 45(12):1757–1790, 1999.

[20] Pooyan Dadvand, Riccardo Rossi, Marisa Gil, X Martorell, J Cotela, E Juanpere, Sergio R Idelsohn, and E Oñate. Migration of a generic multi-physics framework to hpc environments. *Computers & Fluids*, 80:301–309, 2013.

[21] Pooyan Dadvand, Riccardo Rossi, and Eugenio Oñate. An object-oriented environment for developing finite element codes for multi-disciplinary applications. *Archives of computational methods in engineering*, 17(3):253–297, 2010.

[22] Maria Laura De Bellis and Daniela Addessi. A cosserat-based multi-scale model for masonry structures. 9:543–563, 01 2011.

[23] Eduardo de Souza Neto and Raúl Feijóo. Ea de souza neto, ra feijoo. variational foundations of multi-scale constitutive models of solid: Small and large strain kinematical formulation. *LNCC R&D Report*, 11 2006.

[24] W.J. Drugan and J.R. Willis. A micromechanics-based nonlocal constitutive equation and estimates of representative volume element size for elastic composites. *Journal of the Mechanics and Physics of Solids*, 44(4):497 – 524, 1996.

[25] R Faria, J Oliver, and M Cervera. A strain-based plastic viscous-damage model for massive concrete structures. *International Journal of Solids and Structures*, 35(14):1533–1558, 1998.

[26] Frédéric Feyel and Jean-Louis Chaboche. Fe2 multiscale approach for modelling the elastoviscoplastic behaviour of long fibre sic/ti composite materials. *Computer Methods in Applied Mechanics and Engineering*, 183(3):309 – 330, 2000.

[27] Jacob Fish and Kamlun Shek. Finite deformation plasticity for composite structures: Computational models and adaptive strategies. *Computer Methods in Applied Mechanics and Engineering*, 172(1):145 – 174, 1999.

[28] Jacob Fish and Qing Yu. Multiscale damage modelling for composite materials: theory and computational framework. *International Journal for Numerical Methods in Engineering*, 52(1-2):161–191, 2001.

[29] M.G.D. Geers, V.G. Kouznetsova, and W.A.M. Brekelmans. Multi-scale first-order and second-order computational homogenization of microstructures towards continua. *International Journal for Multiscale Computational Engineering*, 1(4):371–386, 2003.

[30] S. Ghosh and Y. Liu. Voronoi cell finite element model based on micropolar theory of thermoelasticity for heterogeneous materials. *International Journal for Numerical Methods in Engineering*, 38(8):1361–1398, 1995.

[31] Somnath Ghosh, Kyunghoon Lee, and Suresh Moorthy. Multiple scale analysis of heterogeneous elastic structures using homogenization theory and voronoi cell finite element method. *International Journal of Solids and Structures*, 32(1):27 – 62, 1995.

[32] Somnath Ghosh, Kyunghoon Lee, and Suresh Moorthy. Two scale analysis of heterogeneous elastic-plastic materials with asymptotic homogenization and voronoi cell finite element model. *Computer Methods in Applied Mechanics and Engineering*, 132(1):63 – 116, 1996.

[33] Somnath Ghosh, Kyunghoon Lee, and Suresh Moorthy. Two scale analysis of heterogeneous elastic-plastic materials with asymptotic homogenization and voronoi cell finite element model. *Computer Methods in Applied Mechanics and Engineering*, 132(1):63 – 116, 1996.

[34] Somnath Ghosh, Kyunghoon Lee, and Prasanna Raghavan. A multi-level computational model for multi-scale damage analysis in composite and porous materials. *International Journal of Solids and Structures*, 38(14):2335 – 2385, 2001.

[35] D. Golanski, K. Terada, and N. Kikuchi. Macro and micro scale modeling of thermal residual stresses in metal matrix composite surface layers by the homogenization method. *Computational Mechanics*, 19(3):188–202, Feb 1997.

[36] JoséMiranda Guedes and Noboru Kikuchi. Preprocessing and postprocessing for materials based on the homogenization method with adaptive finite element methods. *Computer Methods in Applied Mechanics and Engineering*, 83(2):143 – 198, 1990.

[37] Zvi Hashin. The elastic moduli of heterogeneous materials. 29, 01 1962.

[38] Christian Heinrich, Michael Aldridge, A S Wineman, John Kieffer, A.M. Waas, and Khaled Shahwan. The influence of the representative volume element (rve) size on the homogenized response of cured fiber composites. 20, 10 2012.

[39] J.A. Hernández, Javier Oliver, Alfredo Huespe, Manuel Caicedo-Silva, and Juan Cante. High-performance model reduction techniques in computational multiscale homogenization. *Computer Methods in Applied Mechanics and Engineering*, 276:149–189, 07 2014.

[40] R. Hill. A self-consistent mechanics of composite materials. *Journal of the Mechanics and Physics of Solids*, 13(4):213 – 222, 1965.

[41] C. Huet. Application of variational concepts to size effects in elastic heterogeneous bodies. *Journal of the Mechanics and Physics of Solids*, 38(6):813 – 841, 1990.

[42] Christian Huet. Coupled size and boundary-condition effects in viscoelastic heterogeneous and composite bodies. *Mechanics of Materials*, 31(12):787 – 829, 1999.

[43] J. Oliver J. M. Ortolano J., A. Hernández. A comparative study on homogenization strategies for multi-scale analysis of materials. *Monograph CIMNE*, 135, 2013.

[44] Mingxiao Jiang, Iwona Jasiuk, and Martin Ostoja-Starzewski. Apparent elastic and elastoplastic behavior of periodic composites. *International Journal of Solids and Structures*, 39:199–212, 01 2002.

[45] Mingxiao Jiang, Martin Ostoja-Starzewski, and Iwona Jasiuk. Scale-dependent bounds on effective elastoplastic response of random composites. *Journal of the Mechanics and Physics of Solids*, 49:655–673, 03 2001.

[46] T. Kanit, S. Forest, I. Galliet, V. Mounoury, and D. Jeulin. Determination of the size of the representative volume element for random composites: statistical and numerical approach. *International Journal of Solids and Structures*, 40(13):3647 – 3679, 2003.

[47] V. Kouznetsova, W. A. M. Brekelmans, and F. P. T. Baaijens. An approach to micro-macro modeling of heterogeneous materials. *Computational Mechanics*, 27(1):37–48, Jan 2001.

[48] V.G. Kouznetsova. *Computational homogenization for the multi-scale analysis of multi-phase materials*. 2002.

[49] P. Roca L. Pelà, M. Cervera. Continuum damage model for orthotropic materials: Application to masonry. *Computer Methods in Applied Mechanics and Engineering*, 200(9):917–930, 2011.

[50] P. Roca L. Pelà, M. Cervera. An orthotropic damage model for the analysis of masonry structures. *Construction and Building Materials*, 41:957–967, 2013.

[51] Gottfried Laschet, Jörg Sauerhering, Oliver Reutter, Thomas Fend, and Josef Scheele. Effective permeability and thermal conductivity of open-cell metallic foams via homogenization on a microstructure model. *Computational Materials Science*, 45(3):597 – 603, 2009. Proceedings of the 17th International Workshop on Computational Mechanics of Materials.

[52] Paulo Lourenco. Computational strategy for masonry structures. 01 1996.

[53] J Lubliner, J Oliver, S Oller, and E Oñate. A plastic-damage model for concrete. *International Journal of solids and structures*, 25(3):299–326, 1989.

[54] Helen M. Inglis, Philippe Geubelle, and Karel Matous. Boundary condition effects on multiscale analysis of damage localization. 88:2373–2397, 06 2008.

[55] Xavier Martinez, Sergio Oller, Fernando Rastellini, and Alex H. Barbat. A numerical procedure simulating rc structures reinforced with frp using the serial/parallel mixing theory. *Computers & Structures*, 86(15):1604 – 1618, 2008.

[56] T Massart. Multi-scale modeling of damage in masonry structures. 01 2003.

[57] T Massart, R H. J. Peerlings, and Marc Geers. An enhanced multi-scale approach for masonry wall computations. 69:1022 – 1059, 01 2007.

[58] T Massart and B Mercatoris. A coupled two-scale computational approach for masonry out-of-plane failure. 5:3820–3826, 01 2009.

[59] B.C.N. Mercatoris, Ph. Bouillard, and T.J. Massart. Multi-scale detection of failure in planar masonry thin shells using computational homogenisation. *Engineering Fracture Mechanics*, 76(4):479 – 499, 2009.

[60] C Miehe and A Koch. Computational micro-to-macro transitions of discretized microstructures undergoing small strains. 72:300–317, 07 2002.

[61] Christian Miehe, Jan Schotte, and Jörg Schröder. Computational micro–macro transitions and overall moduli in the analysis of polycrystals at large strains. *Computational Materials Science*, 16(1):372 – 382, 1999.

[62] Christian Miehe, Jörg Schröder, and Jan Schotte. Computational homogenization analysis in finite plasticity simulation of texture development in polycrystalline materials. *Computer Methods in Applied Mechanics and Engineering*, 171(3):387 – 418, 1999.

[63] F. Montero-Chacón, S. Zaghi, R. Rossi, E. García-Pérez, I. Heras-Pérez, X. Martínez, S. Oller, and M. Doblaré. Multiscale thermo-mechanical analysis of multi-layered coatings in solar thermal applications. *Finite Elements in Analysis and Design*, 127:31 – 43, 2017.

[64] Suresh Moorthy, Somnath Ghosh, and Yunshan Liu. Voronoi cell finite element model for thermoelastoplastic deformation in random heterogeneous media. 47, 01 1994.

[65] Daniel V Oliveira and Paulo B Lourenço. Implementation and validation of a constitutive model for the cyclic behaviour of interface elements. *Computers & structures*, 82(17):1451–1461, 2004.

[66] J Oliver. A consistent characteristic length for smeared cracking models. *International Journal for Numerical Methods in Engineering*, 28(2):461–474, 1989.

[67] SERGIO Oller. *Fractura Mecánica: Un Enfoque Global*. Ediciones CIMNE y UPC, 2001.

[68] Sergio Oller, J Miquel Canet, and Fernando Zalamea. Composite material behavior using a homogenization double scale method. *Journal of Engineering Mechanics-asce - J ENG MECH-ASCE*, 131, 2005.

[69] M. Ostoja-Starzewski. Random field models of heterogeneous materials. *International Journal of Solids and Structures*, 35(19):2429 – 2455, 1998.

[70] Martin Ostoja-Starzewski. Scale effects in materials with random distributions of needles and cracks. *Mechanics of Materials*, 31(12):883 – 893, 1999.

[71] Martin Ostoja-Starzewski. Ostoja-starzewski, m.: Material spatial randomness: from statistical to representative volume element. *Probabilistic Engineering Mechanics*, 21:112–132, 04 2006.

[72] F. Otero, X. Martinez, S. Oller, and O. Salomón. An efficient multi-scale method for non-linear analysis of composite structures. *Composite Structures*, 131:707 – 719, 2015.

[73] Fermin Otero, Xavier Martinez, Sergio Oller, and Omar Salomon. Study and prediction of the mechanical performance of a nanotube-reinforced composite. *Composite Structures*, 94:2920–2930, 09 2012.

[74] Fermin Otero, Sergio Oller, and Xavier Martinez. Multiscale computational homogenization: Review and proposal of a new enhanced-first-order method. *Archives of Computational Methods in Engineering*, 25(2):479–505, Apr 2018.

[75] Fermin Otero, Sergio Oller, Xavier Martinez, and Omar Salomon. Numerical homogenization for composite materials analysis. comparison with other micro mechanical formulations. *Composite Structures*, 122:405–416, 04 2015.

[76] J. G. Rots P. B. Lourenço. Multisurface interface model for analysis of masonry structures. *Journal of engineering mechanics*, 123(7):660–668, 1997.

[77] E. Oñate P. Dadvand, R. Rossi. An object-oriented environment for developing finite element codes for multi-disciplinary applications. *Archives of computational methods in engineering*, 17(3):253–297, 2010.

[78] S Pecullan, Leonid Gibiansky, and S Torquato. Scale effects on the elastic behavior of periodic and hierarchical two-dimensional composites. journal of the mechanics and physics of solids, 47, 1509-1542. 47:1509–1542, 06 1999.

[79] Luca Pelà, Miguel Cervera, Sergio Oller, and Michele Chiumenti. A localized mapped damage model for orthotropic materials. *Engineering Fracture Mechanics*, 124-125:196–216, 2014.

[80] Luca Pelà, Miguel Cervera, and Pere Roca. An orthotropic damage model for the analysis of masonry structures. *Construction and Building Materials*, 41:957–967, 2013.

[81] Massimo Petracca, Pelà Luca, Rossi Riccardo, Oller Sergio, Camata Guido, and Spacone Enrico. Regularization of first order computational homogenization for multiscale analysis of masonry structures. *Computational Mechanics*, 57(2):257–276, 2016.

[82] Massimo Petracca, Luca Pelà, Riccardo Rossi, Stefano Zaghi, Guido Camata, and Enrico Spacone. Micro-scale continuous and discrete numerical models for nonlinear analysis of masonry shear walls. *Construction and Building Materials*, 149:296 – 314, 2017.

[83] Massimo Petracca, Luca Pelà, Riccardo Rossi, Sergio Oller, Guido Camata, and Enrico Spacone. Multiscale computational first order homogenization of thick shells for the analysis of out-of-plane loaded masonry walls. *Computer Methods in Applied Mechanics and Engineering*, 315:273–301, 2017.

[84] L. G. Nallim R. D. Quinteros, S. Oller. Nonlinear homogenization techniques to solve masonry structures problems. *Composite Structures*, 94(2):724–730, 2012.

[85] Fernando Rastellini, Sergio Oller, Omar Salomón, and Eugenio Oñate. Composite materials non-linear modelling for long fibre-reinforced laminates: Continuum basis, computational aspects and validations. *Computers & Structures*, 86(9):879 – 896, 2008. Composites.

[86] Pere Roca, Miguel Cervera, Giuseppe Gariup, and Luca Pelà. Structural analysis of masonry historical constructions. classical and advanced approaches. *Archives of Computational Methods in Engineering*, 17(3):299–325, 2010.

[87] B.Walter Rosen and Zvi Hashin. Effective thermal expansion coefficients and specific heats of composite materials. *International Journal of Engineering Science*, 8(2):157 – 173, 1970.

[88] Savvas Saloustros, Luca Pelà, and Miguel Cervera. A crack-tracking technique for localized cohesive-frictional damage. *Engineering Fracture Mechanics*, 150:96–114, 2015.

[89] Savvas Saloustros, Luca Pelà, Miguel Cervera, and Pere Roca. Finite element modelling of internal and multiple localized cracks. *Computational Mechanics*, pages 1–18, 2016.

[90] Enrique Sanchez-Palencia. *Non-Homogeneous Media and Vibration Theory*. 127. Springer-Verlag Berlin Heidelberg, 1 edition, 1980.

[91] Javier Segurado and Javier LLorca. A new three-dimensional interface finite element to simulate fracture in composites. *International Journal of Solids and Structures*, 41(11):2977 – 2993, 2004.

[92] Juan C Simo and MS Rifai. A class of mixed assumed strain methods and the method of incompatible modes. *International Journal for Numerical Methods in Engineering*, 29(8):1595–1638, 1990.

[93] R.J.M. Smit, W.A.M. Brekelmans, and H.E.H. Meijer. Prediction of the mechanical behavior of nonlinear heterogeneous systems by multi-level finite element modeling. *Computer Methods in Applied Mechanics and Engineering*, 155(1):181 – 192, 1998.

[94] P. M. Suquet. Local and global aspects in the mathematical theory of plasticity. *Plasticity Today*, pages 279–309, 1985.

[95] İ. Temizer and P. Wriggers. A micromechanically motivated higher-order continuum formulation of linear thermal conduction. *ZAMM - Journal of Applied Mathematics and Mechanics / Zeitschrift für Angewandte Mathematik und Mechanik*, 90(10-11):768–782, 2010.

[96] I Temizer and Peter Wriggers. An adaptive method for homogenization in orthotropic nonlinear elasticity. *Computer Methods in Applied Mechanics and Engineering*, 196:3409–3423, 07 2007.

[97] K. Terada and N. Kikuchi. A class of general algorithms for multi-scale analyses of heterogeneous media. *Computer Methods in Applied Mechanics and Engineering*, 190(40):5427 – 5464, 2001.

[98] Kenjiro Terada, Muneo Hori, Takashi Kyoya, and Noboru Kikuchi. Simulation of the multi-scale convergence in computational homogenization approaches. *International Journal of Solids and Structures*, 37(16):2285 – 2311, 2000.

[99] Kenjiro Terada and Noboru Kikuchi. Nonlinear homogenization method for practical applications. 212:1–16, 01 1995.

[100] W. A. M. Brekelmans V. Kouznetsova, M. G. D. Geers. Multi-scale constitutive modelling of heterogeneous materials with a gradient-enhanced computational homogenization scheme. *International Journal for Numerical Methods in Engineering*, 54(8):1235–1260, 2002.

[101] W. A. M. Brekelmans V. Kouznetsova, M. G. D. Geers. Multi-scale second-order computational homogenization of multi-phase materials: a nested finite element solution strategy. *Computer Methods in Applied Mechanics and Engineering*, 193:5525–5550, 2004.

[102] O. van der Sluis, P.J.G. Schreurs, W.A.M. Brekelmans, and H.E.H. Meijer. Overall behaviour of heterogeneous elastovisco-plastic materials: effect of microstructural modelling. *Mechanics of Materials*, 32(8):449 – 462, 2000.

[103] Peter W. Chung, Raju Namburu, and Kumar K. Tamma. Homogenization of temperature-dependent thermal conductivity in composite materials. 15:10–17, 01 2001.

[104] Jian Ying Wu, Jie Li, and Rui Faria. An energy release rate-based plastic-damage model for concrete. *International Journal of Solids and Structures*, 43(3):583–612, 2006.

[105] Julien Yvonnet and Q.-C He. The reduced model multiscale method (r3m) for the non-linear homogenization of hyperelastic media at finite strains. *Journal of Computational Physics*, 223:341–368, 04 2007.

[106] Stefano Zaghi, Xavier Martinez, Riccardo Rossi, and Massimo Petracca. Adaptive and off-line techniques for non-linear multi-scale analysis. *Composite Structures*, 206:215 – 233, 2018.

[107] I. Özdemir, W.A.M. Brekelmans, and M.G.D. Geers. Fe2 computational homogenization for the thermo-mechanical analysis of heterogeneous solids. *Computer Methods in Applied Mechanics and Engineering*, 198(3):602 – 613, 2008.

[108] Idris Özdemir, W A. M. Brekelmans, and Marc Geers. Computational homogenization for heat conduction in heterogeneous solids. 73:185 – 204, 01 2008.

[109] H.W. Zhang, Q. Zhou, H.L. Xing, and H. Muhlhaus. A dem study on the effective thermal conductivity of granular assemblies. *Powder Technology*, 205(1):172 – 183, 2011.

[110] A. Zucchini and P.B. Lourenço. A micro-mechanical homogenisation model for masonry: Application to shear walls. *International Journal of Solids and Structures*, 46(3):871 – 886, 2009.